

MORPHOMETRIC PROPERTIES AND QUANTITATIVE TRAIT LOCI MAPPING OF THE MOUSE
LIMB SKELETON

DISSERTATION

in fulfilment of the requirements for the degree

“Doctor rerum naturalium”

of the Faculty of Mathematics and Natural Sciences
at the Christian Albrechts University of Kiel

submitted by

WIOLETA JOANNA RASMUS

Plön, 2023

First examiner: Prof. Dr. Paul B. Rainey

Second examiner: Prof. Dr. Eva Stukenbrock

Date of the oral examination: 11 July 2022

ABSTRACT

The tetrapod vertebrates are adapted to diverse ecological niches, which is reflected in their anatomy. From the wings of bats to the powerful legs of kangaroos or the dexterous hands of primates and murine rodents, the skeletons of limbs undergo remarkable rearrangements through evolutionary processes, such as mutations, selection and genetic drift. Nevertheless, nearly all vertebrate limbs still comprise the three main functional modules, which in the proximo-distal axis are stylopod, zeugopod and autopod. Unlike in their reptile ancestors, mammalian front limbs have an additional segment which actively participates in achieving gait – the scapula. This reorganisation affects the overall skeletal anatomy of and allows a great variety of specialisation not seen in any other group of vertebrates. Here, I use the house mouse (*Mus musculus*) as a model system to study the genetics of morphometric properties of the limb bones. Limb bone length is a complex, quantitative trait, affected by multiple genetic regions associated with their development and growth. I set out to characterise the genetic differences underlying not only the variance of bone lengths and their proportions within a population but also to the covariation between front and hind limbs and the segments within them.

In the first chapter, I use a population originated in the Iran (AH mice) to analyse how variance in limb bone length is affected by the method of measurement. I compare morphometric results obtained from the x-ray images and micro-CT scans, and show that they are, in most cases, similar. Analyses of Pearson's correlation has shown that females express stronger integration of bones within the hind limb than males. Additionally, length of the scapula correlated strongly with the femur and tibia in females, but not in males. All measured bones were significantly longer in males, in which the humerus expressed strong correlation with the tibia.

In the second chapter, I perform quantitative trait mapping (QTL) of the limb bone lengths using mice from the 15th generation of a 4-way advanced intercross (called G15). I have also explored the morphometric properties and covariation patterns between limb bones in males and females. By using another bone as a covariate in the mapping model, I attempted to find candidate intervals linked to the relationship between two different traits. The design of this population proved highly useful in detecting genes relevant in bone development, but also genome intervals with yet not recognized role. This includes candidate genes such as *Sox5* and

Cdh10 in the ulna or *Bmp3* in the tibia. A linked interval was also observed on chromosome 13 in several phenotypes. Analyses with the humerus as a covariate, showed that length of the radius is influenced by different genes than lengths of the ulna and tibia within this QTL marker. One of the interesting candidate genes was *Dnajb9*, suggestive in the radius with the ulna as a covariate, and previously reported in QTL mapping of limb proportions. Unlike in the Iranian mice, the hind limb bones of the female G15 were significantly longer than in males. The sex differences in bone proportions are often associated with hormonal regulation, however the model of femur with tibia covariate pointed to the X-chromosome candidate genes *Sh3kbp1* and *Rps6ka3*. Importantly, the mutation of human orthologue *RPS6KA3* are associated with the Coffin-Lowry syndrome, which affects skeletal proportions and causes mental retardation, particularly in men. In females, the scapula was correlated with the tibia, similar to the Iranian mice, and using the shoulder blade bone as a covariate enabled to identify two separate peaks in the chromosome 5 linked to this relationship.

The results from both chapters are a promising advance in our understanding of the evolution of the rodent skeleton. Using the laboratory animal model allowed the identification of candidate genes with causal effects on limb growth and size, including potential links between bone morphology and pathology. Future molecular research of these candidate genes could advance our knowledge on human skeleton diseases, as well as improve health and welfare of agriculturally important animals.

Zusammenfassung

Landwirbeltiere sind an unterschiedliche ökologische Nischen angepasst, was sich in ihrer Anatomie widerspiegelt. Von den Flügeln der Fledermäuse bis zu den kräftigen Beinen der Kängurus oder den geschickten Händen der Primaten und den feingliedrigen Pfoten von Nagetieren haben sich die Knochen der Gliedmaßen durch evolutionäre Prozesse wie Mutationen, Selektion und Gendrift erheblich verändert. Dennoch bestehen fast alle Gliedmaßen der Wirbeltiere nach wie vor aus den drei wichtigsten funktionellen Modulen, die in der proximal-distalen Achse Stylopod, Zeugopod und Autopod heißen. Im Gegensatz zu ihren reptilischen Vorfahren verfügen die vorderen Gliedmaßen der Säugetiere über ein zusätzliches Segment, das aktiv am Gang beteiligt ist: das Schulterblatt. Diese Umstrukturierung wirkt sich auf die gesamte Skelettanatomie aus und ermöglicht eine große Vielfalt an Spezialisierungen, die bei keiner anderen Wirbeltiergruppe zu finden sind. In dieser Arbeit verwende ich die Hausmaus (*Mus musculus*) als Modellsystem, um die Genetik der morphometrischen Eigenschaften der Gliedmaßenknochen zu untersuchen. Die Länge der Gliedmaßenknochen ist ein komplexes, quantitatives Merkmal, das von mehreren genetischen Regionen beeinflusst wird, die mit ihrer Entwicklung und ihrem Wachstum zusammenhängen. Ich habe mir vorgenommen, die genetischen Unterschiede zu charakterisieren, die nicht nur der Variation der Knochenlängen und ihrer Proportionen innerhalb einer Population zugrunde liegen, sondern auch der Kovariation zwischen Vorder- und Hintergliedmaßen und den Segmenten innerhalb dieser.

Im ersten Kapitel analysiere ich anhand einer Population Hausmäuse, die ursprünglich aus dem Iranischen Flachland stammen, wie die Varianz der Knochenlänge der Gliedmaßen von der Messmethode beeinflusst wird. Ich vergleiche morphometrische Ergebnisse aus Röntgenbildern und Mikro-CT-Scans und zeige, dass sie in den meisten Fällen vergleichbar sind. Analysen mittels Pearson-Korrelationen haben gezeigt, dass Weibchen eine stärkere Integration der Knochen innerhalb der Hintergliedmaße aufweisen als Männchen. Darüber hinaus korrelierte die Länge des Schulterblatts bei den Weibchen stark mit dem Oberschenkelknochen und dem Schienbein, nicht jedoch bei den Männchen. Alle gemessenen Knochen waren bei den Männchen signifikant länger, wobei der Humerus eine starke Korrelation mit dem Schienbein aufwies.

Im zweiten Kapitel führe ich eine quantitative Merkmalskartierung (QTL) der Gliedmaßenknochenlängen an Hausmäusen aus der 15-ten Generation eines 4-Wege

komplexen Intercross Verfahrens durch (G15 genannt). Ich habe auch die morphometrischen Eigenschaften und Kovarianzmuster zwischen den Gliedmaßenknochen von Männchen und Weibchen untersucht. Durch die Verwendung eines anderen Knochens als Kovariate im Kartierungsmodell habe ich versucht, Kandidatenbereiche zu finden, die mit der Beziehung zwischen zwei verschiedenen Merkmalen verbunden sind. Das Design dieser Population erwies sich als sehr nützlich bei der Entdeckung von Genen, die für die Knochenentwicklung relevant sind, aber auch von Genomintervallen, deren Rolle noch nicht näher bekannt ist. Dazu gehören Kandidatengene wie *Sox5* und *Cdh10* in der Elle oder *Bmp3* in der Tibia. Ein starkes Signal wurde auch auf Chromosom 13 in mehreren Phänotypen beobachtet. Analysen mit dem Humerus als Kovariate zeigten, dass die Länge des Radius von anderen Genen beeinflusst wird als die Länge von Ulna und Tibia innerhalb dieses QTL. Eines der interessanten Kandidatengene war *Dnajb9*, das für den Radius mit der Elle als Kovariate naheliegend ist und über das bereits bei der QTL-Kartierung von Gliedmaßenproportionen berichtet wurde. Im Gegensatz zu den Mäusen der iranischen Population waren die Knochen der Hintergliedmaßen der weiblichen G15 signifikant länger als die der männlichen Tiere. Die geschlechtsspezifischen Unterschiede in den Knochenproportionen werden häufig mit hormoneller Regulierung in Verbindung gebracht, das Modell der Kovariate Femur und Tibia deutet jedoch auf die X-Chromosom-Kandidatengene *Sh3kbp1* und *Rps6ka3* hin. Wichtig ist, dass die Mutation des menschlichen Orthologs *RPS6KA3* mit dem Coffin-Lowry-Syndrom in Verbindung gebracht wird, welches die Skelettproportionen beeinträchtigt und zu geistiger Retardierung führt, insbesondere bei Männern. Bei den weiblichen Tieren korrelierte die Länge des Schulterblattes mit dem Schienbein, ähnlich wie bei den Mäusen der iranischen Population, und die Verwendung des Schulterblattknochens als Kovariate ermöglichte es, zwei separate Signale auf Chromosom 5 zu identifizieren, die mit dieser Beziehung verbunden sind.

Die Ergebnisse aus beiden Kapiteln sind ein vielversprechender Fortschritt in unserem Verständnis der Evolution des Nagerskeletts. Die Verwendung des Labortiermodells ermöglichte die Identifizierung von Kandidatengenen mit kausalen Auswirkungen auf das Wachstum und die Größe der Gliedmaßen, einschließlich möglicher Verbindungen zwischen Knochenmorphologie und -pathologie. Die künftige molekulare Erforschung dieser Kandidatengene könnte unser Wissen über menschliche Skeletterkrankungen erweitern und die Gesundheit und das Wohlergehen von Tieren in der Landwirtschaft verbessern

Thanks to dr. Nico Fuhrmann and dr. Anja Guenther for their kind help with translating this Abstract.

Table of Contents

ABSTRACT	3
Zusammenfassung.....	5
1. GENERAL INTRODUCTION.....	9
1.1. Strategies for linking genotype to phenotype	9
1.2. The house mouse	13
1.3. Vertebrate skeleton.....	14
1.4. Development and genetic pathways	18
1.5. Measurement and estimating error	22
1.6. Aims of the thesis	24
Limb bone morphometrics in Iranian mice	25
2. Abstract	25
2.1. Introduction	26
2.2. Methods	27
2.2.1. Mouse population	27
2.2.2. X-ray cabinet procedure	28
2.2.3. μ CT scanning.....	29
2.2.4. Measurements.....	30
2.2.5. Statistical analyses.....	32
2.3. Results	32
2.3.1. Comparison of the measurements.....	32
2.3.2. Morphometric properties and female – male difference in AH mice.....	34
2.4. Discussion	41
Bone length QTL mapping in an advanced intercross of the house mouse	45
3. Abstract	45
3.1. Introduction	46
3.2. Methods	49
3.2.1. Population G15	49
3.2.2. Imaging and measurements	50
3.2.2. Statistics.....	56
3.2.3. QTL Mapping	57
3.2.4. Bone covariate models.....	58
3.3. Results	59
3.3.1. Final measurements – statistics	60
3.3.2. Genome mapping	69
3.3.3. Bone covariates – mapping of residual bone values.....	90
3. 3. DISCUSSION.....	106
4. General Conclusions.....	113
Supplementary material.....	114
BIBLIOGRAPHY	120

List of Figures.....	134
List of Tables.....	137
Acknowledgements	140
Authors' contributions	142
Declaration.....	142
Outline of the Academic career	143



1. GENERAL INTRODUCTION

1.1. Strategies for linking genotype to phenotype

The association between genotype and phenotype is a vital part of biological study. Since Mendel's findings of heritability, generations of scientist have pushed the boundaries of our understanding of how traits vary and change in macro and micro evolutionary scale. Traits such as the pea seed shape or rare diseases of humans, which can be inherited by single genotypic change are referred as Mendelian traits (Bhattacharyya et al., 1990). However, it is now widely recognised, that most traits express continuous variation (Zwick et al., 2000; Quintana-Murci and Barreiro, 2010). These are known as complex, quantitative traits, and include animal phenotypes such as body weight (Wuschke et al., 2007), limb bone lengths (Leamy et al., 2002) or susceptibility to diseases (Rosemann et al., 2014). Hence, they are of interest not only to scientists, but also have important application in agriculture and animal breeding, as well as medicine. A challenge for evolutionary biology is to understand how the genetic interactions and novelties arise and are altered through time, and the integral part of this in building a genotype-phenotype map, which links the information of the genome sequence and observed morphotype (Kemble et al., 2019).

The process of genetic mapping is bound to methods such as genome-wide association studies (GWAS) or quantitative trait loci (QTL) mapping, where phenotype diversity is tested for correlation with the dense marker information in a large population (Schacherer, 2016). Since the time GWAS was developed, it has become possible to define small genomic regions encoding a variety of traits, thanks to availability of fully sequenced genomes, such as that of the human and mouse. Many GWAS studies use genome-wide SNP arrays due to their lower costs (polymorphism of markers with known location on a chromosome), as well as whole-genome sequencing (Tam et al., 2019; Kim et al., 2018). The downside is that the variants might not have a true causative biological relevance to the phenotype (Tam et al., 2019).

A quantitative trait locus (QTL) is a polymorphic region of the genome, that co-varies with the trait polymorphism in a studied population (Broman, 2001). Typically, traits of interest in QTL studies, are continuous, with examples such as body mass, height, cholesterol level etc.

Mineral bone density is one of the primary quantitative traits to investigate in the skeleton as it determines likelihood of bone fractures (Koller et al., 1998). Similar as in GWAS, QTL mapping can use an array where known markers (SNPs) are genotyped densely across the chromosomes (Belheouane et al., 2017; Liu et al., 2018). Mapping of QTLs uses a population developed by crossing different parental strains and finding the linkage between the QTL markers and possible genes encoded within it. Both in QTL and GWAS it is currently common to account for population structure, through using linear mixed models, as opposed to the Haley-Knott regression model (Wang and Xu, 2019). It is of great advantage, because it accounts for relatedness of individuals (Yu et al., 2006). One of the most important parts of the QTL mapping strategy is a cross design (Broman, 2009). Typically, inbred and outbred populations can be used to map QTLs of continuous traits. In case of a laboratory mouse, an inbred strain is expected to be delivered by at least 20 generations of brother and sister mating, which guarantees homozygosity at each locus (Beck et al., 2000). Inbreeding in most animals is considered harmful for their wild populations, because it can decrease survival of the individuals due to accumulation of deleterious alleles (Jiménez et al., 1994). However, in laboratory setting, mapping of the QTL traits in the crosses of inbred strains is common, for example in designs such as backcross or intercross (Fig. 1.1. A).

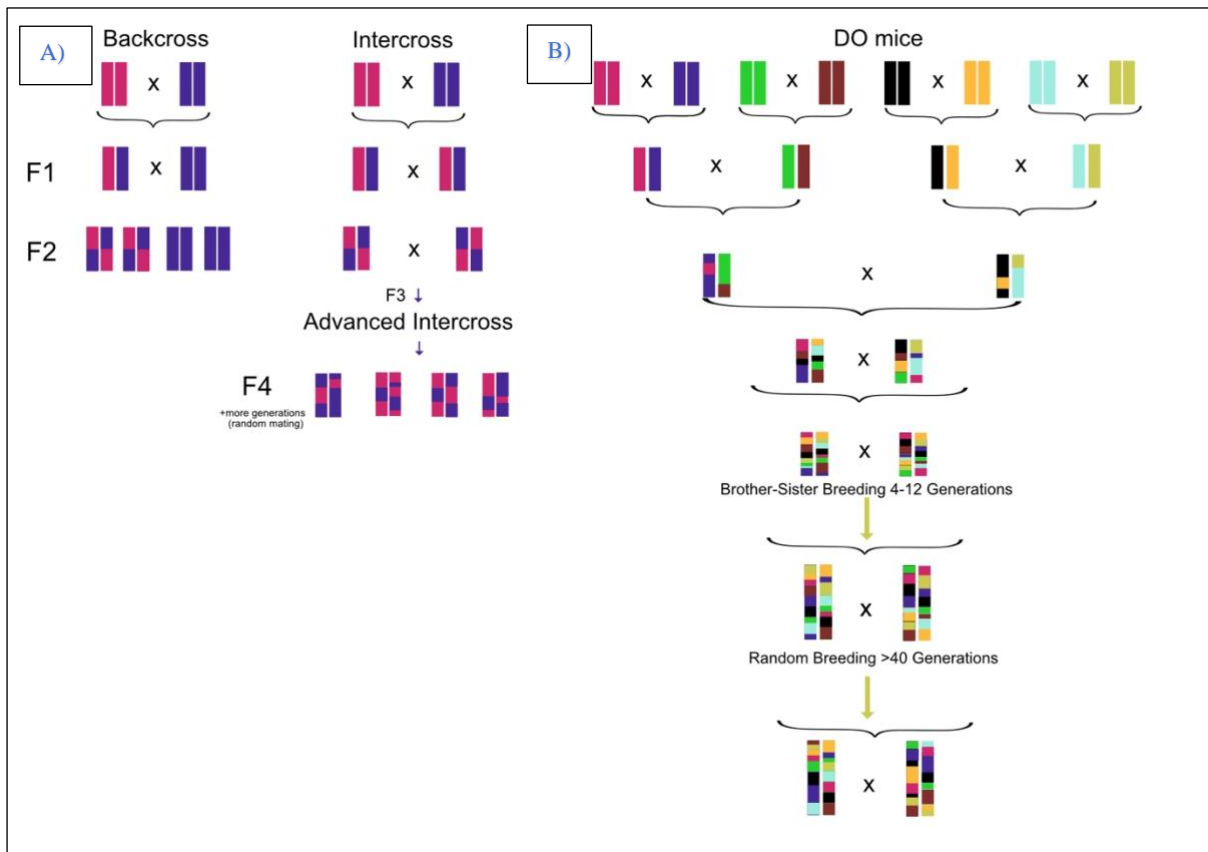


Figure 1.1. Examples of simple cross designs used in QTL mapping – backcross, and intercross which after multiple generations is referred as an advanced intercross (A); Cross design of the diversity outbred (DO) mice (B); the same-colour blocks represent inbred specimen chromosomes (homozygous), as a result of recombination events, the crossed heterozygous offspring represents genotype where the loci are not in a linkage anymore, hence after many generations, the genotype of the DO mice is a diverse mosaic of the parental lineages (modified, after Solberg and Woods, 2014)

In backcrossing, two congenic strains are crossed, and the first heterozygous offspring is mated back to one of the parental strains. We can expect half of the F2 to be heterozygous, and half to have the genotype of the backcrossed parent at each locus (Ishikawa and Namikawa, 2004). Another breeding strategy involves the intercross, where in the second-generation heterozygotes are crossed thus producing both homozygotes and heterozygotes in the population. Intercross simplifies identification of a dominant allele (Broman, 2001). Because of low number of recombinations per chromosome, these models do not require highly dense marker maps (Darvasi and Soller, 1995; Gonzales and Palmer, 2014). Importantly, the phenotype between the crossed populations should express considerable variance (Sugiyama et al., 2001). Mapping using simple designs has been traditionally favoured, because of limited bioinformatic possibilities, which could not account for complex population structure defining

the connection between specimen, and therefore biasing randomness of the phenotype. Simple crosses could identify chromosome regions associated with particular quantitative phenotypes, but limited number of markers, as well as lack of recombination events could not allow for very precise mapping. Consequently, mapped QTL regions contained hundreds of genes. In 1995, Darvasi and Soller introduced the term “advanced intercross” (AIL – advanced intercross lineage) which was a strategy to provide better resolution than standard backcross populations. Unlike in the standard backcross and intercross, the AIL population is crossed for multiple generations, which produces multiple recombination events and increases precision of mapping by decreasing regions of linkage disequilibrium (Darvasi and Soller, 1995). The difficulty of using advanced intercross populations, especially in vertebrates, is the time needed to obtain a large enough population. Naturally occurring hybrid animals are also interesting models, because they provide additional opportunity to study speciation where selection acts on unique genetic variants, and in addition, can identify existing selection patterns. The very important difference expected from these populations, is that in the wild they are unlikely to hold mutations of large effects gene, because these would be selected against (Bierne et al., 2002; Škrabar et al., 2018).

Advanced intercrosses from two parental strains have been used intensively, for example in mapping sensory phenotypes (Samocha et al., 2010), and body weight (Parker et al., 2011) in mice. Multi-parent designs have been increasingly used in the QTL mapping attempts and are especially popular in plant research (called MAGIC populations (Ongom and Ejeta, 2018)), as well as in animals such as mice. The Collaborative Cross (CC) is a valuable recombinant inbred strain (RI) developed from eight inbred founder mouse strains. Another established cross, the Diversity Outbred (DO) mice (Fig. 1.1.B), descends from the CC and is maintained by random crossing. Such outbred designs are highly valuable in dissecting the genetic architecture of complex traits and characterising alleles of known genes, due to their high level of recombination events and minimized effect of genetic drift (Chesler et al., 2016). The downside of using populations such as the DO mice, is that the results cannot be reproduced, because each mouse is unique (Svenson et al., 2012). However, the aim is that they are reproducible at the population level. Using these complex strains has the advantage of obtaining reproducible outcomes, which is valuable in medically and agriculturally important questions which are also critical in our understanding of evolutionary genetics. But such fine-mapping studies also have

disadvantages. For example, large sample size is needed, of over 200 specimens (Churchill et al., 2012).

1.2. The house mouse

Rodents are one of the most numerous group of mammals in term of species, and highly successful in colonizing diverse environments (Churakov et al., 2010). Together with lagomorphs they belong to the clade Glires, which share common ancestor with primates (Huchon et al., 2002). The house mouse (*Mus musculus*) is a cosmopolitan, murine rodent, which originated from the Iranian Plateau, and followed human colonization through the past 10,000 years. The taxon consists of genetically distinct subspecies spread across continents. In fact, the South East and Central Iran were also reported to host genetically separate mice populations, as well as those belonging to *M. m. musculus* and *M. m. domesticus* (Hardouin et al., 2015). The *M. m. musculus* inhabits most of the Asia, and meet with the *M. m. domesticus* in the narrow hybridization zone across Germany. The latter one is also spread in Africa. Another subspecies, *M. m. castaneus* inhabits south-eastern Asia (Harr et al., 2016).

The house mouse is one of the most important model organisms in genetics and medical research and currently large number of inbred strains are commercially available. Molecular research show that they are primarily descends from *M. m. domesticus*. Variable level of introgression among different strains has been reported (Yang et al., 2011). In 2002 the first sequence analysis of the mouse genome was published, which was a key to revolutionizing biomedical research (Mouse Genome Sequencing Consortium, 2002). At the time strain C57BL/6J was used and was later followed by another 17 strains, among which four were wild type strains, including the *M. m. castaneus*, CAST/EIJ (Keane et al., 2011). The house mouse is one of the most widely recognized animals and aside of its use as a model organism, can be considered as agricultural pest, and is an invasive species with negative impact on many newly colonized regions (Bolton et al., 2014), where it can exhibit especially intense morphological adaptation (Parmenter et al., 2016).

Widely available genetic resources for analysis of the house mouse makes it an even more favourable model system (Bućan and Abel, 2002). Other characteristics include fast reproduction rate and genetic similarity to humans in terms of protein coding genes. Mice and

humans also have largely similar skeletons, which makes them a great tool in modelling of bone diseases (Youtten and Baldock, 2019). High rate of nucleotide substitution rates in mice and rats is what distinguish them from higher primates (Li et al., 1996). It could be speculated that inbred strains can't reflect the natural diversity of the species, however by expanding the efforts to obtain maps of other subspecies such as the *M. m. castaneus* and complex crossing we can obtain more diverse genetic backgrounds and still track novel or known loci to understand their contribution to the complex phenotypes (Carver and Stubbs, 1997; Svenson et al., 2012). On the other hand, mice are thought to have less developed social interactions than rats, which are therefore more suitable in models of human behavior (Parker et al., 2014). Relatively small size of these animals might also prove difficult for detailed phenotyping of small organs or body parts. They also require sufficient space and enrichment, which is more challenging than in case of *Drosophila* or nematode models, which enable use of larger populations. Compared to most invertebrates such as insects or nematodes, more complex regulations are in place to minimize potential suffering of mice and other vertebrates (Olsson et al., 2016). As of yet, cell or tissue cultures do not hold enough possibilities to study evolution of complex traits in the population level, which is however important to improve our understanding of many complex questions. The current standards of animal research state to reduce, and reuse the material, for example by sharing the genetic information, tissues and other materials, which makes it then possible to study multiple traits in limited number of animals ("The 3Rs | NC3Rs"; Annys et al., 2014).

1.3. Vertebrate skeleton

In this thesis, the phenotypes of interest are lengths of limb bones and variability of their proportions in relation to sex and populations. Studying biology of vertebrate skeleton calls attention to the numerous processes which shape it in a specimen and which can contribute to the morphological fluctuations observed within and across the population, as well as ultimately between the species.

Bones are units of the vertebrate skeleton, which is a scaffold for the body. But the purpose of bones is more complex than this, and includes locomotion, feeding, protection of vulnerable

body parts - such as brain or lungs, production of blood cells in the bone marrow and repository of important mineral elements such as calcium (Weatherholt et al., 2012). Bones of the vertebrate skeleton can be classified according to their morphology, function or by developmental origin. They incorporate cell types such as osteocytes which are the main component of fully developed bone, the osteoblasts which are important in energy homeostasis and are responsible for bone mineralisation, as well as osteoclast that reabsorb bone tissue (Dirckx et al., 2019). It is hypothesised, that genome duplication in the early chordates was an important event in forming the large diversity of connective tissue which eventually formed the vertebrate skeleton (Zhang and Cohn, 2008).

Similar to human and other tetrapod vertebrates, the skeleton of mouse consists of two main parts: axial (skull, vertebra and ribs) and appendicular (limb) skeleton. Front and hind limbs are thought to be serial homologues, as their skeleton has similar morphology consisting of the three parts in proximo-distal axis: autopod, zeugopod and stylopod (Fig. 1.2).

Limb part	Bone of a front limb	Bone of a hind limb
Stylopod	Humerus (H)	Femur (F)
Zeugopod: Proximal Anterior	Radius (R) Ulna (U)	Tibia (T) Fibula (Fi)
Autopod	Metacarpal (Mc)	Metatarsal (Mt)

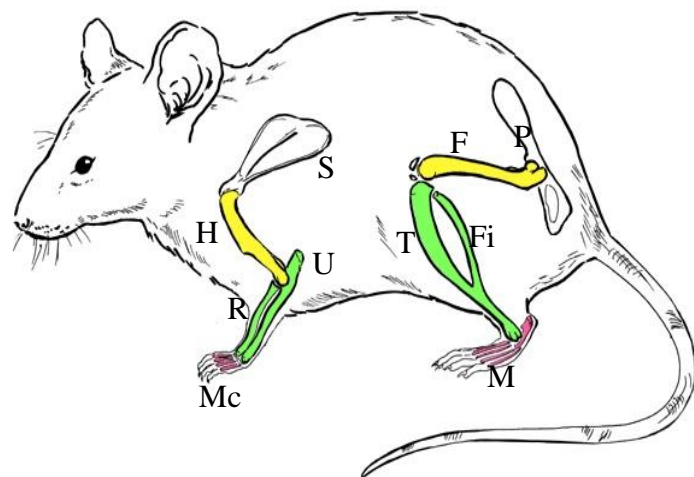


Figure 1.2. Concept of integrated bone elements as in the example of the house mouse; Letters in the drawing correspond to each bone, as specified in the table; additionally, S – scapula and P – pelvic bone are additionally shown in the illustration;

The limbs share similar developmental pathways, and the corresponding elements exhibit morphological integration (Young and Hallgrímsson, 2005), which constrains their

diversification. However, skeletal anatomical changes can also occur very rapidly, as is especially vivid in dogs and other domestic animals, such as poultry (Duggan et al., 2015).

In the process of adaptation to specific ecological niches, proportions, morphology and microstructure of limb bones of mammals (and other tetrapods) have been shaped, with striking examples such as elongation of the bat forearm (Sears, 2008) or increased robustness and density of bones of the ancestors of whales (Sun et al., 2019). Mechanical loads experienced by each elements can be considered as a functional aspect that drives evolution of anatomical properties of limbs (Lieberman et al., 2004). Limbs of extant mammals are exceptionally diverse in this context, ranging from running, jumping, swimming or flying animals and similar patterns of divergence between the homologous limb elements took place many times independently in their evolution. For example an elongated hind limb is found in jumping animals such as hopping mice and jerboa (allowing bipedal locomotion) (Berman, 1985). Macroevolutionary challenge of limb length and proportions of mammals reflects adaptation to these types of movements. For example, a short proximal element, and elongated distal element of the front limb gives ungulate mammals increased speed delivering long strides and rapid steps. But shorter distal parts of the cat limb provide it with powerful acceleration (Gough-Palmer et al., 2008). Such high diversity of limb anatomy is not observed in marsupials, a sister group of placental mammals, in which specific developmental rates constrain morphological evolution of the distal forelimb (Cooper et al., 2010).

A very special aspect of the therian mammalian limb anatomy, is the pectoral girdle, freely connecting front limb with the axial skeleton (McGonnell, 2001). Compared to other tetrapods, such as reptiles, which move in a sprawling condition, the terrestrial mammals move in the parasagittal plane, which is achieved through limbs that are positioned under the body. This is possible through the scapula, attached by muscles and scapulothoracic joint to the body, which gives mobility. It became a functional homologue of femur, while further reorganization made tarsus and metatarsus homologues to forearm bones (Schmidt and Fischer, 2009). The genetic covariation between limbs is thought to be affecting integration of the bone elements, as well as proportions between them. There is still lack of knowledge on the molecular pathways that affect covariance between different bone elements. One of studied patterns is that of FGF/FGFR signalling which was shown to positively affect magnitude of covariation in the mouse skull (Martínez-Abadías et al., 2011). Deletion of *Fgf9* is associated with shortened

stylopod elements in mouse (Hung et al., 2007). But there is still lack of understanding on how the strength of correlation is maintained in the limb bones, and what causes the corresponding elements to diverge in various natural and domestic animal models.

The front limb is made of the pectoral girdle: scapula and clavicle (absent or rudimentary in many animals), the humerus bone of the arm, radius and ulna of forearm, and the bones of hand and digits. The complex of radius and ulna compose the skeleton of the forearm (zeugopod) of many tetrapods (Sears et al., 2007). Radius and separate ulna were present in the fin structure of Tiktaalik, a sarcopterygian (lobe-finned fish), in which they individually articulated with a primitive humerus bone (Shubin et al., 2006). Similar to *Acanthostega*, the radius became elongated while the ulna had an unregular shape, without the olecranon process. In mammals such as mice or primates, the radius has a mobile articulation with the ulna and the wrist bones, which allows rotational movement of the hand – supination and pronation, as well as climbing or the holding food while eating (feeding behaviour) (Barrett et al., 2020). The two bones articulate with wrist bones, to enable movement of the hand – the front limb autopod part.

Compared to pectoral girdle, the pelvic bone has a very different developmental origin in the sense that it grows from embryonic somatopleuric cells (Capellini et al., 2011). It provides articulation with the stylopod of the hind limb, which is made of the femur bone that then articulates through the hinge joint with tibia and the fibula (zeugopod). Among mammals, similar to the radius and ulna, these two bones can exist as a fused unit (Sears et al., 2007). Murine shaft is made of such a fused tibio-fibular complex, where the two bones are connected at their posterior end (Bab et al., 2007). It is therefore different than, for example in humans, where fibula and tibia exist as separated bones. Limb evolution includes also a process of reduction of certain elements, which is a key part of evolutionary specialisation. Such reduction often involves loss of signalling from developmentally important genes (Swank et al., 2021). In the house mouse we observe reduction of fibula, which is a zeugopod element homologous to the ulna (posterior elements, as opposed to anterior radius and tibia). In the bat *Carollia perspicillata*, the ulna and fibula are reduced, in both species the identified mechanism was connected to slower growth rates and is an example of repeated evolution (Sears et al., 2007). It is however interesting, that the bone equivalents – ulna and fibula are not affected in the same direction in the mouse.

It was previously shown that degree of association between limb elements can differ between species (Martín-Serra et al., 2015) and subspecies (Škrabar, 2018). For example, the strength of morphological integration between front and hind limb homologues, which is expressed as a covariation of the elements in question (the length or shape variation) can differ in cursorial and non-cursorial mammals, showing that discrepancy of function of limbs is of great importance. Loss of function of rhinoceros fibula, was linked to weak correlation of this bone with other limb elements (Mallet et al., 2020). Some of the most important concepts in evolution of these parts is modularity, morphological integration and developmental stability. It has been shown, that in terrestrial mammals the limb bone size and shape scale allometrically with body mass within population and across species (Ruff, 1987; Christiansen, 2002). It has been suggested that these associations in scaling can also diversify with functional adaptation of the limb. Genetic factors can explain partially the covariance, of lean body mass and bone density (Seeman et al., 1996). In artificially selected mice for increase of bone length, this occurred independently of the body mass (Marchini et al., 2014).

The length and shape of bones is known to be a polygenic, complex trait, reflecting their development and functional importance (Castro et al., 2019; Pallares et al., 2014). Morphometric properties of two separate bones can also be bound by morphological integration, which is their ability to covary in a population (Klingenberg, 2014). Common developmental pathways or functional similarity of the features can create such covariation, and genesis was of recent scientific interest.

Pavlicev et al. (2013), has used covariate models, to pin genome regions responsible for the diversification of the limbs in mice, which was introduced as relationship QTL (rQTL), and showed that limb proportions are represented at the genetic level. Decrease of genetic covariance can also cause the correlated elements to shift leading to the generation of new phenotypes (Young and Hallgrímsson, 2005).

1.4. Development and genetic pathways

The embryonic growth of the skeletal elements has been extensively studied in the house mouse and other vertebrates, such as chicken, amphibians and zebrafish (Yan et al., 2002), which gives us a wide spectrum of how the specific bones arise and what is their evolutionary

potentials (Sanger et al., 2011). The skeleton is also subject to many diseases, such as cancer and osteoporosis, which makes it even more important to understand its development and genetics. In the mouse model research, knowledge of the timing of growth of the structures and organs, including bones and limbs is important in experimental approaches such as constructions of deletions in disease-related genes. However, because mice of different populations and breeding background can have different rates of development, the defined Theiler stages (TS) are commonly used, where stage 1 marks egg formation, and the 28th stage is the last before adulthood and indicates the postnatal development.

The formation of vertebrate limb bud is a fairly conserved process, and became a study model of embryonic regulatory networks and patterning giving the rise to the limbs (Zeller et al., 2009; Petit et al., 2017). Though their development is initially similar among most mammal species, the limb exhibits strong divergence during the life span of bat or jerboa (Sears, 2008; Cooper, 2011; Saxena et al., 2021) while in these examples the direction of these changes affects homologous elements of the front and hind limb differently. Timing of gene expression is one of the crucial stages in formation of the limb (Loebel et al., 2014). Given the complex construction of long bones and their multiple functions in the body, Atchley and Hall (1991) provided the model of factors and their interactions which are crucial in skeleton formation. Precisely, the morphology (length, proportions) of the adult skeleton is the outcome of developmental (genetic) pathways, uterine effects and postnatal growth. During these steps, genetics can play a role in mitosis rate, hypertrophy (enlargement) and apoptosis of the cells (Sanger et al., 2011). Of less importance, epigenetic effects might seem to contribute solely to maintenance of the patterning of adult bone covariation patterns (Young et al., 2009). Through the constant process of bone remodelling, the mineral bone density can also be affected in adult animals. Recent research in artificially selected mice shows that proliferation rates of the cells, rather than their size or timing is the crucial factor in elongation of limb bones (Marchini and Rolian, 2018). Shedding light on the most important developmental pathways is nevertheless important to understand properties of this complex system.

The skull bones are examples of flat bones, which typically are formed by intramembranous ossification (Franz-Odenaal, 2011). In this process, the mesenchyme cells transform into osteoblasts, which then synthesize bone matrix. Unlike the endochondral ossification, it does not involve formation of cartilage tissue. Interestingly, certain variance in skull anatomy exists

between mouse strains, for example in terms of presence of intrerfrontal bone of the cranium. Particularly, while it is almost always present in C57BL/6J, it is predominantly missing in the CAST/Ei mice (Zimmerman et al., 2019). Intramembranous ossification is also an important pathway in the process of bone fracture healing (Thompson et al., 2002). On the other hand, the long bones, which are the main elements of the limb skeleton, form through the process of endochondral ossification. Here, the cartilage is formed first and builds a scaffolding, which is then occupied by blood vessels, bone marrow cells, osteoclasts and osteoblasts. The process of long bone development through the endochondral ossification is continued postnatally (Carter et al., 1998). Additionally, trabecular and cortical bone can be distinguished. The long bones include these two types, where the cortical is found in the shaft, while the trabecular (“spongy bone”) is what makes the distal parts of it, and enables absorption of mechanical shocks. Type VI Collagen, coded by *Col6a2* was recently found to contribute to loss of trabecular bone (Pham et al., 2020). Collagenous proteins are among most important ones, which compose bone (Paschalis et al., 2003).

The house mouse, like other mammals and bilaterian animals poses three embryonic plates: ectoderm, endoderm and mesoderm. From the perspective of limb development, mesoderm (of the lateral plate origin - LPM), which first appears during gastrulation is the most important (Hirasawa and Kuratani, 2015). It gives rise to the mesenchyme, which then forms limb buds, surrounded by the ectodermal wall – the first “visible” stage of forming the limbs of mammals (Gros and Tabin, 2014). The front limb buds form before the hind limbs, consequently, within the 15th and 16th Theiler Stage (Bard et al., 1998). The mesenchyme is composed of loose cells embedded in extracellular matrix, in which they can migrate and give raise to the skeletal and connective tissues of limb. It has been experimentally shown, that the *Hoxa13* protein is expressed in distal mesenchyme cells, which also diversify in proximo-distal axis (Saiz-Lopez et al., 2015). Positioning of the limb which exist in three different planes is controlled by specific genes. Protein coding gene families such as *Hox*, *Wnt*, *Fgf* and *Shh* among many others. While the *Hox* genes are mainly involved in proper positioning of the segments of the body (somites), *Shh* (Sonic Hedgehog) signalling is responsible for antero-posterior development (Ingham and McMahon, 2001). *Gli* repressor and *Hand2* works upstream of *Shh* (Galli et al., 2010). The protein coded through the *Wnt* are beta-catenin dependent. The latter, is one of the cell-cell adhesion proteins (CAMs), which are extremely important in diversification of tissues. Calcium-dependant cadherins have been reported to play important roles in formation of skeletal

tissues, such as *Cdh11*, *Cdh9* and N-Cadherins (Oberlender and Tuan, 1994; Kimura et al., 1995). The allelic variants might not alter protein structure, but some can be related to human disease. Families such as Hox and Shh are conserved among most vertebrates, and even all metazoans. For example, the Hox protein in a fruit fly and other insect product the segments characteristics, such as for example the *Ubx* type of Hox transcription factor alters formation of second pair of wings (Grenier and Carroll, 2000). Mice with missing *Hoxa-11* and *Hoxd-11* simultaneously, do not develop zeugopod bones of the forearm (Davis et al., 1995). The Sox family of regulatory genes is just as important in embryonic development. Particularly, *Sox8* and *Sox9* are essential in chondrogenesis preceding formation of skeletal limb tissue (Akiyama et al., 2005). The process of bone condensation takes place, during which the cells create the cartilage through proliferation of chondrocytes. Further, the formation of extracellular matrix made of collagen takes place, where transcription factor *Sox9* is one of the key contributors (Arostegui and Underhill, 2021). The forming diaphysis is invaded by blood vessels, making way for osteoblasts. On the other hand, BMP signalling is essential in prechondrogenic condensations. It can be inhibited by overexpression of either *Smad7*. BMPs are also upregulating N-cadherin expression. Specifically, *Bmp2* upregulates *Wnt-3a* expression and overexpression of *Wnt-3a* enhances BMP-2- mediated chondrogenesis.

The neural crest cells (of ectodermal origin) have just as important a role, however they are mostly involved in formation of skull bones (Noden and Schneider, 2006). The skull has undergone many anatomical changes through the evolution of Tetrapoda, but most often can be divided into two modules – the craniofacial part and the braincase. In mice, as well as other rodents, the mandible has two separate bones: left and right. On the other hand, scapula of the pectoral gridle is somewhat unique, because of a very complex embryonic origin, from various embryonic cell layers including the dermomyote and NC. It was hypothesised, that scapula is in fact a large sesamoid bone (Young et al., 2019). The limb is also composed of elements, such as muscles, tendons and ligaments as well as fat tissue and neural and blood vessel systems. In the vicinity of joints, another type of bone – sesamoid bones are present, with examples present in the mouse such as the patella bone (kneecap) and the fabella, also associated with the knee joint. Despite their similar appearance, they can be formed by action of distinct genes or their co-expression (Eyal et al., 2019). Most of the sesamoid bones are small, and some can form as a result of physical strain (Young et al., 2019). Attachment of the

muscles etc has impact on the adult bone anatomy, which additionally shows complexity of this system.

As shown, development of limbs depends strongly on a small number of gene families and their interactions. Mutations in any of these large effect genes have usually has drastic effects on the developing embryo (Morikawa et al., 2007). The products of these key genes, and others which remain to be discovered, interact with each other, for example by upregulation or downregulation. Therefore, these interactions are the key for development process, and it can be speculated, that by changing them we can also expect the traits to diverge. It can however have also detrimental effect on the specimen, so evolutionary speaking, the development of the skeleton has to be constrained enough by the natural selection processes to provide necessary scaffolding for muscles and other organs, and support the processes such as blood cell production or adipose. For example, the BMP signalling is also essential for the adipogenesis. Shape and length of the skeletal elements are highly polygenic, and so are the proportions of the skeleton. It is therefore a basic expectation, that formation of the skeleton, will also impact on the formation of other systems, and vice versa. Recently Škrabar et al. (2018) used mice from hybrid zone of *M. m. musculus* and *M. m. domesticus* to map genetic association with limb bone length and covariation with integrated bone elements. Inbred and outbred stocks of different mice populations were used to compare between these covariation patterns. Limb bone length was confirmed to be highly polygenic, while covariation between lengths of correlating elements was shown to be influenced by genetic interactions. The study provides fundamentals for further analyses in different strains, and possibly different skeletal traits.

1.5. Measurement and estimating error

The delicate skeleton of mouse and other rodents and small mammals, such as shrews can be difficult to phenotype in the most informative way. Precision and accuracy are two valuable determinants when obtaining morphometric data. Precision is explained as self-similarity among repeated measurement to its true value, while accuracy (validity) means closeness of measurement to actual value (Stallings and Gillmore, 1971). The anatomy of long bones is reasonably complicated, because aside from articulation with other bones, their surface also provides structures where muscles and other elements have to be attached (Bab et al., 2007).

The lifestyle of the species often depicts more detailed anatomical properties of various skeletal structures, which in turn is a valuable knowledge to model paleoecological characteristics of extinct vertebrates. It is important to realize that length, regardless of measurement method is just one of the quantitative properties of a long bone. Keeping that in mind, repeatability of the method is of greater consideration than its accuracy. In previous studies authors have used x-ray pictures, micro tomography scanner (μ CT) or callipers (Perez et al., 2017) to phenotype skeletal elements, such as limb bones or skulls. Skrabar et al. (2017) have evaluated the precision of bone length measurements based on μ CT Scans, while no such evaluation for x-ray-based measurements has been found in recent literature. However, it is reasonably quick and easy way to obtain the measurements. The time range of x-ray exposure can be easily controlled, and even as short as 3 seconds can provide a good quality picture. In comparison, the time of taking a μ CT scan can extend to even 30 minutes (ScanCO), depending on the size of animal and requires laborious mounting and dismounting of the anesthetized animal on the sample holder, in case of in vivo studies.

1.6. Aims of the thesis

This thesis is composed of the general introduction and two main chapters. In the first one, I explore concordance of different morphometric methods used in murine skeleton research as well as patterns of correlations between bone lengths in male and female Iranian mice.

In the second chapter I explore morphometrics and correlation patterns of bone lengths in a population of mice from 15th generation of advanced intercross (G15). The morphometric measurements are then used in subsequent QTL mapping, where I look for genes related to the bone lengths. Finally, by using another bone as a covariate, I provide five new models to explore genetic intervals involved in the divergence of two different skeletal elements of the front and hind limbs.

1. To compare the analyses of skeletal morphometric properties in mouse populations with the use of different imaging methods.
2. To describe patterns of lengths and morphological correlation between distinct bones of the limbs in male and female house mouse.
3. To pinpoint key genomic regions contributing to the length of bones of fore- and hind limb in the experimental population of the house mouse.
4. To suggest genetic causes for morphological correlations between bones of the limbs.

Chapter I

Limb bone morphometrics in Iranian mice

2. Abstract

In this chapter *ex-vivo* morphometric methods of limb bone morphometrics are presented using 36 mice from an Iranian population. Additionally, correlation of the limb bone length and variance of limb lengths and proportions is evaluated in males and females of Iranian mice (called AH mice). The results show that *ex-vivo* methods – using x-ray and μ CT are both highly useful in phenotyping the mouse skeleton. The correlation analyses show different patterns in males and females bone integration, which might reflect variable backgrounds, such as differences in underlying genetics or endocrine regulation.

2.1. Introduction

The suitability of morphometric and imaging method used to quantify variation of skeletal morphology depends strongly on the research question and the setup of the experiment. Mouse limb bones are anatomically complex structures, involved in more functions than just locomotion, therefore, various properties can be quantified, such as their length, mid-shaft diameter or shape (Cretekos et al., 2008; Tommasini et al., 2009). Direct methods of taking the measurements include the usage of callipers or a microscope, but given the small size of mouse bones, they require careful handling and preparation, for example removing the skin and muscle tissue. In case of the embryonic stages or juvenile animals, staining of the tissue with is usually performed to determine properties of ossified skeleton and surrounding cartilage (Ovchinnikov, 2009).

The non-invasive visualisation of murine skeleton, which utilises the x-rays can be advantageous in observation of skeletal diseases progression, such as bone fractures, arthritis or tumors (Perilli et al., 2015). Taking an x-ray picture requires only very short time of the exposition, shortening time necessary for immobilizing the animal. The quality of picture can be maintained by manipulation of exposure time, intensity and kilovoltage of the machine (Butterfield et al., 2019). The downside of using the two-dimensional pictures is the parallax error, which can cause the structure to appear shorter than it really is (Shikhaliev and Tartoni, 2019; Mullin and Taylor, 2002). This is not a problem in case of 3-dimensional visualisation, such as achieved through the μ CT scanner. Similar to human medical purpose tomographic examination, the μ CT provides three-dimensional view of the specimen or selected part, and takes many separate x-ray pictures from x, y, z plane. A volume model is then reconstructed from the obtained picture stacks. Micro-tomography can be used for the *in-vivo* and *ex-vivo* examination (Cantley et al., 2009). In case of *in-vivo*, some machines have the possibility to install inhalant anaesthesia equipment, such as that of isoflurane, widely used in rodents. Live specimen needs to be then restrained to take an x-ray picture by application of anaesthetic (Gargiulo et al., 2012). But as a matter of fact, difficulty in phenotyping can be associated with various situation, and one of them is when museum specimens are used and damage to the material has occurred (Claude J, 2008).

Correlation and degree of variance of bone lengths is affected by many genetic and non-genetic factors (Atchley and Hall, 1991). These patterns are known to vary between species and populations (Gough-Palmer et al., 2008; Škrabar, 2018). The proportion of radius to other bones is rarely inspected in the murine model, and only the ulna is used (Pavlicev et al., 2013; Parmenter et al., 2016). Although they belong to the same zeugopod part, their diversification occurs through the vertebrate lineage, for example the radius becomes the main weight bearing bone of the front limb in artiodactyls (Christiansen, 1999). The scapula is also an interesting bone because of its varied embryological origin, and functional similarity to femur in the cursorial movement of murine rodents. Therefore, it was additionally inspected in the x-ray pictures and tomography scans. Because of large measurement error (ME) reported before for small autopod bones (Škrabar, 2018), they were not included in this or the next chapter.

The aim here was to evaluate properties of mouse limb bones in the *ex-vivo* measurements, compare results from two different imaging methods, and investigate morphological integration of limb bone lengths in males and females AH mice.

2.2. Methods

2.2.1. Mouse population

A subset of Iranian mice (AH) consisting of 18 females and 18 males was used to examine morphometric properties of long bones and the scapula of shoulder girdle. The animals were descendants from outbred colonies kept at the MPI for Evolutionary Biology (Veterinary License permit from the Veterinäramt Kreis Plön: 1401-144/PLÖ-004697). Parental specimens, which were progenitors of this colony, were collected in Iran, Ahvaz. Two lines were present, called “AH” and “AHE”, which were bred in separate buildings, but the same cage types (See the supplement Tab.S2.1.).

Prior to the experiment, all mice cages were moved to the Mouse House building at the MPI. All of the 36 selected animals were fully grown adults (over 200 days), to avoid age covariation on the bone elements. The mice were bred together in standard cages, up to 5 specimens per

cage, and had unlimited access to food and water, thorough their lives. The mice were weighed at the time of the sacrifice. They were reduced by CO₂ asphyxiation prior to the imaging procedure.

2.2.2. X-ray cabinet procedure

After the individual mouse was reduced, its body was used to take the *ex-vivo* x-ray picture. The Faxitron X-Ray Cabinet (Fig. 2.1.A) was beforehand calibrated and ready to take new picture and the time of x-ray exposure was set to the 5 seconds (Fig. 2.1. B). One picture of the front and one of the hind body parts were taken, which were then saved to individual folder as a DICOM file. At the same time, the mice which had already undergone the x-ray picture were prepared for μ CT scanning (see the next section).

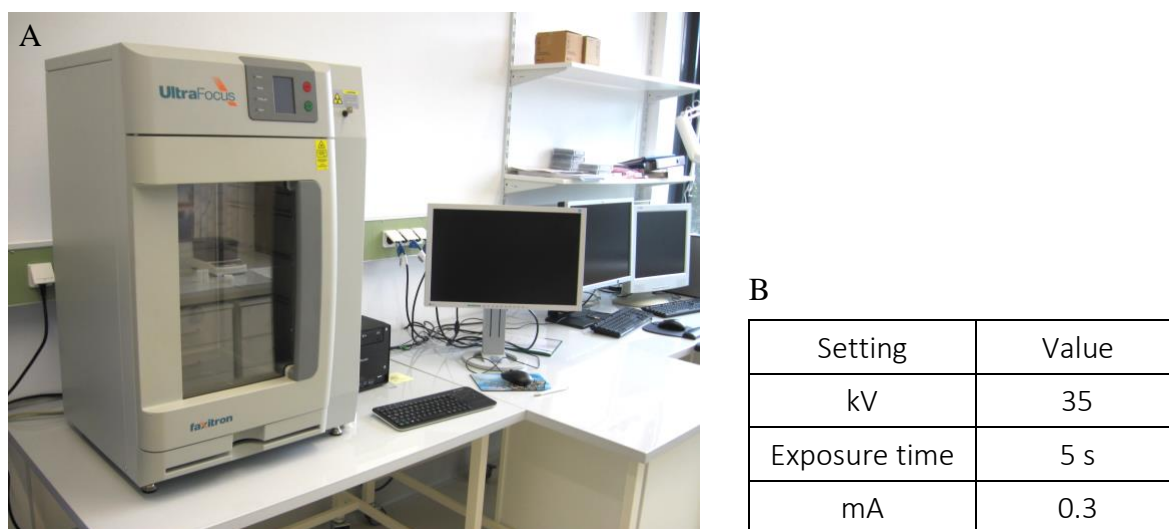


Figure 2.1. The Faxitron x-ray machine used in the experiment (A), and the settings of the machine used in this study (B)

To get good quality pictures of bones of interest (humerus, radius, ulna, scapula, femur, tibia), the mouse was placed flat on their dorsal side on a plastic tray. The limbs were positioned as presented on the Fig.2.2., with their front (A) and hind limbs (B) in midway flexion. Described in detail in the method section of Chapter III in this thesis.



Figure 2.2. Examples roentgen pictures of front (A) and hind (B) part of the AH mouse

2.2.3. μ CT scanning

In the next step, the ScanCo μ CT device was used to obtain 3-dimensional scan of each animal. After the x-ray picture was taken in the Faxitron cabinet, each mouse body was placed on the μ CT-purpose holder with a foam bedding designed for small rodents (Fig. 2.3. A). The front and hind limbs were additionally fixed to the bedding with a plastic tape. The machine was previously automatically calibrated. When the scanner was ready to use, the hood was opened, and the holder with specimen was placed inside. The process of scanning was manipulated through the computer. Given the large body size of Iranian mice, especially males, the tomography scan was divided in two batch scans, for the front and hind part of the body. Each took around 15-20 minutes, taking together approximately 35 minutes per mouse. The most important settings programmed for every specimen are summarized in the Fig. 2.3.B.

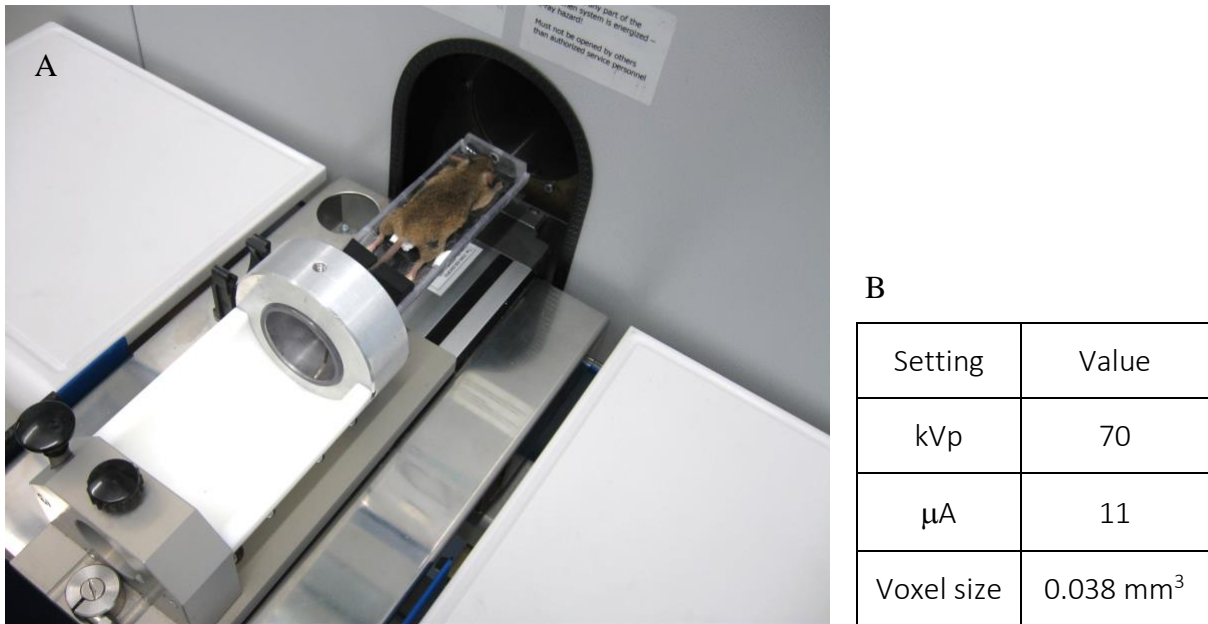


Figure 2.3. Inserting a mouse body into the ScanCo micro-tomograph (A); parameters of the scanner in AH mice (B).

After the mice were scanned, the bodies were packed in separate plastic bag with the ID of the mouse and preserved in a freezer at -20°C .

The resulting raw image sequence was obtained after the scanning. The raw image set was cropped to remove any unnecessary visible background (such as the holder), and converted to the DICOM image sequence. The scans were stored in the server for further measurements.

2.2.4. Measurements

Bones of stylopod: humerus (front limb) and femur (hind limb) and three bones representing the zeugopod part (radius, ulna and tibia respectively) were chosen for morphometric analyses. In all cases, bones of the right side were used. Additionally, scapula was measured in x-ray method and in the uCT scans. The exact landmarks are specified below (Tab. 2.1):

Table 2.1. List of landmark anatomical positions in each measured bone

Bone	Anterior landmark	Posterior landmark
Humerus	head of humerus	capitulum
Radius	head of radius	distal growth plate
Ulna	olecranon	distal growth plate
Scapula	coracoid process	caudal inferior angle
Femur	Tip of greater trochanter/head of femur (D)	Medial condyle
Tibia	head of tibia	lateral malleolus

D - landmark used for measurement from the x-ray cabinet-based dorsal view;

Fiji (Schindelin et al., 2012) was used to obtain measurements from the x-ray cabinet pictures. The pictures in the DICOM format were imported in the software, one at a time, and the landmarks were placed using point tool at two ends of each measured bone. The coordinates of each point were saved in the Excel spreadsheet, with ready formula, accounting for the two-dimensional plane and magnification of the x-ray cabinet (the details on the method are provided in the chapter III).

To obtain measurements from the tomography scans, the landmarking tool, TINA (Schunke et al., 2012) was used. The DICOM stacks for a half body scan were uploaded in the platform, and the landmarks were placed on two ends of each measured bone (see Tab. 2.1.). The results were saved as TPS file, and lengths were obtained in the Excel spreadsheet. To do that, the formula accounting for position of the two landmarks in each plane (X-Y-Z) was applied:

$$L = \left(\sqrt{(X_2 - X_1)^2 + (Y_2 - Y_1)^2 + (Z_2 - Z_1)^2} \right) \times 0.038$$

where 0.038 is the voxel size.

2.2.5. Statistical analyses

All statistical analyses were performed in R Studio and MS Excel. Base R function were used to calculate basic statistics, such as variance and standard variation. To make correlation plots, *corrplot* (Wei, 2021) package was used. Weight residuals were obtained from a linear model for entire dataset, and saved as a new data frame. The principal component analysis (PCA) plots for the cumulated male and female specimens, as well as separate sexes were constructed using R package *ggbiplot* (Vu, 2011). Due to small sample sizes, and different degree of weight effect on males and females, the residuals were not used for the sex-specific PCA. In both cases, scale and center arguments were used to account for different variance of bone lengths. Additionally, Kendall-*tau* was also calculated to test for correlation between each bone/sex and weight of the animals.

2.3. Results

2.3.1. Comparison of the measurements

The measurement error of the x-ray-cabinet-based method is evaluated in the Chapter II. Importantly, the G15 mice, which were used in the next chapter were more difficult to position in the x-ray because of the condition of G15 specimens, which was not the case with the AH mice. It can be therefore expected, that the x-ray-based measurements in Iranian mice were more precise. The methods of measurements based on the micro tomography scans followed that of Skrabar (2018), where the measurement error was evaluated.

It is important to point out that the landmarking methods were adjusted individually to be reproducible in each method, and therefore, the lengths of bones differed between them, which is summarised in the Table 2.2. Particularly, the tibia bone appears to be shorter in μ CT-based measurements than in the x-ray based. The standard deviation of the bone measurements was similar between methods in the AH mice, with scapula being reasonably higher in the x-ray-based measurements, while it was lower in case of the humerus with this method.

Table 2.2. Basic statistic of ex-vivo morphometric measurements; var – variance, sd – standard deviation.

Method	bone	min	mean	median	max	var	sd
x-ray measurements	Humerus	11.180	12.583	12.700	14.050	0.331	0.575
	Radius	10.910	12.101	12.135	13.050	0.245	0.495
	Ulna	13.560	14.779	14.800	16.220	0.318	0.564
	Scapula	11.260	13.053	13.200	14.330	0.634	0.796
	Femur	15.000	16.322	16.360	18.170	0.547	0.740
	Tibia	18.550	20.576	20.600	22.280	0.787	0.887
μ CT measurements	Humerus	11.030	12.349	12.505	13.830	0.442	0.665
	Radius	10.730	11.729	11.700	12.820	0.235	0.485
	Ulna	13.300	14.398	14.445	15.650	0.302	0.550
	Scapula	11.360	12.629	12.660	13.940	0.483	0.695
	Femur	15.240	16.548	16.575	18.320	0.575	0.758
	Tibia	17.820	19.790	19.900	21.170	0.677	0.823

Differences were observed in the correlation strengths between individual bones in the two methods (Fig. 2.4.). In the x-ray-based measurements, the Pearson's r was usually lower than in the μ CT based measurements. This is most evident for the humerus.

The overall patterns of strong correlation within the forelimb zeugopod are observed in both methods. The strength of correlation of these two bones and tibia are also roughly similar between the methods. Interestingly, in the dorsal measurements the scapula shows higher correlation with radius and ulna than with humerus, which is not the case in μ CT measurements, but both has equally strong correlation with tibia. Both methods show that the shoulder blade bone is more correlated with femur than humerus, even though strength of the correlation is lower in the x-ray-based results.

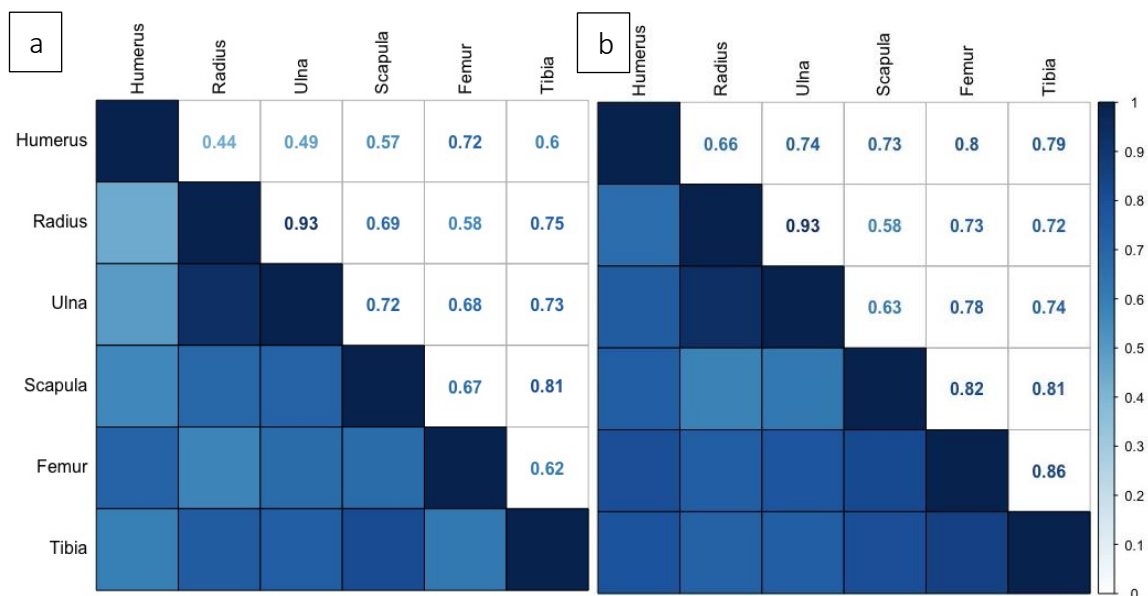


Figure 2.4. Heatmaps of Pearson's correlation of bones measurements in x-ray-based (a) and μ CT-based (b) measurements

To further explore the morphometric properties of the AH mice skeleton, μ CT based measurements were used. The differences between males and females were explored, and the weight of the mice was used as a covariate.

2.3.2. Morphometric properties and female – male difference in AH mice

All measured bones are significantly longer in males than in females (Fig. 2.5, Tab. 2.3). The distribution of the measurement was not normal, especially in male mice, for example in case of tibia (Fig. 2.5., Tab. S.2.2). Outliers were detected in both sexes, in humerus, but also in male scapula and ulna and in the female tibia. Given the small sample size, they were not excluded from the further analyses. Male mice were also heavier than females, and included specimen as large as 50g (Tab. 2.3, Tab S2.1).

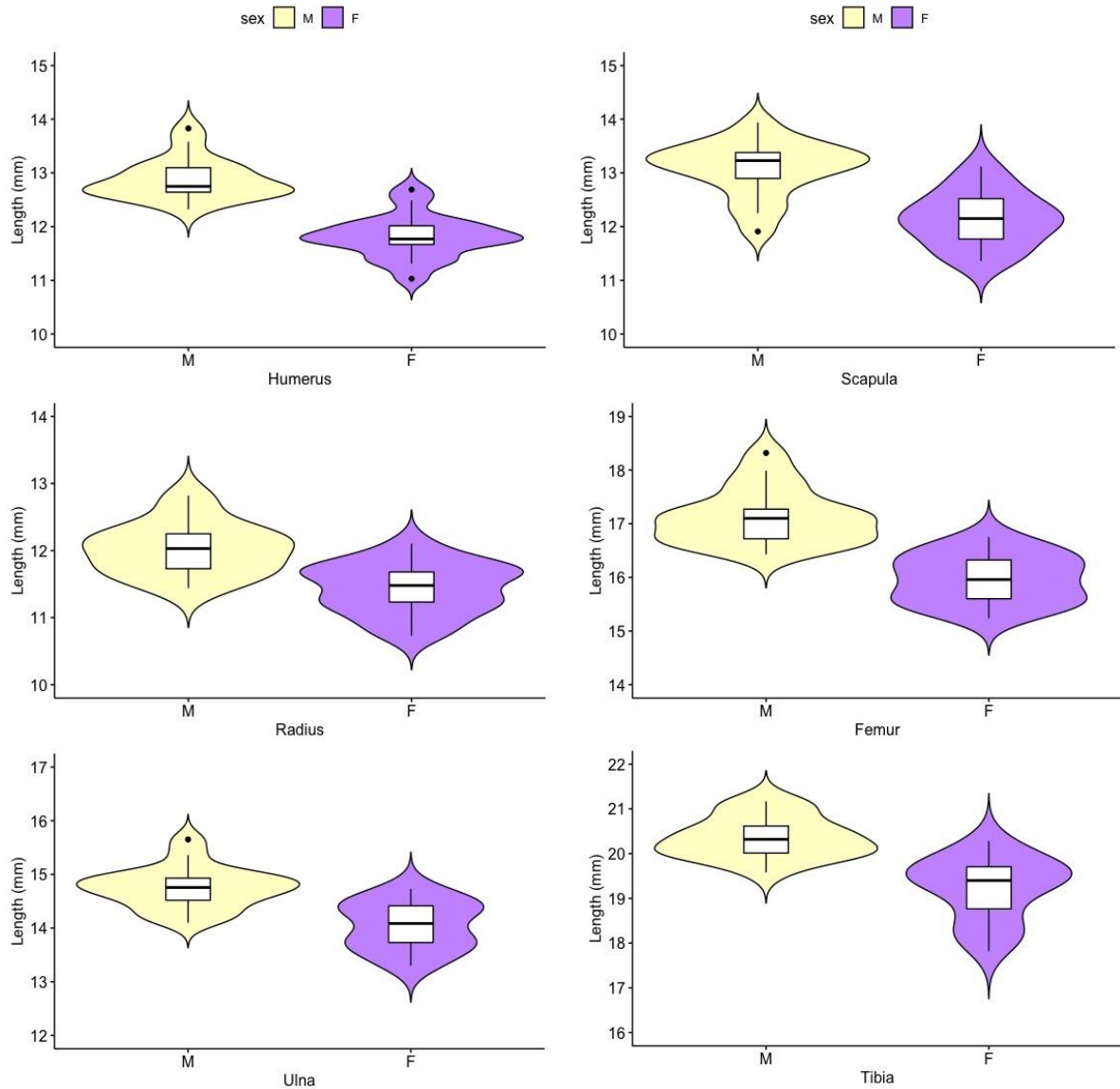


Figure 2.5. Violin plots representing male (M) and female (F) distribution of each bone length in the AH mice; the boxplots represent the median values and the black dots represent outlier values;

Table 2.3. Length properties (the values are given in millimeters) of each measured bone in females and males and the statistical test (Wilcoxon test) of the bone length and weight difference in males and females; min – the minimum value, max – the maximum value.

Bone	Females				Males				Wilcoxon Test	
	min	mean	median	max	min	mean	median	max	W	p
Humerus	11.03	11.82	11.77	12.69	12.32	12.88	12.75	13.83	8.5	<0.0001
Radius	10.73	11.43	11.48	12.1	11.44	12.03	12.03	12.82	44.0	0.0002
Ulna	13.3	14.04	14.09	14.73	14.1	14.75	14.76	15.65	37.5	<0.0001
Scapula	11.36	12.14	12.15	13.12	11.91	13.09	13.23	13.94	29.0	<0.0001
Femur	15.24	15.97	15.96	16.75	16.43	17.13	17.1	18.32	9.0	<0.0001
Tibia	17.82	19.22	19.4	20.28	19.58	20.36	20.32	21.17	19.0	<0.0001
Mean Weight (g)	24.19				33.25				34.0	<0.0001

Weight is a significant covariate, affecting bone lengths when both sexes are considered as a single dataset, which might be a reflection of better distribution of data, and because females are smaller and have on average shorter bones than males (Fig. 2.6, Tab. 2.4). In females (Tab.2.4) a significant correlation with weight was observed in humerus, scapula, and also both hind limb bones. In males however, only scapula was correlated with weight, radius and ulna do not correlate with weight either in males or females. In cumulated dataset, the radius has the lowest correlation with weight among other bones. The relationship of this covariate is only to small degree represented by the linear models, particularly in case of scapula in females (Fig 2.8, Fig 2.9)

Table 2.4. Kendall's tau correlation between weight and bone length in cumulated samples, females and males. Non-significant values ($p > 0.05$) are marked with red color; n – number of specimens.

group	Humerus	Radius	Ulna	Scapula	Femur	Tibia	n
all	0.517106	0.315793	0.437551	0.574075	0.528991	0.457143	$n=36$
females	0.348692	-0.0329	0.170493	0.420667	0.424837	0.385621	$n=18$
males	0.084967	0.098039	0.209837	0.393445	0.118033	-0.05882	$n=18$

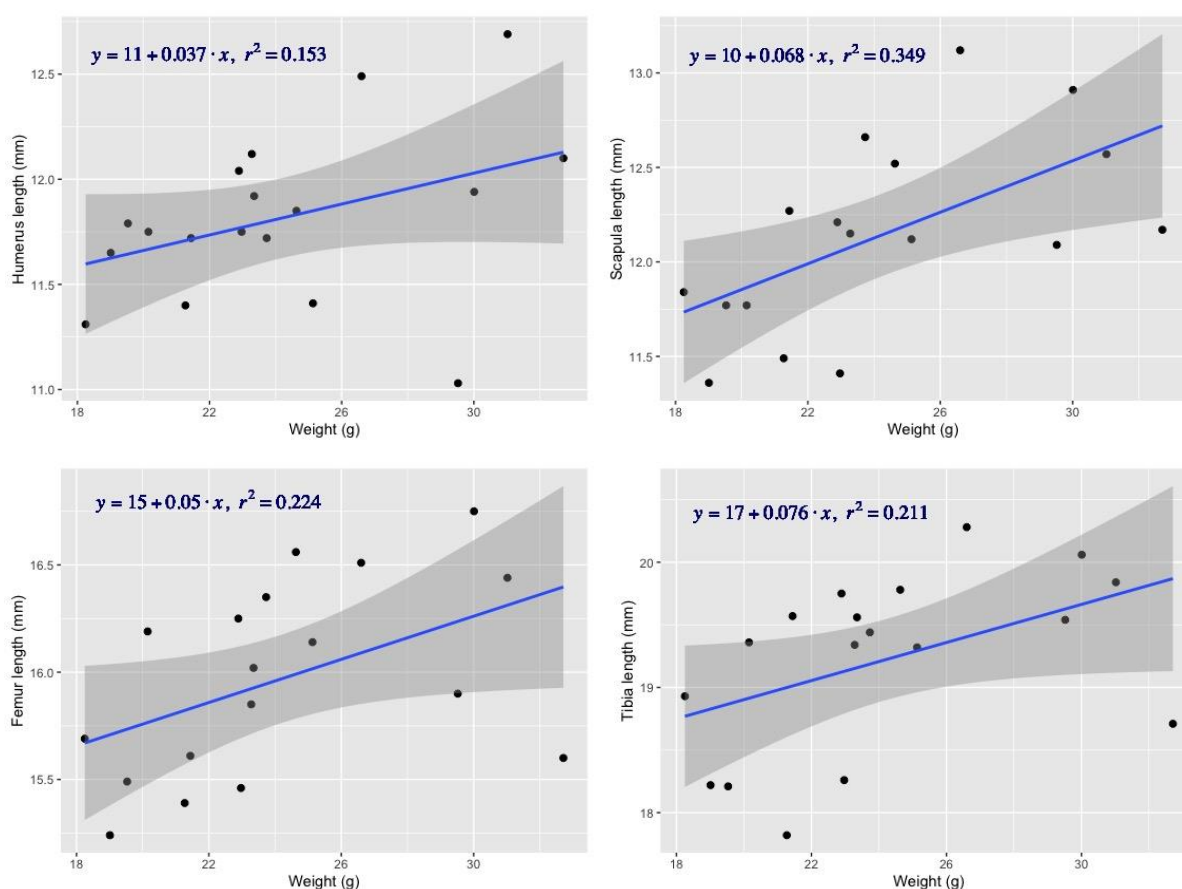


Figure 2.8. Relation of weight and bone length in female AH mice; humerus: F-statistics = 2.90, DF = 16, p-value > 0.05 (not significant); scapula: F-statistic = 8.06, DF = 15, $p < 0.05$; femur: F-statistics = 4.62, DF = 16, p-value < 0.05; tibia: F-statistics = 4.27, DF = 16, p-value = 0.05.

The Kendall rank correlation between male scapula and weight was significant, however not strong. As could be expected, it is not supported by the linear model (Tab. 2.7, Fig. 2.9). Since there were also very large male mice in the dataset (two males of around 50g), these could have caused error. However, there was no difference in the correlation significance of the correlation, after removing the large males from dataset (data not shown).

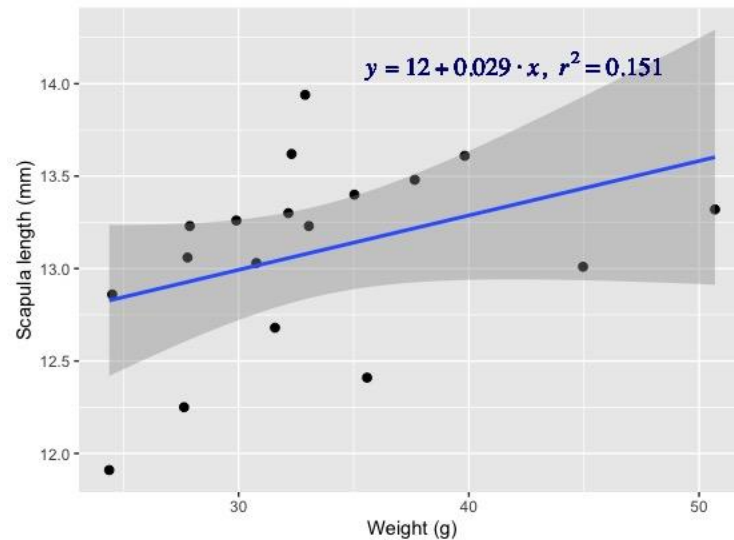


Figure 2.9. Male scapula correlation with the weight of animals; F-statistic = 2.85, DF = 16, $p > 0.05$ (not significant);

The patterns of correlation between bone lengths differ strongly between male and female mice, and in both sexes change slightly after removing the effect of weight of the animals (Fig. 2.10). One of the most evident differences between sexes is a very strong correlation of tibia and humerus in males, which is only moderately strong in females. In females, bones of the hind limb, femur and tibia are correlated much stronger than in males. These two patterns appear to be unaffected by weight. Stronger correlation of forelimb bones in males is also observed, although it does not include the scapula. In females, the shoulder blade bone appears to be more evidently correlated with tibia, as well as femur, which might be linked to the relation of these bones with weight, absent or weak in males.

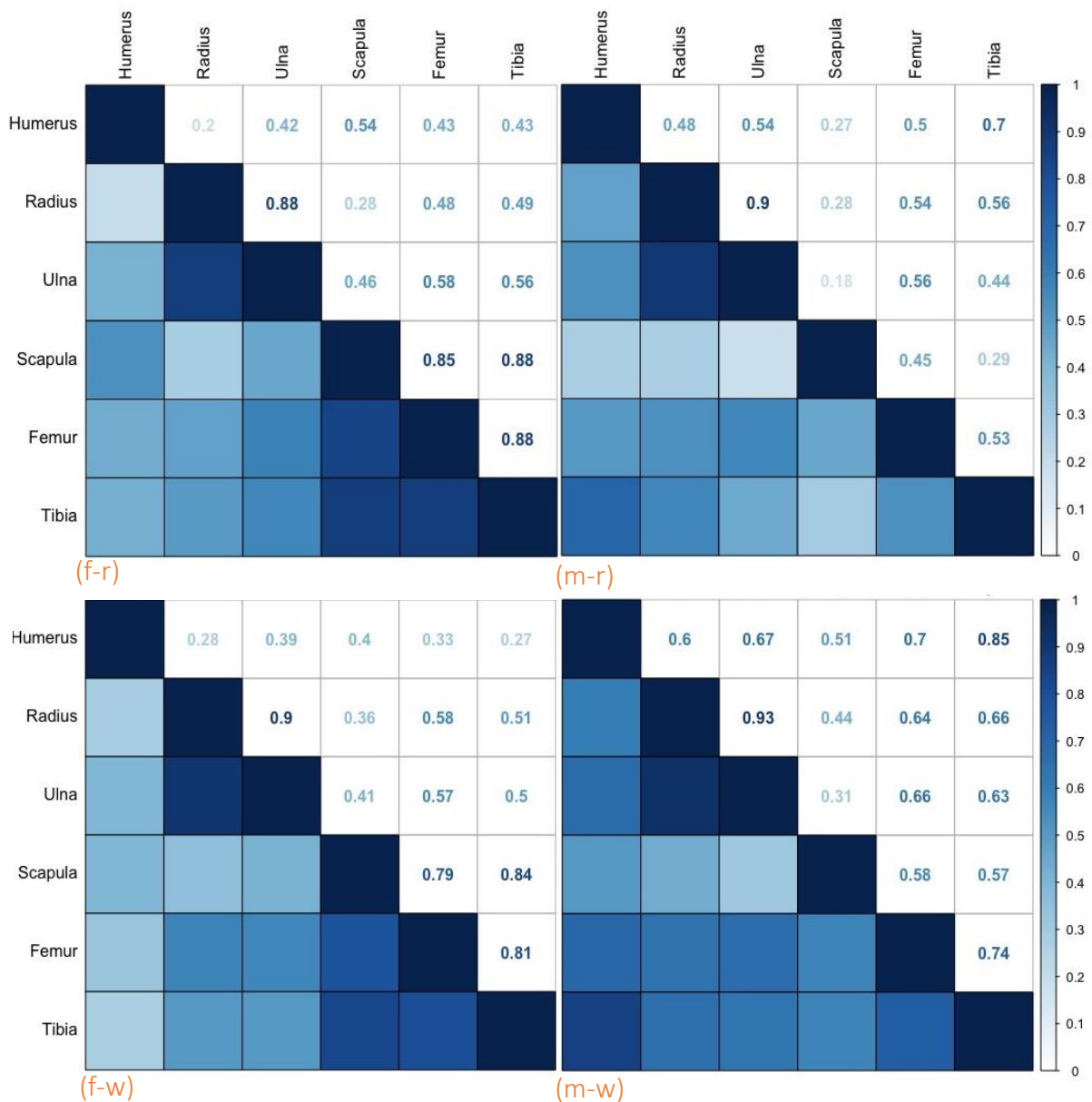


Figure 2.10. Correlation between bones in μ CT-based measurement for raw female (f-r) and male (m-r) data, and for weight residual dataset (female: f-w, males: m-w).

To explain how individual bones contribute to the total variance of skeletal morphometrics in AH mice, a PCA analysis, using weight residuals was performed. One specimen, with missing scapula measurement was removed from dataset (female with ID: 71202). After regressing the data over weight covariate, the PCA shows that there is a separation between males and females based on bone length variance (Fig.2.11, Tab.S2.3).

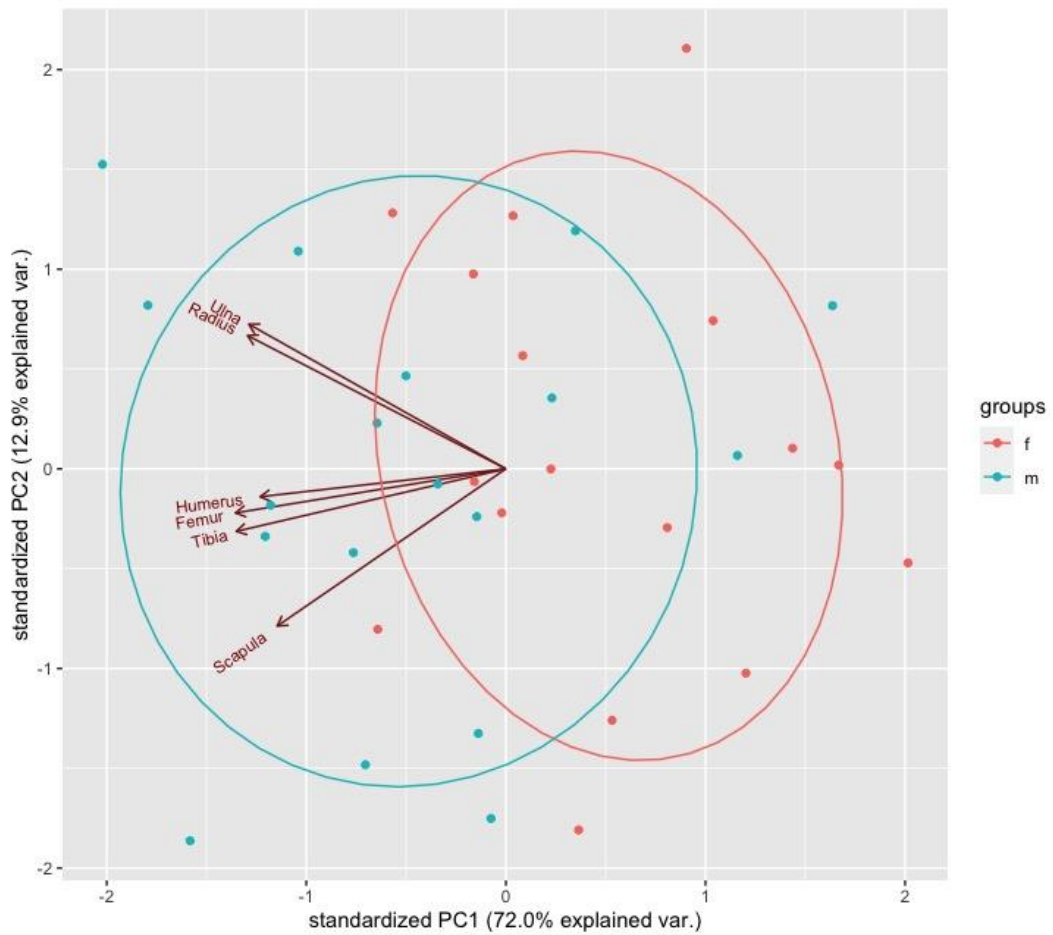


Figure 2.11. Residual weight measurements of AH mice show division between male and female. The ulna and radius show a similar direction of variance.

The PC1 and PC2 explain together 83 and 74 percent of variance in females and males respectively (Fig 2.12, Tab.S2.3). In males, scapula has a stronger negative effect in the second PC, and the loading shows it is separated from other traits. In females, the ulna and radius have negative effects in the PC2. The opposite is in the cumulated dataset regressed on weight, which could reflect these bones as more independent of this covariate (while scapula reflects it the most).

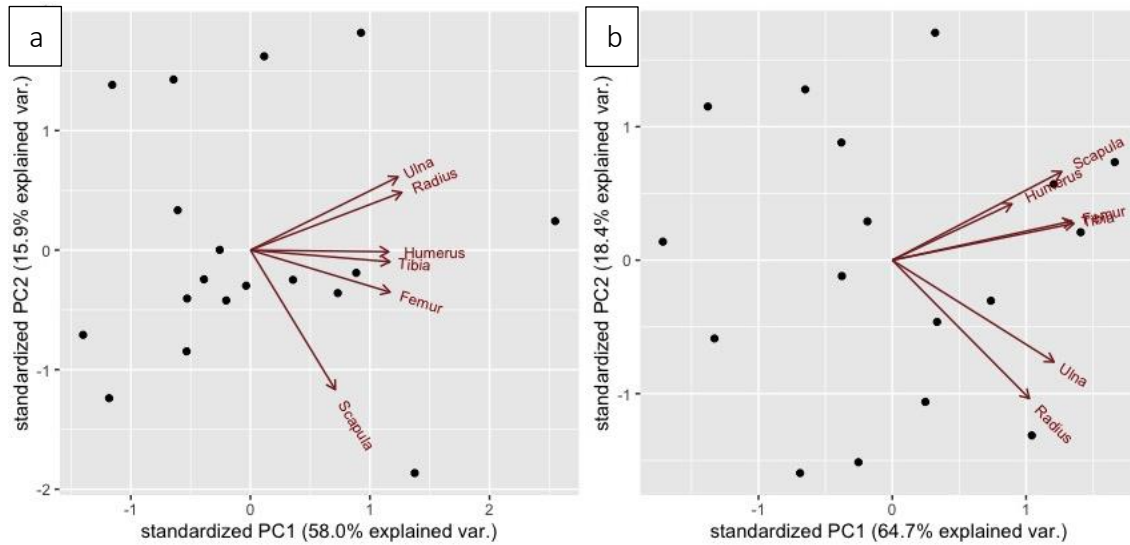


Figure 2.12. PCA showing loadings of each trait in males (a) and females (b) AH mice

2.4. Discussion

In this chapter I show that two measurement methods, which are based on different imaging methods are useful to quantify lengths of animal bones, although x-ray-based measurements can be more prone to the measurement error caused by positioning of the animals. Fast methods of quantifying rodent skeleton are indispensable, for example to measure the seasonal changes of skull size in shrews, which were also studied through the x-ray cabinet (Lázaro et al., 2021). Live imaging of bones is also a basic part of medical and veterinary examination, and parallax error can be the factor which obscures performed assessment (The et al., 2006). It is also naturally bound to other bioimaging techniques, for example microscopy. While museum specimens can be studied with more precision, there can also exist measurement error due to quality of the samples. For example, preservation method and possible decay of specimens could create higher level error (Claude J, 2008).

Results obtained from the x-ray measurements, could reflect similar patterns of limb bone correlations to the μ CT results, although the humerus is possibly bound to higher levels of morphometric error (see Chapter III). Together with bone length, muscle length might also be grasped within this method. However, x-ray limb measurements were nevertheless used with good results in genetic mapping (Parmenter et al., 2016). Tomography scans were previously

intensively used in *ex vivo* measurements, including for very delicate analyses such as fluctuating asymmetry. Such measurements can also be used in genome wide mapping studies (Pallares et al., 2015). Another way is to use callipers, or an optical microscopy on prepared bones for example with staining agents. The advantage of it is the possibility of visualisation of cartilage tissues, such as in developing limbs or joints (Pan et al., 2012). Commonly dermestid beetles are used to obtain the animal bones.

The analyses have shown interesting patterns of correlation between the measured bones in males and females. Here, longer limb bones of males might partly reflect their larger body size compared to the females. The correlation between skeletal size and weight differs between each bone and sex of the animals. In mammals, it is known that bone size as well as bone mass scale allometrically with body weight. It is observed in populations and between species, although regression of proportions of limb bones in larger mammals is less fit, as they are shorter in length than could be expected, while animals below 50kg show positive allometry with weight (Christiansen, 2002). Appendicular bone parameters can also be used to predict body mass (Christiansen and Fariña, 2004).

Dimorphism of bone lengths proportions are observed across species, including human. One of the interesting examples, is digit proportions, where males (on average) have shorter fourth but longer second finger, while in females these digits have similar length (Zheng and Cohn, 2011). This is also observed in hind leg digits in mice (Bailey et al., 2005). The observed dimorphism is thought to have its source in prenatal hormonal exposure (Manning et al., 2003). Thyroid hormones are important contributors in the adult bone formation. They are essential for the endochondral processes (Bassett and Williams, 2016) and are also associated with higher digit ratio in women (Pruszkowska-Przybylska et al., 2021). Otherwise, oestrogens play important roles in homeostasis of bones in both sexes (Noirrit-Esclassan et al., 2021).

The analyses of the skeleton of Iranian mice show distinct patterns of correlation, particularly between the humerus and scapula. Strong differences are not observed in this ratio of most pairs of traits, but it exists within the forelimb, where males have a higher ratio between the ulna and humerus (Fig.2.13). Interestingly, the human finger ratio does not appear to be characterised by strong heritability (Kalichman et al., 2019). Here, although a subgroup of the

AH mice were bred separately, I did not find it to be a factor in overall variance of limb bones (data not shown).

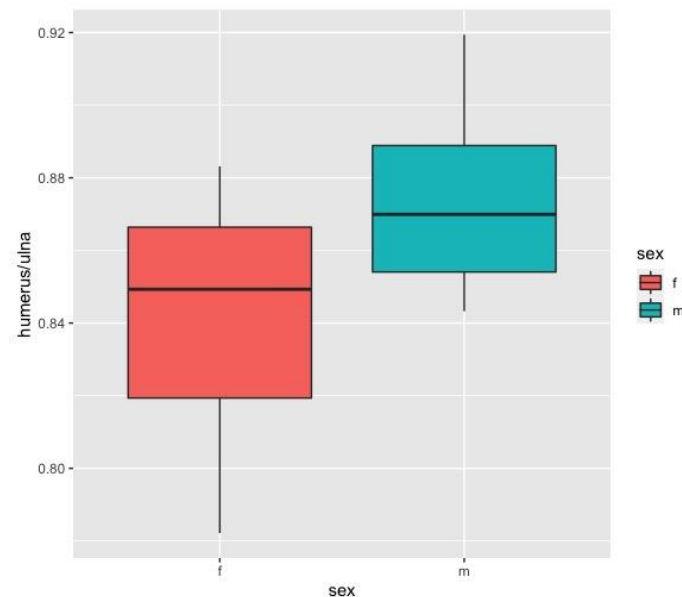


Figure 2.13. Front limb bone length proportions in males and females (Wilcoxon test: $W = 77$, p -value = 0.006402)

In many studies of murines, only the ulna of the forearm is investigated (Parmenter et al., 2016). Here, in my study, both bones have been used, and it can be observed that some slight changes between the correlation of these two bones appear, especially when the dataset is uncorrected for weight. The scapula, which was highly correlated with the weight, is an important contributor of locomotion in mammals, and therefore essential in investigating limb bone proportions (Lilje et al., 2003). Although simply using the length of this bone might not give a full picture of relationship between other bones, it appears that it already shows unique patterns in males and females. Similarly, long bones are also geometrically complex structures, which motivates for further more detailed investigation of shape. The bone length themselves are also diversified among mouse population, where outbreds were characterised with longer bones than inbred strains (Škrabar, 2018).

Previous research showed high correlations of bone length within the hind limb, which are lower for example between femur and ulna – bones which belong to developmentally different parts (Parmenter et al., 2016, Škrabar et al., 2018). These correlation patterns can vary, which is also true for male and female fluctuations. Skeletal proportions can be associated with timing

of growth plate aging. Although correlation or covariation was argued to be insufficient enough to represent the phenomena of morphological integration (Hallgrímsson et al., 2009), it is still used to represent the morphological integration, and here the results show important aspects of the skeletal proportion, dimorphism and patterns between less and more frequently investigated bones.

CHAPTER II

Bone length QTL mapping in an advanced intercross of the house mouse

3. Abstract

The house mouse is a perfect model system for genetic and evolutionary studies, with its skeletal elements being used to explore the concept of morphological integration. Morphological integration is the tendency for characters to covary as the result of common underlying genetic, developmental, and functional factors. In this study 264 mice from 15th generation of an Advanced Intercross Lineage (AIL) were used to map possible regions linked to bone length. The specimens were photographed in Faxitron X-Ray Cabinet, and the length of humerus, ulna, radius, femur, tibia as well as scapula was used for further analysis. Candidate genes identified in this setup include essential regulatory elements such as *Sox5* and *Bmp3*, but also genes with less recognized roles, such as *Cdh10*. By including another bone as a covariate to other traits, relationship QTLs affecting covariation between traits were detected. One identified region overlaps with previous findings, but many other genes were found to be spread across the entire genome. Genes, such as *Dnajb9* and *Rps6k3* present interesting new opportunities to study individuation of skeletal elements.

3.1. Introduction

QTL mapping has been performed in many animal and plant models, including wheat (Buerstmayr et al., 2009), tomatoes (Chaim et al., 2006), cattle (Grisart et al., 2002) and pigs (Ernst and Steibel, 2013), and is a powerful technique for linking genes to phenotype. Quantitative genetic mapping has been developed before the molecular markers enabled the direct observation of genotype-phenotype interactions (Botstein et al., 1980).

Currently, various types of markers and assemblies are used in murine model research, while SNP arrays provide reliable genotype information in known loci. According to Fisher's model (Orr, 1998), polygenic traits are shaped by multiple genes of very small effect - mutations in small effect genes are expected to be the primary contributor to evolution, because changes in sequence of a large effect loci are likely to be harmful and thus lost. However, these assumptions are being challenged (Waxman and Welch, 2005). Genes of large effect play the main role of orchestrating development, and formation of traits, while many small effect genes calibrate the final effect. On the other hand, mutations – especially duplications, of key development genes as the previously mentioned members of the Hox family, could produce drastic phenotype change, that sometimes lead to shaping new or repeated traits, such as in arboreal species of deer mice (Monteiro, 2021). Additionally chromosomal inversions were reported to affect evolution of pairs of traits (Hager et al., 2021).

On a genetic level, the variability of phenotype can be attributed to different allelic variants that may contribute to changed structure of a coded protein, as well as affect genetic interactions (through epistasis) (Sunyaev et al., 2001; Azevedo et al., 2006; Negrão et al., 2013) In the case of pleiotropy, it is recognised that QTLs affecting properties of bone can also affect susceptibility to disease, which makes it very important to narrow down existing intervals, and map those yet unknown (Jiao et al., 2007). Markers, extending to a whole genome together with suitable models can improve detection and narrowing down candidate genomic interval (Knott et al., 1996). Syntenic loci, which are physically situated within one chromosome can exist in a linkage, and be inherited together, the closer they are, the more likely this is to happen. Crossing over during meiosis is necessary to break this linkage, and create new

haplotypes, but the number of spots of this process are limited within pairs of chromosomes. Therefore, increasing the number of generations of the experimental cross creates more possibilities for crossing over, and provides better resolution of mapping. Backcrosses do not allow to use densely placed markers in QTL mapping, because of large chromosomal regions tend to be in linkage. Therefore, breeding models of multiple-lineage experimental populations, through multiple generations are now widely used to map various traits. As the main assumption of QTL analyses is that the frequency of the phenotype is random, accounting for the population structure is a necessary step in.

Haley-Knott regression is suitable for simple models such as half-sib populations. Complex family relationships require more heavy computations, which is increasingly possible. Therefore, linear mixed model is used, with a polygenic effect estimated under the null hypothesis of no (major) QTL, and then taken as fixed as known in the genome scan (Kang et al., 2008). Recent studies also implement the linear mixed model in GWAS. Additionally, sample size is an important contributor to the possibility of finding candidate genes with best precision. QTL mapping remains indispensable in the populations of controlled structure.

Although many studies have been conducted on the genetic basis of proportions in the rodent limbs, there is a lot of disassociations on the morphometric methods in use, as well as selected bones of interests, and the context of analyses. For example, genetic mapping often accounts for only one of the zeugopod bones. Scapula, a mobile part of the mammalian gait enabled their typical, parasagittal movement style, which forced functional diversification of other limb parts (Schmidt and Fischer, 2009). Although proportions of limbs are diverse among the amniotic metazoans, the segmentation pattern of limb anatomy is conserved among them, and modularity of the proximal elements is evident (Young, 2013). In mammals, events of reduction of autopod or zeugopod bones happened multiple times in many species independently, which has functional aspects to it. While autopod, particularly the digit elements, are widely studied in this context (Galis et al., 2001; Wagner, 2005; Cooper et al., 2014), there are not many genetic studies on what controls the diversification of bones in the fore arm or hind limb shanks – and within them. Two bones per zeugopod is largely conserved in animals. For example, the two bones: radius and ulna are present in Acanthostega fin, wing of bird and a fin of a killer whale. In the mouse skeleton, radius and ulna are well-developed, but the fibula is merged with the tibia (Bab et al., 2007). In larger mammals, radius, as a

proximal part of the limb, bears most of the weight, while the ulna is reduced. Therefore, the tibia has a functional similarity to the radius. The space between the radius and the ulna is maintained by the interosseous membrane, which is essential for the stability of forearm (McGinley and Kozin, 2001). Diversity of limb musculature or articulation can also reflect the mechanical capabilities of the animal (García-Esponda et al., 2021).

The observed phenotype is dependent not only on the allele, but also covariates, such as weight, sex, or the environment, which regulate the development of the trait. The phenotypic relationship between traits can be reflected in genetic mapping, through rQTL mapping. Relationship QTL (rQTL) had been used on many traits in the murine model, such as long bone lengths, but also properties of teeth (Navarro and Murat Maga, 2018) or mandible. Furtherly, genetic interaction between rQTLs are the sources of genetic variation affecting trait relationships (Pavlicev et al., 2013). Mapping of relationship QTL between two skeletal traits have been performed on two-strain crosses of mice populations. In earlier attempts they lacked a dense map to narrow down eventual candidate intervals. On the other hand, natural populations might not provide results relevant from functional, macroevolutionary perspectives, because they will mostly reflect variants segregating in a specific ecological system. Additionally, in G15 mice, the genetic background of a relationship between two traits have been successfully explored in terms of microbial composition (Belheouane et al., 2017).

Here, I extend this method to the six bones of front and hind limb: humerus, radius, ulna, scapula, femur and tibia on the G15 mice. As the information of genomic structure of the house mouse is widely available, it is of great importance to expand understanding of function of each gene, and contributions to phenotypes, especially in the light of their evolutionary inputs. Importantly, one of the main purposes of genetic studies is to understand function of the specific genes and how they contribute to phenotypes. The genome of the house mouse, which consists of over 24 thousand protein coding genes situated on 19 autosomes and the sex chromosomes is a perfect model to pinpoint novel loci relevant for limb bones morphology, disease susceptibility and evolutionary perspectives.

3.2. Methods

3.2.1. Population G15

The fifteenth generation of Advanced Intercross Lineage mice (further called G15, Fig.3.1.) of four different strains, were bred for an unrelated microbiome study (Belheouane et al., 2017). Genomes of the animals involved in this study were sequenced with MegaMuga Illumina Array which provides over 77,000 informative SNPs. The detailed procedure was specified in the above mentioned study and Srinivas 2013 (Srinivas et al., 2013).

After the samples for genotyping were taken, the bodies (with their internal organs removed) of G15 mice were stored in -20°C freezer, each of them was wrapped in individual plastic bag with an ID sheet attached.

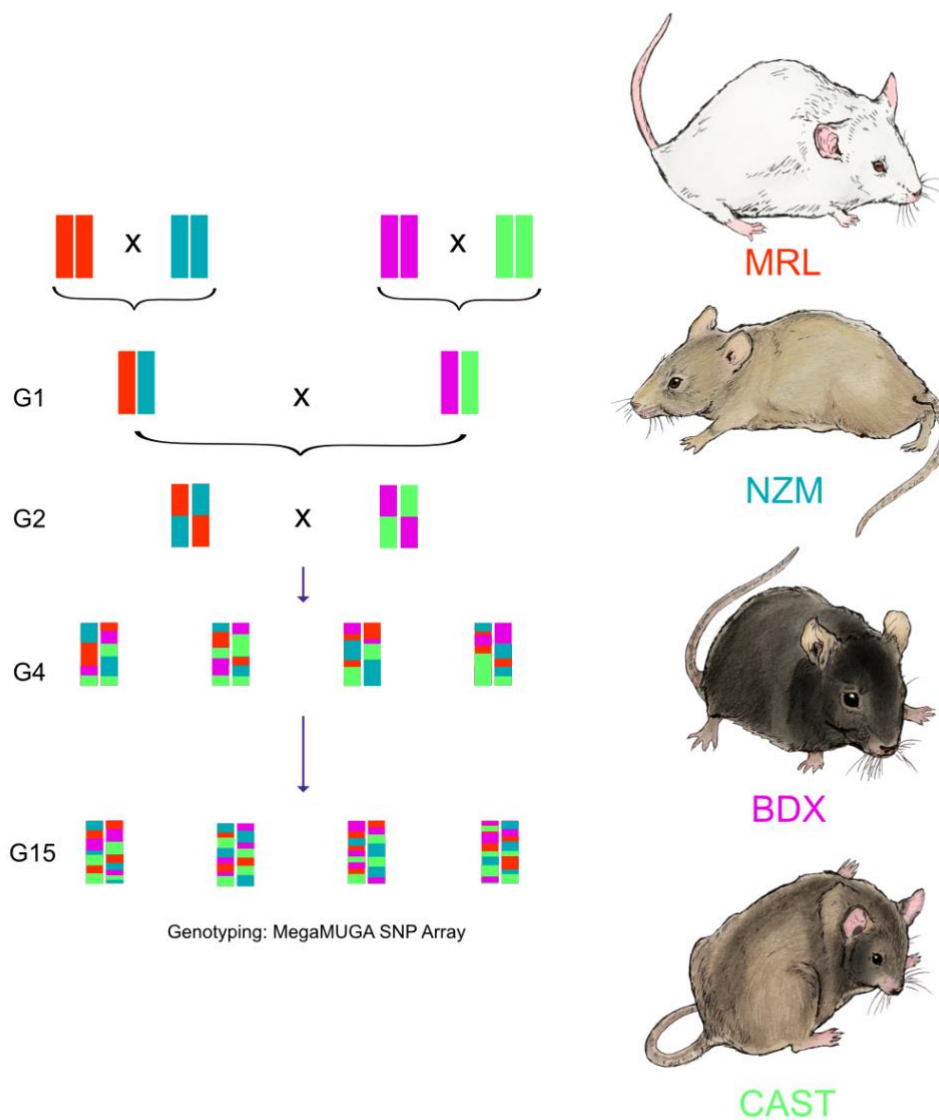


Figure 3.1. Schematic figure of the G15 mice breeding; the three parental lines are laboratory inbred mice of *M. m. domesticus* origin, which were crossed for 15 generations together with the wild-type mice *M. m. castaneus*;

3.2.2. Imaging and measurements

The bodies were intended for morphometrics analyses of skeletal elements. For this purpose, each mouse was radiographed in the x-ray cabinet (Faxitron), and digital photos were taken. As a first step, mice were removed from the freezer and placed in a fridge (at +4°C) overnight to thaw. The next day ice-free specimens were x-rayed. This procedure made it possible to increase flexibility of joints and muscles and to have more control on the positioning of the limbs. Just before positioning, the animals were taken out of the individual plastic bag, and one

mouse was photographed at a time. A body was put flat on a plastic tray on its ventral side, with the elbow and knee joints flexed in a mid-way, and secured with a plastic tape, to restrict limb movement. Bones of interest, which were included in the study: humerus, radius, ulna and scapula of front limb, and femur and tibia of the hind limb. Bones of limbs of right side were used, but in some specimens, due to damage or problems with positioning of the body, the left side was substituted. In some cases, the limbs were also very little flexible, and the muscles were contracting, which could have effect on eventual position and visibility of desired landmarks.

Two separate pictures in double magnification were taken of each mouse – one of the front, and one of the hind limbs. Because of the rather large size of the animals, this procedure allowed a full, clear view of bones that were considered in this research to be obtained. In comparison, single pictures without magnification could normally cover the whole mouse skeleton, however, due to lower resolution, it provided worse quality, which stood to affect subsequent measurements. The magnification of the machine was achieved by putting the sample on the second, fixed shelf of the cabinet. In some cases, additional pictures of full mouse without magnification were also taken, but they were not later used in the analyses of morphometrics. All pictures were saved as DICOM files in ready folders named with the ID of a specimen, all files were then stored on the mpistaff server for the further processing. The name of each saved file consisted of a 4-digit ID number, a number of the photo, which was informative if more repeats were made (for example due to bad quality of the first picture), and a code “FL” or “HL” which would indicate front limb or hind limb. The folders, where the pictures were saved, were simply named by the ID of each mouse.

Landmarking

The limb bones were measured from digital pictures using *Fiji* software, by placing one landmark at the two ends of each bone of interest. The point tool, which is available in the software, was used, and the x-y coordinates were provided in the “Results” window, after pressing “m” key on the keyboard (or manually, by selecting “Measure” from “Analyze” menu). They were then copied to earlier prepared excel spreadsheet (Fig.3.2.).

9473	Landmark	X	Y	Length	
humerus	1	86.01781	68.41696		
	2	62.47403	76.18348	12.39585	
radius	1	63.52422	74.46573		
	2	58.10232	52.7781	11.17755	
ulna	1	65.95431	79.41138		
	2	54.48771	53.7306	14.06223	
scapula	1	86.38415	67.88373		
	2	82.8306	91.5374	11.95955	
femur	1	57.22309	74.39246		
	2	88.72876	69.2392	15.96217	
tibia/fibula	1	88.82645	67.61508		
	2	84.8455	29.64952	19.08685	

Figure 3.2. Spreadsheet example for calculating the length of each bone in first and second attempt.

The spreadsheet incorporated columns, with the ID of the sample, landmark number, x and y coordinates of landmarks, and the length of bone – were formula for calculating it from coordinates has been implemented. Length of each bone was calculated as follow:

$$L = \frac{\sqrt{(x_2 - x_1)^2 + (y_2 - y_1)^2}}{2}$$

Where x and y are the landmarks of each bone.

This procedure was repeated twice for the entire dataset. Whenever more pictures were taken for a single specimen, the ones of best quality were used for measurements (i.e., not an average measurement from multiple pictures).

Choosing the measurement landmarks in each bone was based on their importance as anatomical features, but also their presence and clarity on the two-dimensional view. Some of the landmarking methods were previously used by other researchers (Parmenter et al., 2016) (humerus, femur), others were developed specifically in this study (Tab.3.1.).

Table 3.1. List of anatomical placements of landmarks

Bone	Anterior landmark	Posterior landmark
Humerus	head of humerus	capitulum
Radius	head of radius	distal growth plate
Ulna	olecranon	distal growth plate
Scapula	coracoid process	caudal inferior angle
Femur	head of femur	condyle
Tibia	head of tibia	lateral malleolus

After all measurements were obtained, the calculated bone lengths were then moved to a new Excel spreadsheet and saved as a csv file. In R Studio, the file was reshaped to include only the IDs and the lengths of each bone, which was then used to quantify summary statistics and perform further analyses in R-Studio. This included mean, variance, standard deviation, distribution of measurements, and correlation patterns between the bones (Tab.3.2.).

Table 3.2. Summary of the two sets of measurements; min – minimum, max – maximum, var – variance, SD – standard deviation, data distribution test: W - Shapiro-Wilk statistics and p-value; vales are given in millimetres where applicable;

Statistics	Humerus	Radius	Ulna	Scapula	Femur	Tibia
Min (mm)	9.370	10.107	12.444	10.845	13.461	17.234
Max (mm)	13.921	12.142	14.766	14.127	17.752	20.425
Mean (mm)	12.178	11.160	13.761	12.611	15.621	18.839
Variance	0.510	0.130	0.181	0.328	0.591	0.390
SD	0.714	0.360	0.425	0.572	0.769	0.625
Shapiro's W	0.972	0.996	0.996	0.995	0.998	0.995
Shapiro's p	<0.001	0.747	0.588	0.379	0.986	0.457

Quality score control

High variance and long data tail was noted in measurements of the humerus (Shapiro's p <0.001). This might indicate a biological feature, or unwanted parallax error, arising from sample quality. As it could falsely influence the mapping results, it was necessary to find out possible source of unwanted error. To check if variance of bone length was affected by the

quality of the picture, the measurements were repeated in May 2020, and each bone was given a score from 1 (best quality) to 5 (worst quality). The quality score was defined by clarity of a picture, but also a visibility of specific landmark in respect to the anatomy of measured bone. The quality score was especially important in humerus and femur, which were the most difficult to position (because of their larger mobility and attachment to the body), which could have resulted in measurement error, and could shift the actual position of landmarks. Because the mice bodies were handled for previous studies, the muscles, and tendons holding the front limb in place were damaged. The joint holding the scapula to the rib cage (scapula-thoracic joint) should be intact, but it could have not been sufficient, to keep natural position of the stylopod of forelimb. On the other hand, landmarks position in zeugopod bones could have been affected by complicated anatomy of joints between them and the autopod and stylopod parts (especially wrist in case of ulna and radius, and foot in case of tibia). A large number of specimens were shown to be affected by skeletal deformations, which included unidentified lesions, tumors or syndactyly, so this time, an additional column with comments was added with eventual information recorded on any relevant issues. In most cases, obtaining a measurement was unaffected, so the mice were included in the study. The “comments” column was filled only if there were any deformations or problems with any skeletal part of the specimen, and it was left empty if skeleton was normal (Fig. 3.3.).

After saving a spreadsheet with all results as a csv file, it was loaded in R Studio, where, using prepared beforehand script, the IDs, bone lengths (without the coordinates), quality scores and comments were extracted at once, and saved as a new csv file, which was used in further steps.

1	lp	ID	x	y	Length	quality score	comments
humerus	1	8833 1 FL.dc	92.3841	69.687		2	
	2	8833 1 FL.dc	69.6218	61.839	12.0386192		
radius	3	8833 1 FL.dc	70.729	60.8295		1	
	4	8833 1 FL.dc	70.957	39.2722	10.7792528		
ulna	5	8833 1 FL.dc	70.0452	66.7562		1	
	6	8833 1 FL.dc	67.4726	39.1745	13.850708		
scapula	7	8833 1 FL.dc	92.8725	68.1565		2	
	8	8833 1 FL.dc	89.2579	92.8888	12.4975197		
femur	9	8833 1 HL.dc	60.2597	77.3395		2	
	10	8833 1 HL.dc	88.5578	67.7331	14.9420998		
tibia/fibula	11	8833 1 HL.dc	88.395	65.7467		3	
	12	8833 1 HL.dc	79.2445	30.3822	18.2645799		

Figure 3.3. Example of the new Excel spreadsheet layout used to calculate the bone lengths. The ID column implies the name of the file which this time was also automatically generated in ImageJ in “Results” window. It therefore included the 4-digit ID, number of a picture, in case there were more than one for said specimen, and a code FL or HL indicating whether it was a photo of front or hind part of the mouse.

The initial summary of the quality control check shows, that humerus was much more often assigned to lower quality score (Q2 = 110 specimen, Q3 = 69 specimen), than other bones. It also had the highest number of cases assigned to the lowest quality score (Q5 = 24 specimens), while single tibia and two scapula cases, and no cases in other bones were noted.

Bone length relation with the quality score

The quality score reflects a part of variance caused by the positioning of the animal during radiography. As mentioned before, in case of humerus and femur, it is of a parallax nature, which means, that the photographed objects (or it’s part) were positioned in closer distance to the camera (or detector), causing them to appear relatively shorter. In some cases, it is acceptable, as long as it is consistent through all specimens (Mullin and Taylor, 2002).

The quality score had the highest impact on the length of humerus, were the least good quality resulted in much shorter bone length. Hence, this could have been the reason for the skewed distribution of measurements. The R2 in linear model in humerus equalled 0.39 (Fig.3.4.). In femur the linear model does not bring statistical importance, due to only single sample being assigned in Quality score 4.

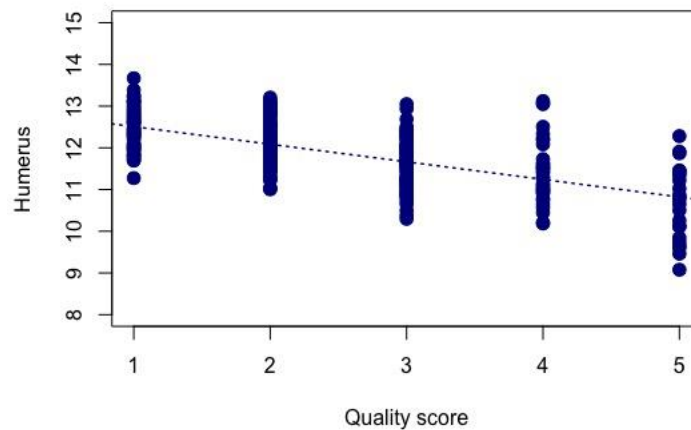


Figure 3.4. Bone length change due to quality in humerus and femur; DF = 290, F-statistic = 189.7, p-value < 0.0001, R2 = 0.39

3.2.2. Statistics

The bone lengths obtained in May 2020 were analysed in the R Studio. This includes basic statistical tests, such as mean, median, variance and standard variation, calculated with *base* R package. These parameters were first calculated for entire dataset with all quality score. Analyses of morphometric properties, as well as genome mapping were then performed on the dataset after removing all quality 5 measurements. Differences between male and female were calculated using t-test. ANOVA was performed to find possible association between the traits and covariates. Violin plots were made in *ggpubr* package with boxplots, to depict length differences between the sexes. Correlation matrices were calculated in *corrplot* package, similar as in Chapter I.

To calculate the measurement error, the ANOVA design was used on the datasets from May 2020 and July 2020. It estimates a percentage measurement error, defined as the ratio of the within-measurement component of variance to the sum of the within- and among-measurement components.

$$\%ME = \frac{s_{within}^2}{(s_{within}^2 + s_{among}^2)} \times 100$$

3.2.3. QTL Mapping

r/qt12 package

The dataset from the MegaMUGA used in this study were earlier processed as indicated in (Belheouane et al., 2017). The data filtered for 10% MAF were used in this genome screening, and consisted of total 53,203 markers spread through 19 autosomes and the chromosome X. Custom R code was built to adapt the array for *rqt12* package. The disagreed genotypes were removed by using a loop on the genotype output file. The control file in json was coded to specify the files' names: genotypes and founder genotypes, genetic and physical marker maps, phenotype file, covariate file and the kinship. The type of cross was also specified in the json as "genail4" which stands for general (outbred) advanced intercross of four parental lineages. The four alleles were coded in respect to the parental lineages names as: CAST, BdX2, MRL and NZM. Physical map was designed in NCBI37/mm9 annotations. The *r/qt12* package was further on applied in the following genome mapping. The genotype probabilities were calculated for the entire dataset with the *calc_genoprob* function using the physical marker map and error probabilities set to 0.002 in the arguments. They were then converted to allele probabilities, with *genoprob_to_alleleprob*. The kinship was calculated using the allele probabilities, with the LOCO method (leave one chromosome out), which produces a matrix for each chromosome. The mapping was conducted on all chromosomes including chromosome X. Permutation tests were used to calculate the threshold of significance for each measured bone (the phenotype). The arguments included the allele probabilities, phenotype data frame, kinship, covariates: sex, weight and age. X chromosome was indicated with *Xcovar*. The permutations were run to calculate autosomes and chromosome X thresholds separately, as according to Broman (2006) (Broman et al., 2006). They were then saved in separate objects. In both cases I used the threshold of 5% and 10% (suggestive) to pinpoint the peaks with possible role in bone length in G15 mice. To calculate logarithm of odds scores of each chromosome and phenotype, genome scan was performed, using *scan1* functions, and saved in an object "out". The arguments, similar as in the permutations, were the allele probabilities, phenotype data frame, kinship, X covariate, and the matrix of additive covariates (weight, age and also sex).

Finding the QTL candidate intervals

To pinpoint the significant regions of the mapping, the results of the genome scan for a chromosome, where a significant peak was detected was extracted with *subset_scan1* and saved as a csv file with marker physical map in another column. The candidate interval was set from the largest LOD (the peak LOD value) score, and the confidence interval was estimated by subtracting 1.5 LOD score to upstream and downstream the physical map. The candidate interval and the peak physical position was transferred to the *LiftOver* web tool and converted from mm9 (NCBI37/mm9) to mm10 (GRCm38/mm10) assembly (Mouse Genome Sequencing Consortium, 2002, Lee et al., 2022). The results of the mapping were visualised for all chromosomes in each trait with *plot_scan1* function.

Genes

The database of Mouse Genome Informatics (<http://www.informatics.jax.org>) as well as Rat Genome Database (RGD) libraries (Smith et al., 2020) were used to screen for relevant candidate genes with known function in the skeleton or limb, as well as the gene in the LOD peak if applicable. Information on selected patterns of gene expression were extracted from these databases, unless another source was given.

3.2.4. Bone covariate models

All the steps for mapping of the relationship QTLs were the same as for the bone lengths, and included adding covariates of weight and age as well as specifying the X chromosome. Model of the radius as a covariate did not have a significant input to the analyses, and therefore it was not included in the result section. By using another bone as a covariate in the model, it become possible to find candidate genes involved in integration of each pair of bone elements. Five separate models were run for all bones when 1) humerus, 2) ulna, 3) scapula, 4) femur and 5) tibia were added as the covariates, together with sex, weight and age of the animals. These bones were then subsequently removed as phenotypes. The models were also run in the other way around, i.e., with radius as a covariate to ulna, and ulna as a covariate to radius. In many cases this method can unravel even more significant regions affecting bone correlation.

3.3. Results

The total set of measurement was obtained from 292 mice (Tab.3.3., Tab S3.1.). Measurement error between two separate measurement sets conducted on the same image sets was calculated using ANOVA method. Humerus and scapula measurements were the only ones with skewed distribution (Fig.3.5.), which was more evident in humerus (right side skewness, $p < 0.001$). It was also characterised by highest standard deviation compared to other bones. As compared with another measurement set, measurement error was highest in scapula and radius. In case of radius, eventual variance could be caused by landmarking difficulty caused by overlap of the radius styloid process and triangular bone of wrist, or radius head by sesamoid bone or humerus. The measurement error was lowest in femur and humerus, showing the highest landmarking precision of these bones.

Table 3.3. Cumulated measurements on 292 mice of each bone and measurement error percentage; var – variance, SD – standard deviation, W - Shapiro-Wilk statistics and p-value, %ME – percentage measurement error (ANOVA design);

Bone	min (mm)	mean (mm)	median (mm)	max (mm)	var	SD	W	p	%ME
Humerus	9.078	11.877	11.948	13.669	0.608	0.780	0.980	<0.000	0.467
Radius	10.114	11.154	11.179	12.114	0.135	0.368	0.995	0.546	1.186
Ulna	12.453	13.779	13.788	14.792	0.187	0.433	0.996	0.697	0.817
Scapula	10.921	12.601	12.605	13.985	0.326	0.571	0.994	0.348	2.440
Femur	13.434	15.619	15.601	17.798	0.580	0.762	0.998	0.991	0.227
Tibia	17.128	18.836	18.820	20.345	0.382	0.618	0.995	0.538	0.791

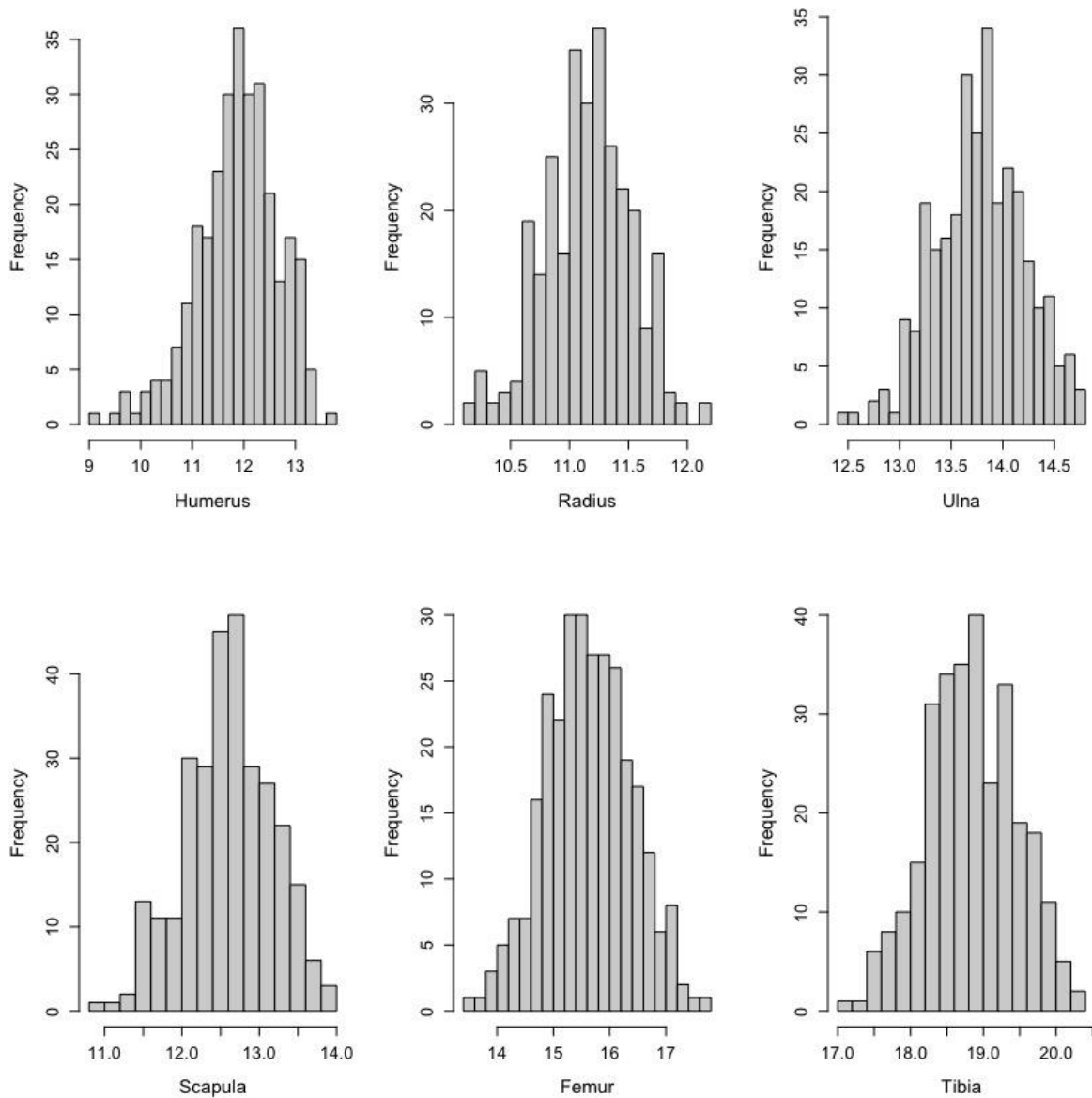


Figure 3.5. Frequency histograms of each measured bone, raw dataset, both sexes; left-side tail is observed in humerus

3.3.1. Final measurements – statistics

The final data used for mapping contained measurements of quality above score 5 (Tab.3.4). Overall, 264 animals were genotyped, and using the IDs of these mice, the final datasets of both phenotyped and genotyped animals was extracted. The humerus measurement dataset contained the least measurements among all bones, 237 measurements were left after removing measurements of uncertain quality. Removed data included the shortest humeri measurements from pictures which were visibly affected by the parallax error. The skewness

of the humerus measurement greatly decreased (p -value of Shapiro test = 0.161) compared to original dataset (Tab.3.3).

Table 3.4. Number of measurements in each quality score per bone

Bone	Q1	Q2	Q3	Q4	Q5	All mice -- Q5	Phenotyped and genotyped
Humerus	58	110	69	34	24	271	239
Radius	259	25	10	1	0	295	259
Ulna	262	25	7	1	0	295	259
Scapula	254	30	7	2	2	293	257
Femur	223	53	18	1	0	295	259
Tibia	205	60	25	4	1	294	258

With mean length of 11.96 mm, the humerus was one of the shortest measured bones, second only to radius. This shorter bone of the forearm had a mean length of 11.1 mm, and the lowest, among other bones variance (0.138). The elbow bone, ulna, was also characterized by relatively small variance (0.19), in regard to the mean length of 13.79 mm. The tibia was the longest of measured bones, with average length of 18.8mm. The highest variance and subsequently, standard deviation was observed in femur followed by humerus. The same as in untreated data, scapula and radius were characterized by highest measurement error compared to other bones. Excluding the mentioned humerus, all datasets appeared to have normal distribution (Tab.3.5, Fig.3.6).

Table 3.5. Primary statistical results of the genotyped and phenotyped mice var – variance, sd – standard deviation, W - Shapiro-Wilk statistics and p-value, %ME – percentage measurement error (ANOVA design)

Bone	n	min (mm)	mean (mm)	median (mm)	max (mm)	var	SD	W	p	%ME
Humerus	237	10.186	11.968	11.995	13.669	0.487	0.698	0.991	0.161	0.578
Radius	259	10.114	11.144	11.186	12.114	0.138	0.371	0.995	0.607	1.150
Ulna	259	12.453	13.767	13.787	14.792	0.190	0.435	0.996	0.693	0.778
Scapula	257	10.921	12.597	12.605	13.985	0.321	0.566	0.995	0.527	2.626
Femur	259	13.434	15.607	15.608	17.798	0.566	0.752	0.998	0.997	0.227
Tibia	258	17.128	18.808	18.811	20.321	0.371	0.609	0.995	0.483	0.762

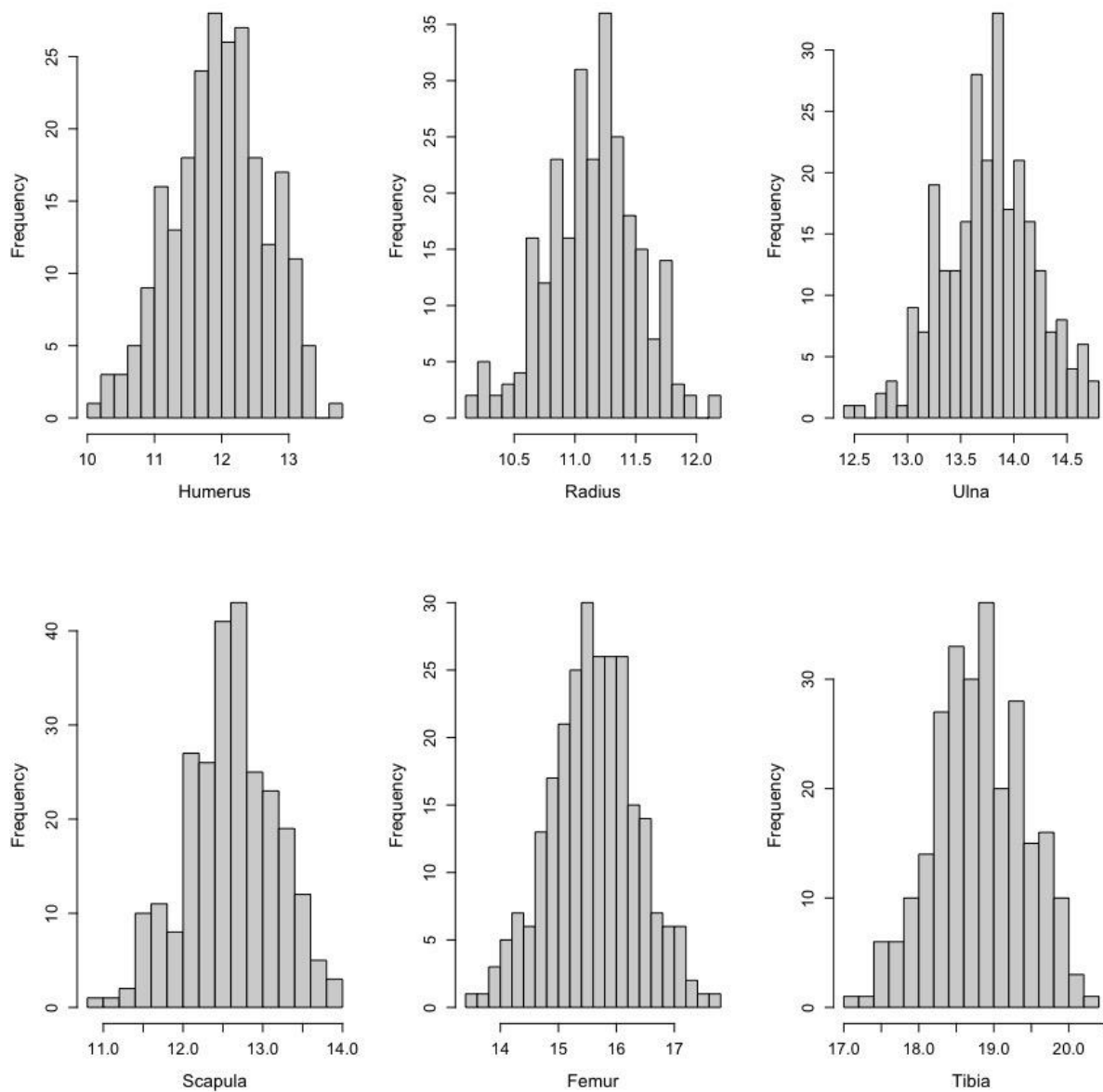


Figure 3.6. Frequency histograms of the final measurement of G15 mice (phenotyped and genotyped specimens)

Weight, age and sex influence on bone length

The final dataset of 259 animals which were both phenotyped and genotyped was used to further estimate the relationship between bone length and the covariates – sex, weight and age of the animals. The mean length of each element was significantly different in males and

females. In the case of the front limb, all bones including scapula are longer in males. However, mean length of femur and tibia of the hind limb was greater in females (Fig.3.7, Tab.3.6, Tab.S3.1.). The dataset consists of 165 females and 94 males. Females are lighter and older than males on average. However, the range of age is much greater, as they also include young mice which were 90 days old at the time of death (Tab.3.6.).

Table 3.6. Female and male statistics in the G15 mice; lengths are given in millimetres

Bone	Females				Males			
	n	length	variance	SD	n	length	variance	SD
Humerus	148	11.79	0.507	0.712	89	12.26	0.321	0.567
Radius	165	11.09	0.139	0.373	94	11.24	0.124	0.352
Ulna	165	13.68	0.186	0.432	94	13.92	0.162	0.402
Scapula	163	12.53	0.312	0.558	94	12.71	0.318	0.564
Femur	165	15.74	0.576	0.759	94	15.37	0.468	0.684
Tibia	165	18.89	0.374	0.612	93	18.66	0.333	0.577
Mean weight (grams)	32.5 (range 22.4 – 48.0)				36.8 (range 27.4 – 57.35)			
Mean Age (days)	180 (range 90-203)				173 (range 127-203)			

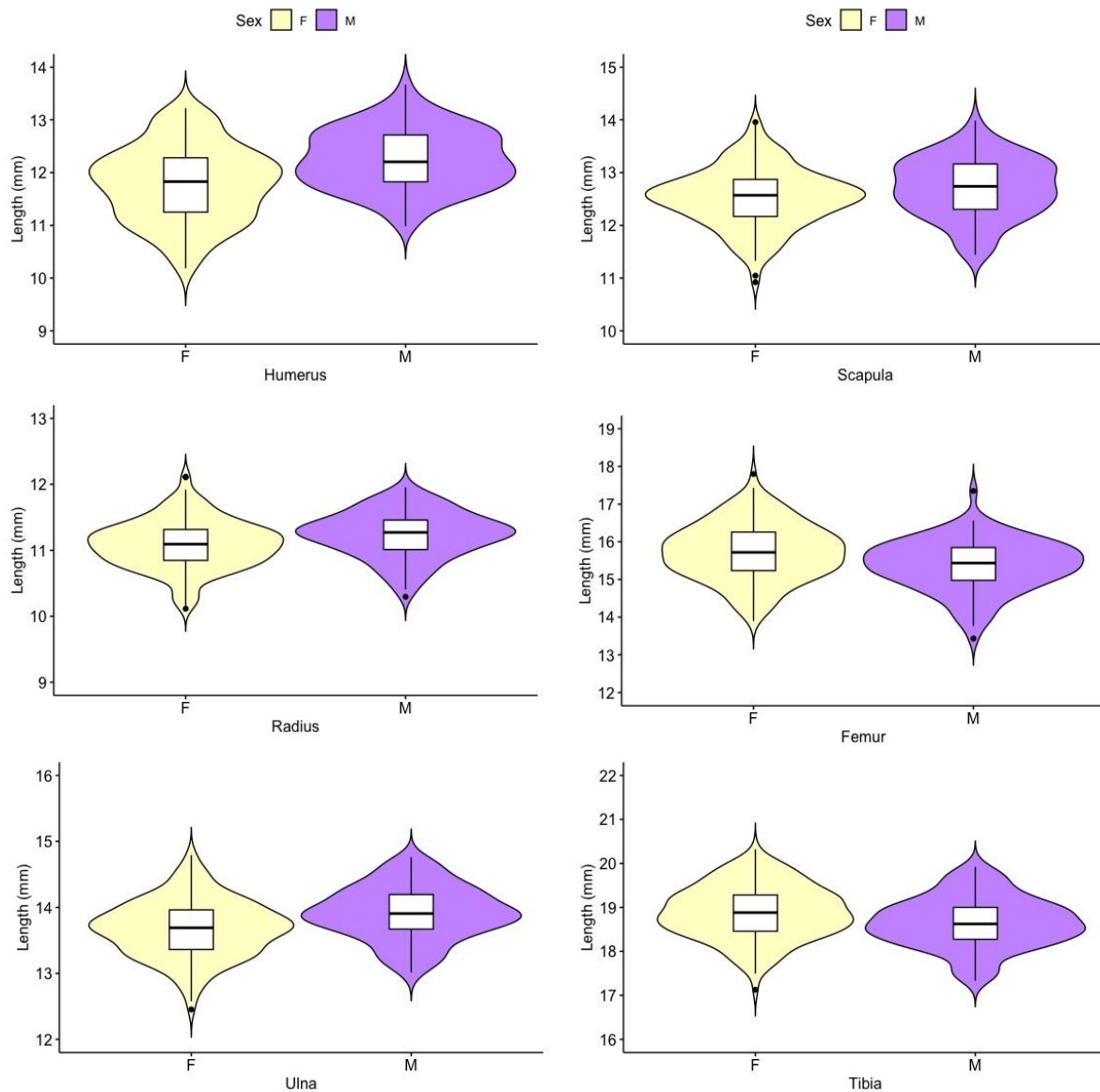


Figure 3.7. Violin plots representing male (M) and female (F) distribution each bone length in G15 mice; the boxplots represent the median values; the black dots represent outlier values; additional statistics are given in Supplementary Table 3.1.

Although the mean bone lengths differed between sexes, the analysis of variance did not suggest that lengths of radius, ulna or scapula were affected by this factor alone (Tab. 3.7). Radius, ulna and also tibia lengths show significant correlation with combined sex and age covariate, which might be related to different ranges of age in females and males, and on average shorter bone length in younger females. It appears, that sex had stronger effect on the hind limb bones overall. Radius has only a very weak correlation with age which is absent in ulna, scapula, and femur (Tab. 3.7, Fig.S3.1). The significance of this relation is observed in

tibia and humerus. As observed in the Figure S3.1 (supplementary material), older mice appear to have shorter humeri, which might be caused by eventual degradation of bone (keeping in mind, that one of the parental lineages, the BXD2, was carrying osteoporosis susceptibility), or simply be an artifact caused by small number of young mice (below 150 days), as there is no linear support of this relationship. Weight of the animals significantly affects all of the measured bones, and in all cases the correlation is positive. The linear relationship between the phenotypes and weight are given in the Figures 3.8 for all specimen used in the mapping (males and females).

Table 3.7. Level of significance of ANOVA test between bone length and covariate, including combination of two of more covariates: *** = $p < 0.0001$, ** = $p < 0.001$, * = $p < 0.01$; grey colour represents lack of correlation, additional test statistics are given in Table S3.2.

	Humerus	Radius	Ulna	Scapula	Femur	Tibia
Weight	***	***	***	***	*	***
Age	***	*				**
Sex	*				***	***
Weight:Age						
Weight:Sex						
Age:Sex		*	*			*
Weight:Age:Sex						

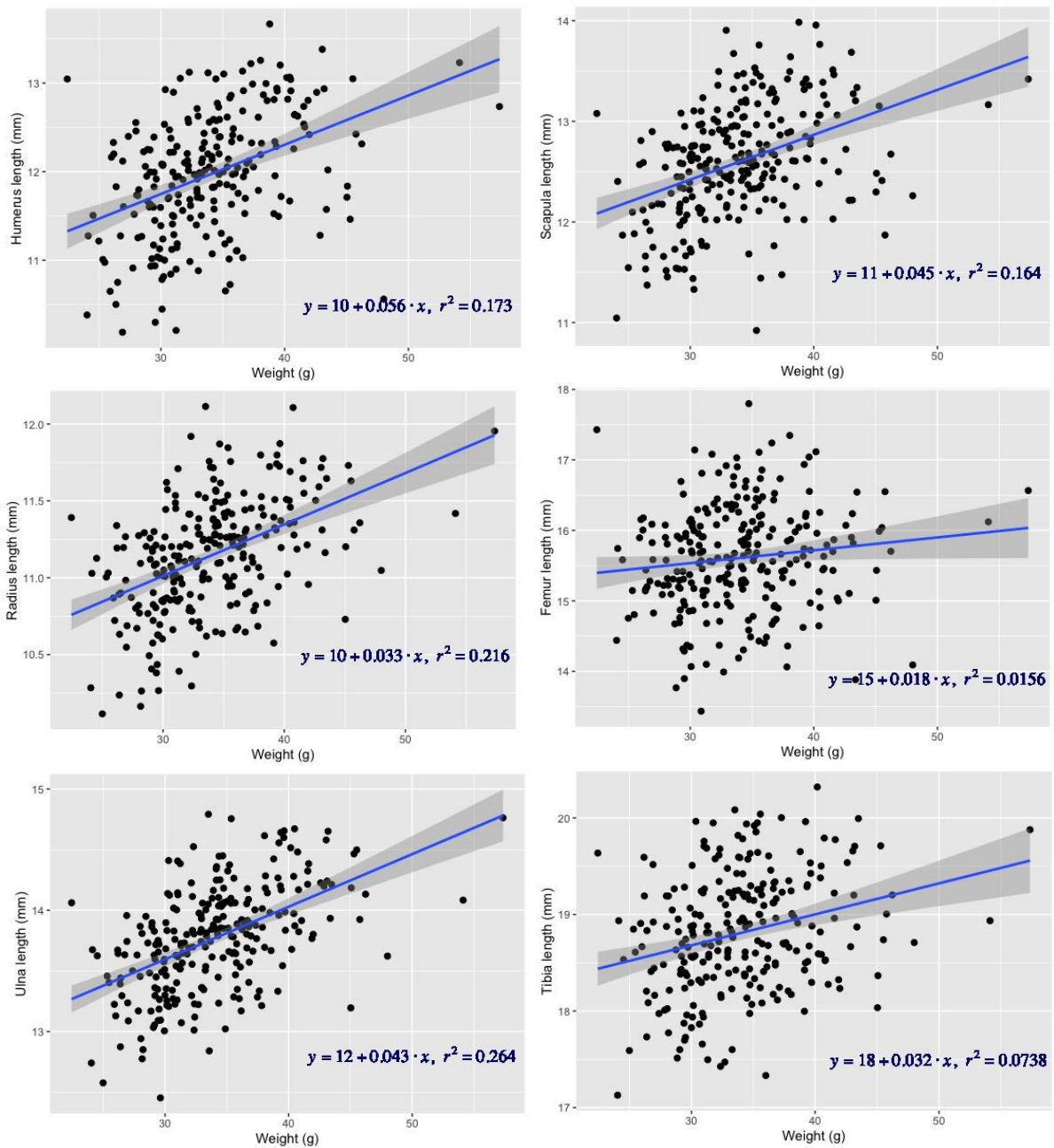


Figure 3.8. Relation of weight and bone length G15 mice; Humerus: F-statistics = 49.32, DF = 235, p-value < 0.0001; Radius: F-statistics = 70.91, DF = 257, p-value < 0.0001; Ulna: F-statistics = 92.21, DF = 257, p-value < 0.0001; Scapula: F-statistics = 50.12, DF = 255, p-value < 0.0001; Femur: F-statistics = 4.08, DF = 257, p-value = 0.04; Tibia: F-statistics = 20.40, DF = 256, p-value < 0.0001

Correlations, differences in males and females

The correlation between bone lengths was calculated by Pearson product moment method, using complete pairwise observation for all phenotyped and genotyped mice (Fig.3.9). Strong correlation is present in bones of forearm, radius and ulna ($R = 0.93$), which both are also correlated with zeugopod element of the hind limb – the tibia bone ($R = 0.71$). Humerus has medium strong correlation with every other bone which is only slightly higher within the front limb bones. Femur is most tightly correlated with radius, while the scapula with all front- and hindlimb zeugopod elements.

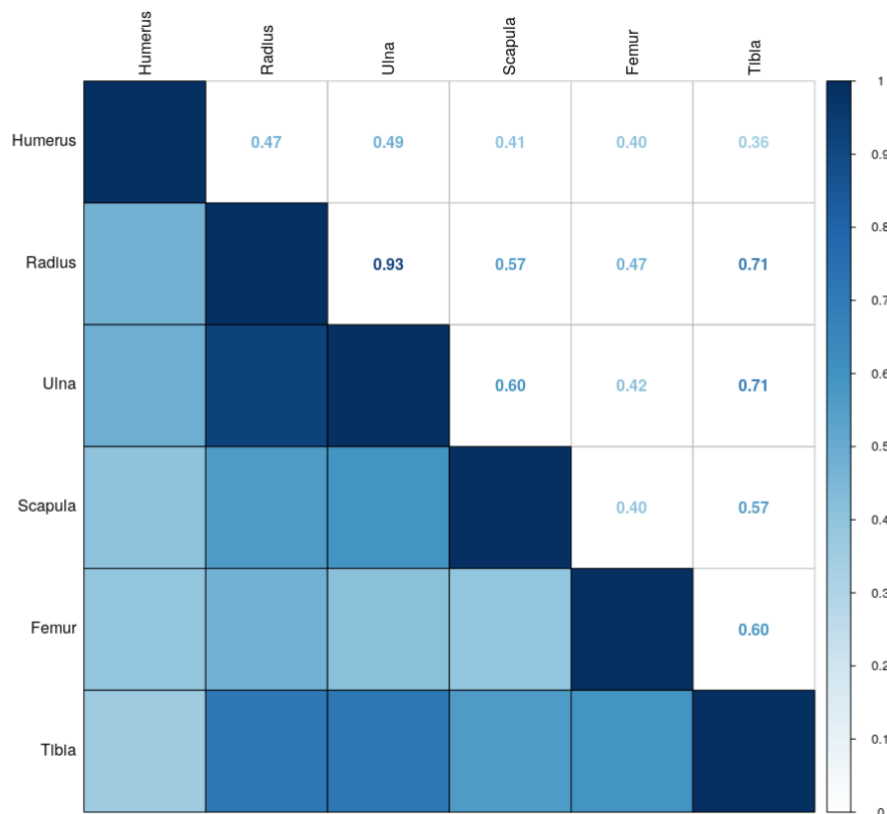


Figure 3.9. Correlation between bone length in G15 mice (both sexes, no covariates added, all results are significant with $p < 0.05$), with r values in the upper squares; method: Pearson product moment correlation, complete pairwise observation

Interestingly, males and females present different patterns in correlation of the specific bones (Fig.3.10). The humerus correlate with other bones most strongly in males. While in females the humerus correlates with the femur ($R = 0.50$), in males the arm bone is characterised by similar between all bones except for scapula, which is the lowest ($R = 0.43$). In both sexes the scapula also has a rather strong correlation with the lengths of zeugopod elements. While it is comparable in the case of the ulna and radius ($R = 0.50-0.60$), the length of the shoulder blade correlates strongest with the length of the tibia within females ($R = 0.70$), than within males ($R = 0.46$).

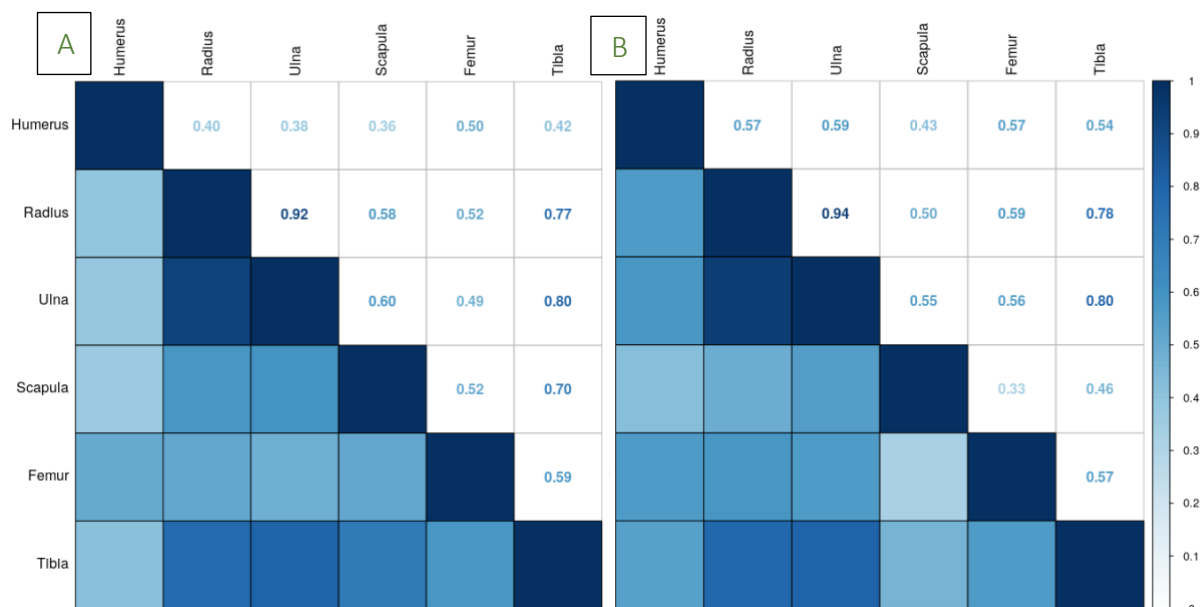


Figure 3.10. Correlation patterns between bone length in females (A) and males (B); method: Pearson product moment correlation (Pearson's R), complete pairwise observation, all results are significant with $p < 0.05$

After removing the effect of weight on the bone lengths, the principal component analysis does not show separation of males and females based on the first and second PC. The loading scores show similar direction of four strongly correlated bones: scapula, radius, ulna and tibia (Fig.3.11, Tab.S3.3). When males and females datasets are considered separately, this trend is observed in females, while in males the scapula has clearly different direction than the zeugopod bones (Fig. S3.2).

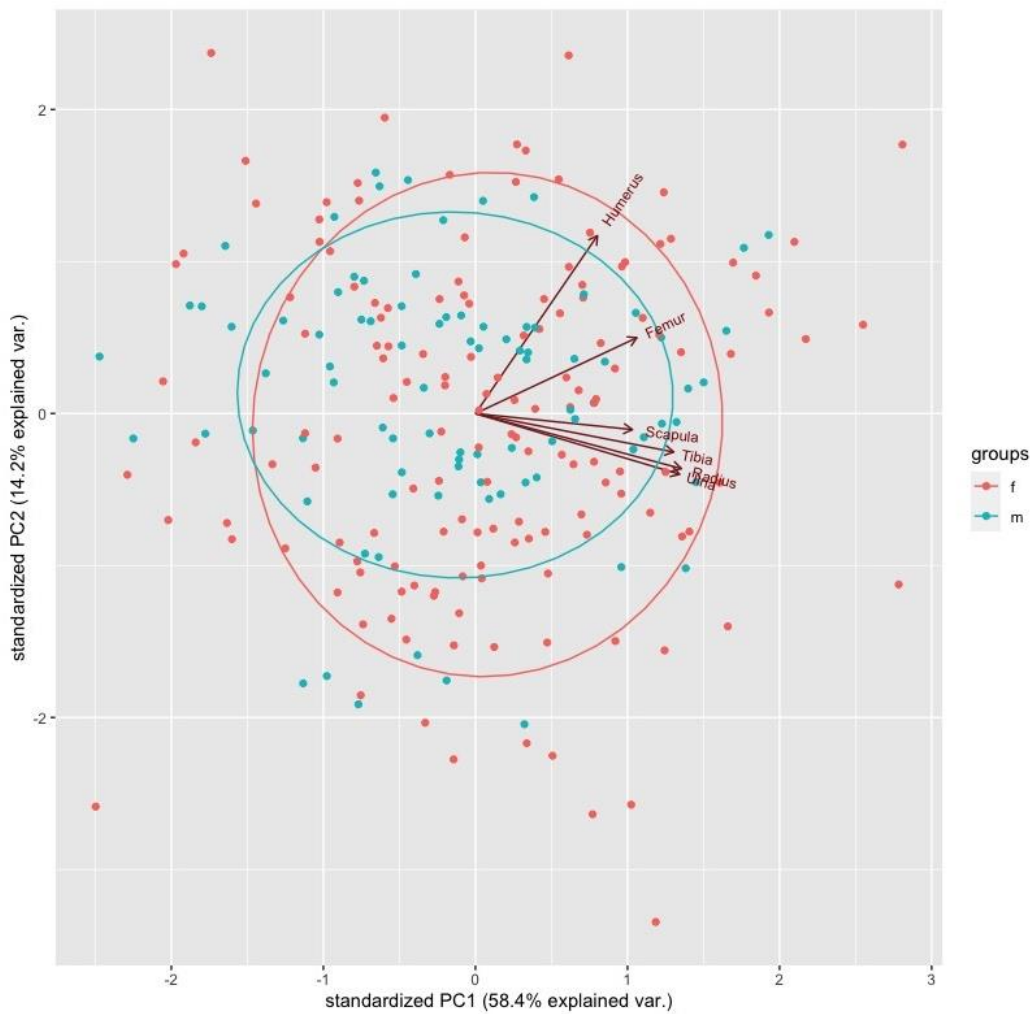


Figure 3.11. PCA graph on weight residual dataset (complete observation) of the G15 mice with eigenvectors for each bone

3.3.2. Genome mapping

Permutations

The mapping was conducted on all chromosomes including the chromosome X. The permutation test was used to calculate the threshold of significance for each measured bone (the phenotype). Separate tests were performed for autosomes and chromosome X, in both cases the threshold of 5% and 10% (suggestive) was used to pinpoint the peaks with possible roles in bone length in G15 mice. The results for autosomes (Tab.3.8) were similar in all phenotypes, ranging from 5.28 to 5.34 LOD score at the 5% threshold, and from 4.93 to 4.98 LOD score at 10% threshold. In case of chromosome X (Tab.3.9.), the LOD significance score

was more diverse between the phenotypes, with minimum value of 3.49 and maximum 3.76 at the 5% threshold, and subsequently 3.12 and 3.36 at the 10% threshold.

Table 3.8. Autosome significance threshold in each bone (number of permutations: 10,000)

Threshold	Humerus	Radius	Ulna	Scapula	Femur	Tibia
10%	4.94	4.93	4.93	4.98	4.94	4.94
5%	5.28	5.29	5.3	5.34	5.3	5.31

Table 3.9. Chromosome X significance threshold in each bone (number of permutations: 14,9367)

Threshold	Humerus	Radius	Ulna	Scapula	Femur	Tibia
10%	3.12	3.36	3.32	3.35	3.28	3.34
5%	3.49	3.76	3.72	3.75	3.66	3.73

Genome scan

Each of the measured bones - humerus, radius, ulna, scapula, femur and tibia were included as phenotypes in the genome scan. Afterward, the resulting LOD scores for each were plotted, and the significant (or close to significant) peaks were presented on the specified chromosome. The confidence interval for each peak was estimated by subtracting 1.5 LOD score from the highest peak LOD score.

Out of the six bones, the results from the humerus, radius and scapula were not significant. However, the largest peaks are nevertheless interesting to shortly characterize (Tab.3.10).

Table 3.10. List of highest LOD peaks in humerus, radius and scapula which did not reach significance; the positions of the peak and confidence intervals (CI) were converted to the GRCm38/mm10 (Mbp - mega base pairs)

Bone	chromosome	CI_lo (Mbp)	CI_hi (Mbp)	peak (Mbp)	size (Mbp)	peak marker	Peak LOD
Humerus	chr11	19.015448	20.649015	19.510013	1.63	JAX00305287	4.47
	chr19	32.802285	32.828447	32.828447	0.03	UNC30214345	4.44
Radius	chr13	106.360312	113.703006	110.932973	7.34	UNC23367022	4.43
Scapula	chr13	102.330985	107.245557	106.758218	4.91	JAX00369337	4.33
	chrX	50.730537	99.218385	72.484131	2.02	UNC30956088	3.04

Humerus

In the humerus, the highest peaks were observed on chromosomes 11 and 19 (Tab.3.10, Fig.3.12). They didn't reach significance, as the highest LOD score in chromosome 11 was 4.47 and 4.44 in chromosome 19. Peaks on these chromosomes were not observed on any other bone. The speculated confidence interval of the peak on chromosome 11 covered 1.63Mbp, where one gene called *Spred2* with known mutational effects on limb skeleton is found (Bundschu et al., 2005). The interval in the chromosome 19 was as small as 0.03 Mbp, within which a very important protein coding gene *Pten* is situated. Mutations of this gene are related to increased bone mineral density and abnormal long bone morphology, among many other skeletal deformations (Lynch et al., 2009).

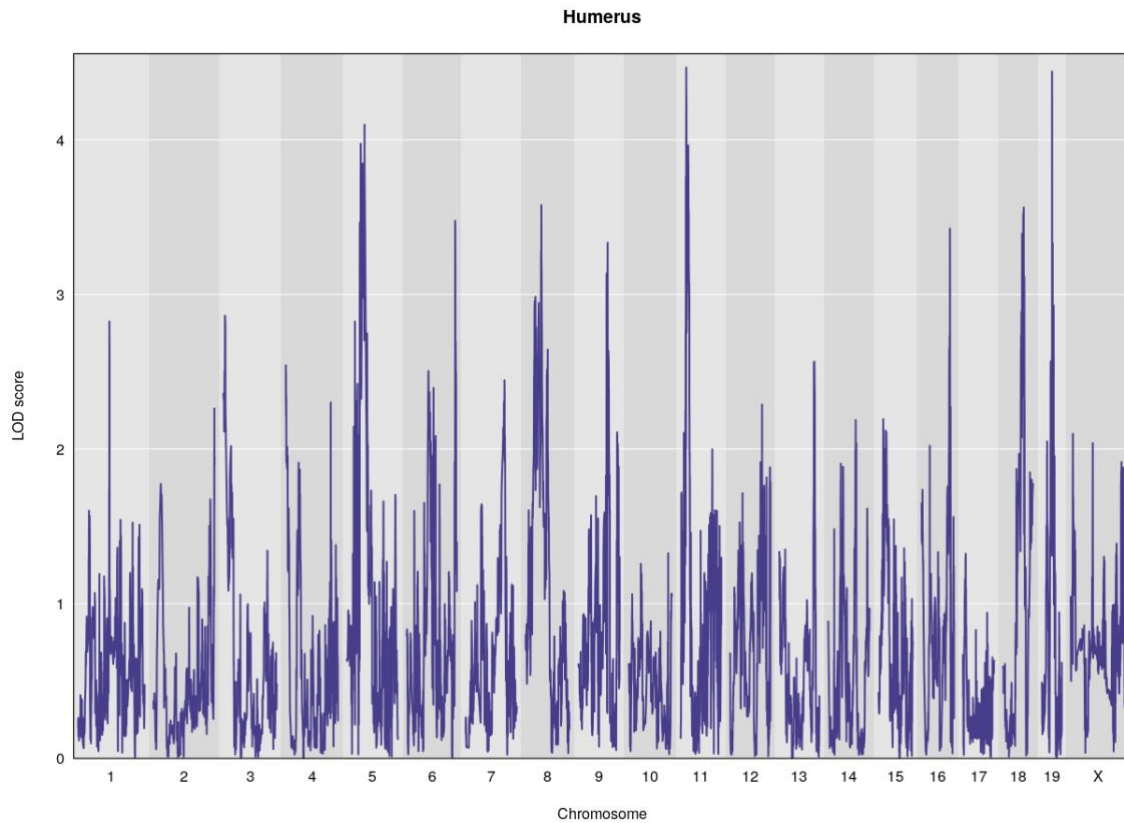


Figure 3.12. LOD scores in each chromosome in the humerus phenotype

Scapula

In case of scapula, the highest peak is observed on chromosome 13 (Fig.3.13.). Although it didn't reach significance, the peak appears to be corresponding with the same region found in radius, ulna and tibia, and is reported in detail in later section.

In the chromosome X, a visible peak with the LOD value of 3.03 is present, and although it did not reach the significance level of 3.35, it might be a suggestive region to investigate further relation with the length of scapula bone.

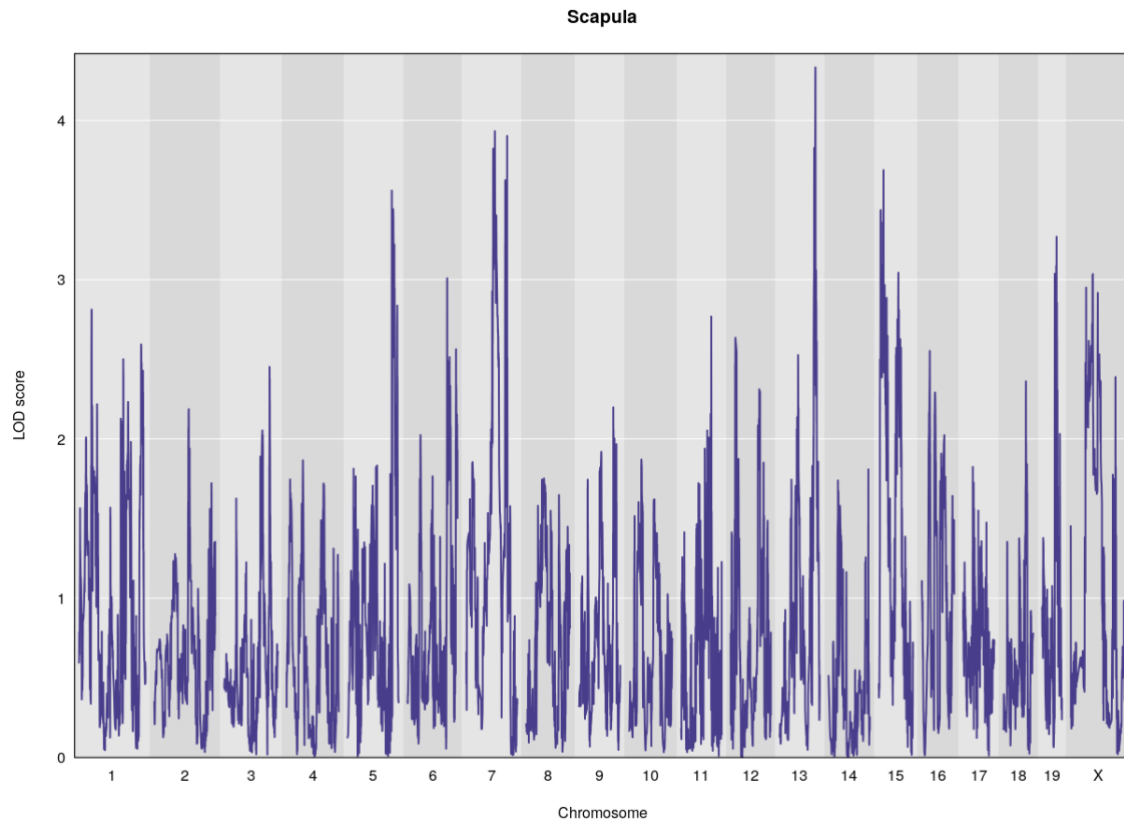


Figure 3.13. LOD scores in each chromosome in the scapula phenotype

In the X chromosome two genes with documented role in skeleton are present: **Mamld1** and **Mtm1**, within the confidence interval of 1.5 LOD score from the peak

Radius

The highest peaks are found in chromosome 13 as well as on chromosome 6 (Fig.3.14), which correspond to the peaks in ulna (Fig.3.15). However, similar to the peaks in scapula and humerus, they do not reach significance threshold. The LOD score of the peak in chromosome 13 reaches the value of 4.43, and the estimated confidence interval is over 7Mbp large. It is therefore larger than in the scapula where it spans of 4.9Mbp. There is no known genetic feature in the peak of the region, but within the confidence interval genes such as *Plk2*, *Map3k1*, *Il6st*, *Il31ra*, *Dhx29* are present, all of them have experimentally proven skeleton phenotype effect.

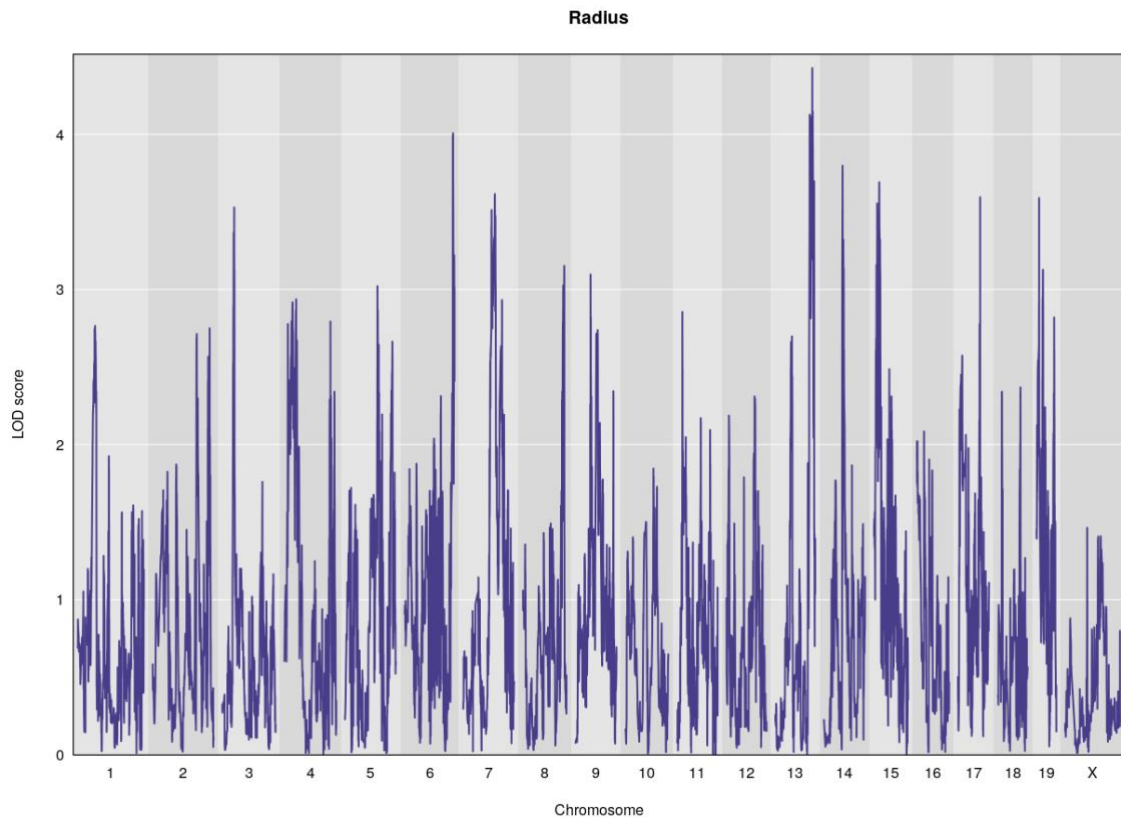


Figure 3.14. LOD scores in each chromosome in the radius phenotype

Genome scan results: Ulna, Femur and Tibia

The genome scan results of the next three bones – ulna, femur and tibia reached significance at the 5% level, and in some cases at the 10% (Tab.3.11), and multiple peaks with interesting candidate genes and other features were found to correspond to the position of the peaks and confidence intervals.

Table 3.11. Highest LOD peaks significant in the bones (blue colour represents significance at the level 10%), the positions (in mega base pairs - Mbp) of the peak and confidence intervals (CI) were converted to the GRCm38/mm10

Bone	chromosome	CI_lo (Mbp)	CI_hi (Mbp)	Peak (Mbp)	size (Mbp)	peak marker	Peak LOD
Ulna	chr6	144.467621	146.372836	145.304160	1.91	UNC12310385	5.70
Ulna	chr6	147.396366	149.516148	149.256921	2.12	UNC12364773	5.20
Ulna	chr13	102.187043	107.439136	104.186732	5.25	UNC23268059	5.53
Ulna	chr15	18.535992	20.094186	18.862132	1.56	JAX00394898	5.22
Femur	chr8	95.711951	103.530655	101.749607	7.82	UNC15386001	5.35
Tibia	chr5	97.763911	99.267893	97.843261	1.50	UNC9738464	5.20
Tibia	chr13	102.403921	106.089354	103.266184	3.69	UNC23253941	4.92

Ulna

In the ulna bone very clear peaks are present on chromosomes 6, 13 and also 15 (Fig.3.15, Tab.3.11). The significance threshold of 5.3 LOD score (level 0.05) is reached in chromosome 6 and 13. With the LOD drop value of 1.5 two peaks can be distinguished in chromosome 6 (Fig.3.16 A), one of which has a LOD score of 5.70 and is significant at the 5% threshold, and the other one with the 5.20 LOD is significant at the level 10%. The peaks are separated by roughly 1Mbp distance on the chromosome. However, no known genes or other markers are present in the second interval on the chromosome 6. It is the very end part of the chromosome (positioned between 147.396366 - 149.516148Mbp of the physical chromosome map). Visually, two peaks are also present in chromosome 13 (Fig.3.16 B), but the LOD score drop between them is smaller than 1.5, so they were not reported as separate features.

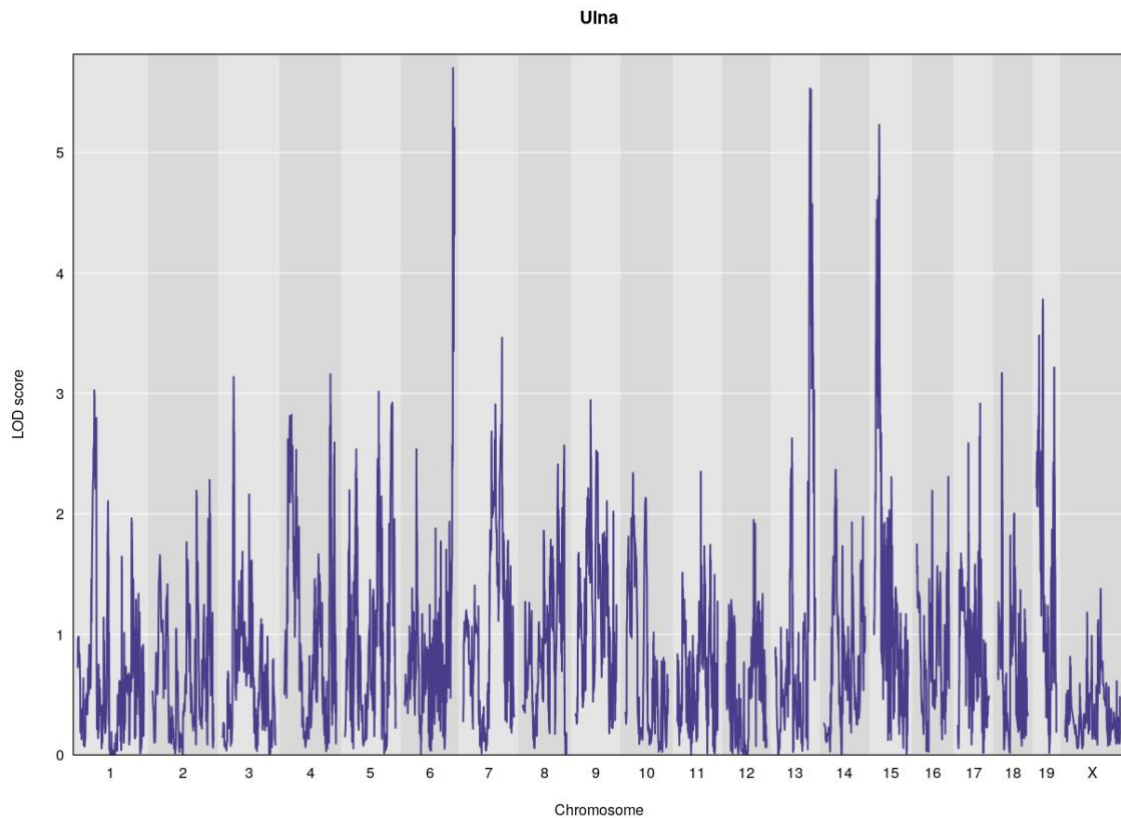


Figure 3.15. LOD scores in each chromosome in the ulna phenotype

The peak on chromosome 13, is in a reasonably small distance to the one in the radius, scapula and tibia (Fig.3.16 B, Fig.3.20). It is 5.25Mb large, which makes it the second largest interval among all significant peaks (Tab.3.11). The size of the peak on chromosome 15 is the smallest among all reported in ulna (1.56 Mbp), and it does not appear in any other phenotype.

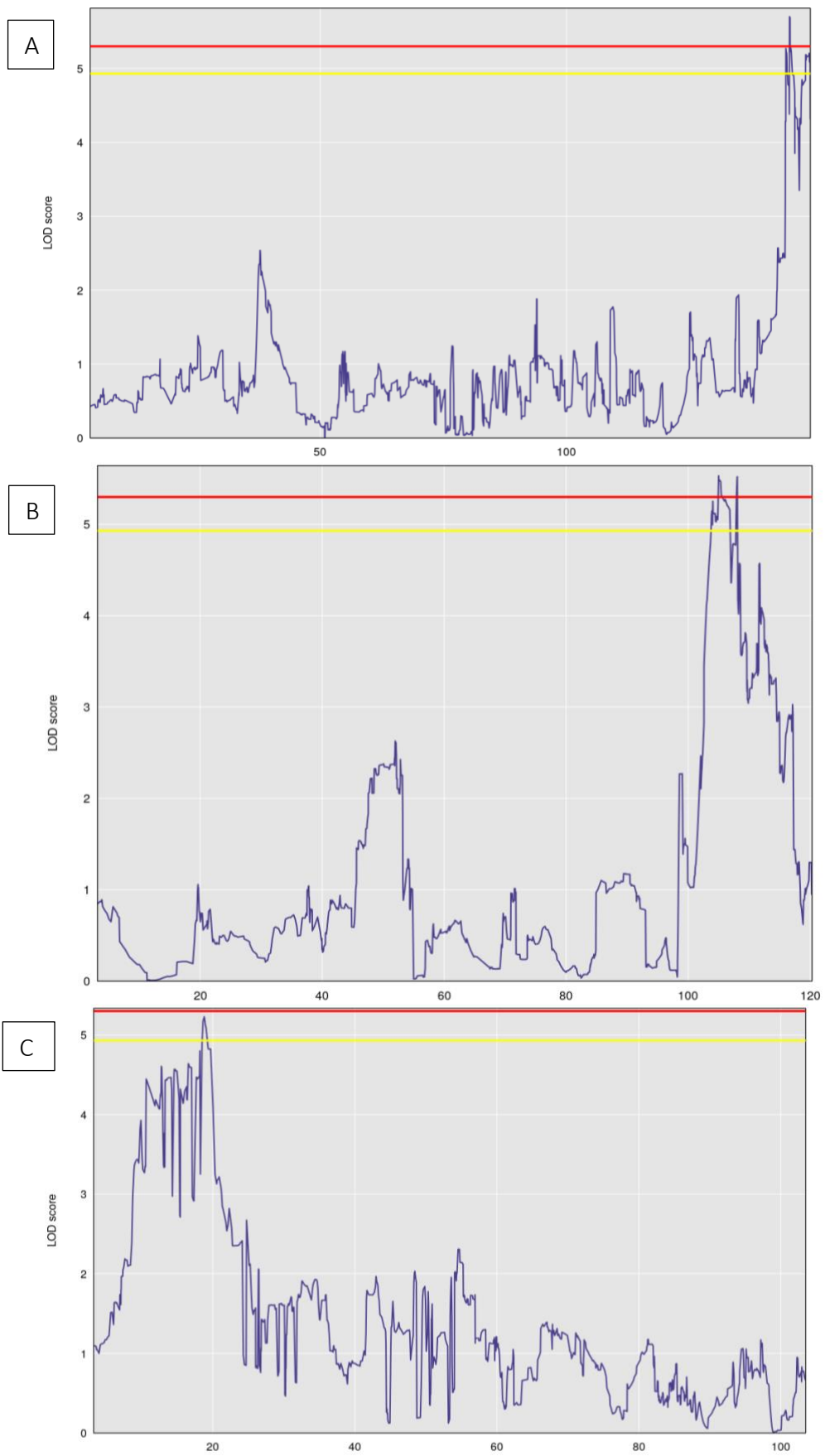


Figure 3.16. LOD scores in the ulna phenotype on chromosomes 6 (A), 13 (B) and 15 (C), with the significance level lines: **red**: 5% and **yellow**: 10%

Femur

For the femur a clear peak is observed on chromosome 8. Considering the confidence interval drop by 1.5 LOD score of the highest peak value, it is as large as 7.82Mbp. No skeleton-phenotype candidate gene was found in the peak, but it is situated directly in the QTL marker *Desp1* and NCBI predicted gene *Gm32477*. A peak reaching 4 LOD score is also observed on chromosome 6, which might correspond to the one found in ulna.

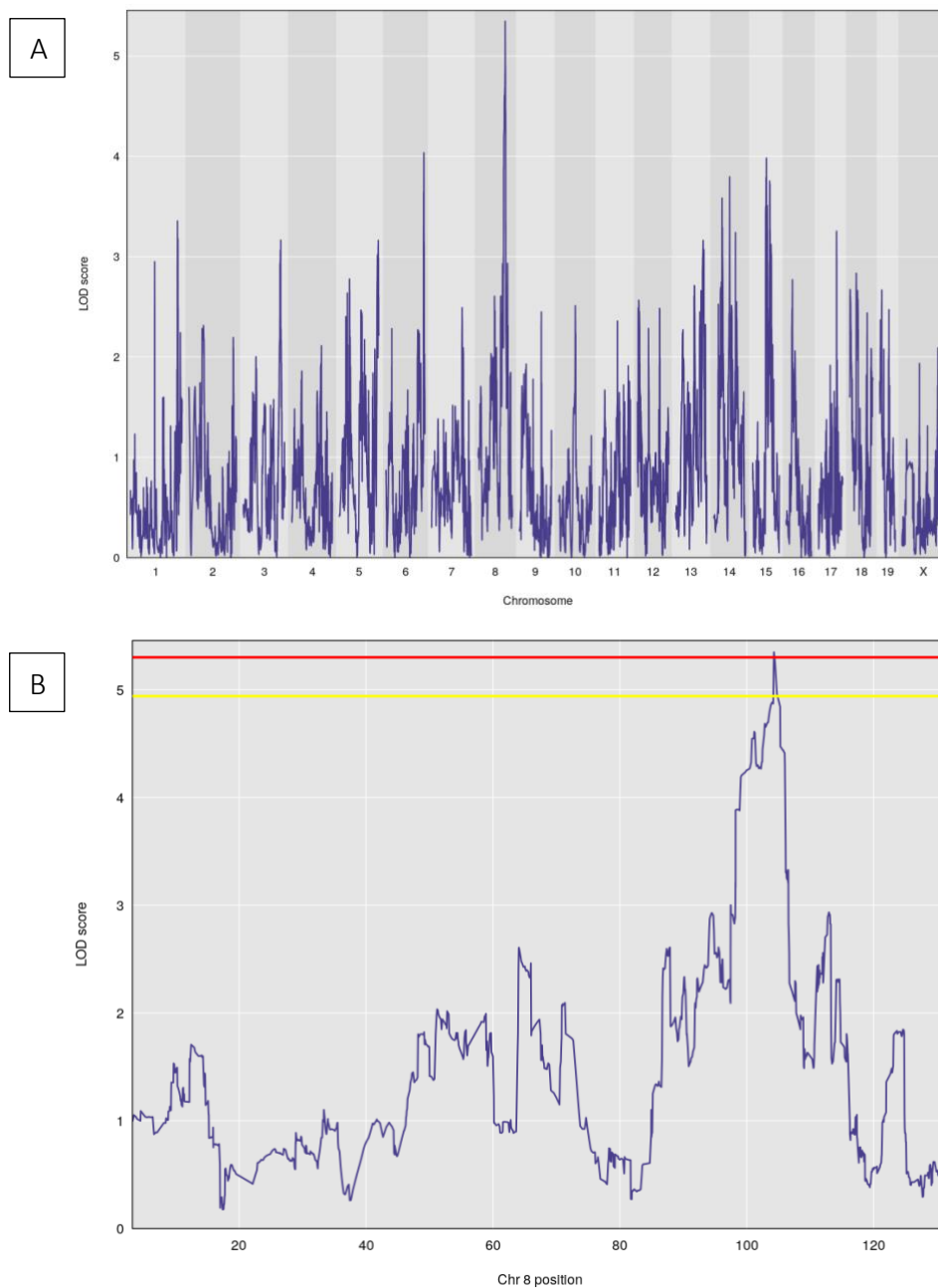


Figure 3.17. LOD scores in each chromosome in the femur phenotype (A) and visualization of the peak in chromosome 8 (B), with the significance level lines: red: 5% and yellow: 10%

Tibia

In the tibia, there are peaks on chromosome 5 and 13 (Fig. 3.18, Fig.3.19). The one on chromosome 5, with LOD score 5.20 is significant at level 0.1, and is very close to the significance at the level of 5%, which require minimum 5.31 LOD score. The peak on chromosome 13 with LOD score 4.92 is very close to significance at the level of 10%, which is 4.94 LOD.

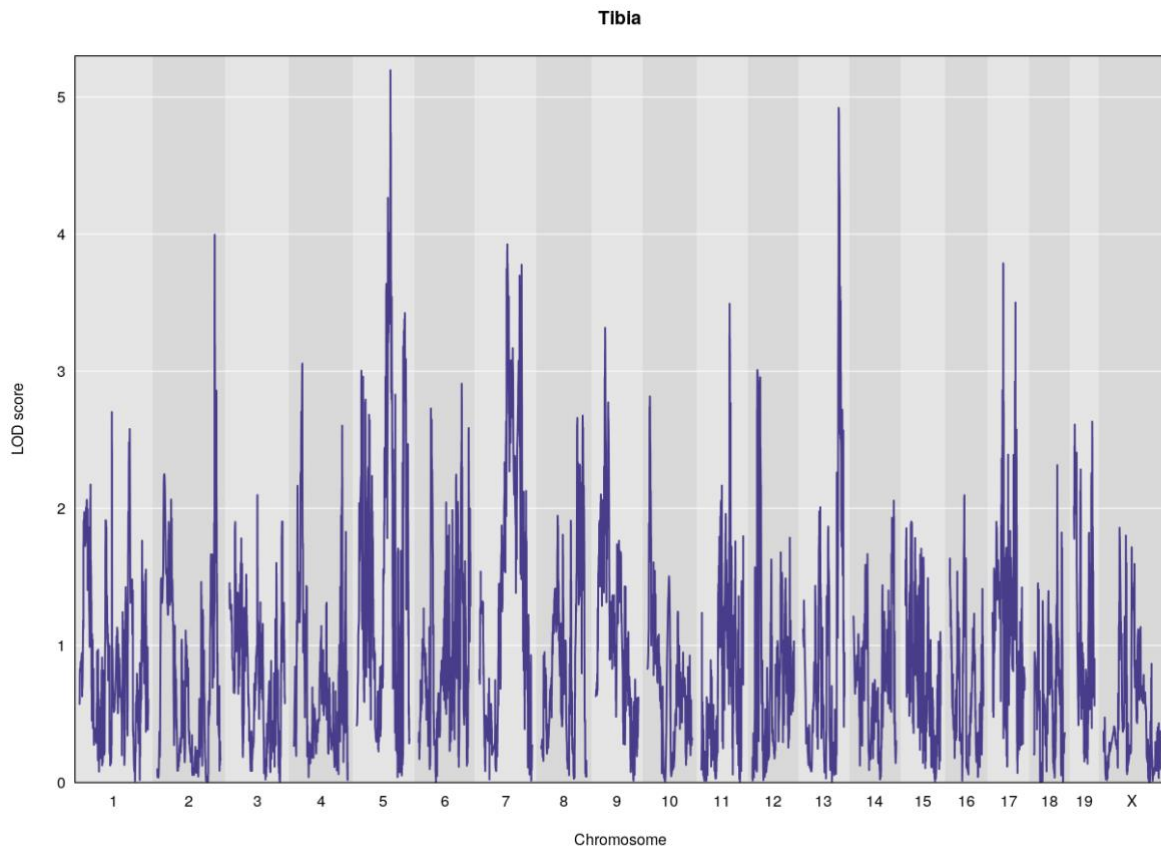


Figure 3.18. LOD scores in each chromosome in the tibia phenotype

The peak on chromosome 5 does not appear in any other tested phenotype. The region within confidence interval on this chromosome is 1.5 Mbp. The peak on the chromosome 13 is 3.69 Mbp size, which is the smallest among other phenotypes pointing to this region (Tab.3.11, Fig.3.20).

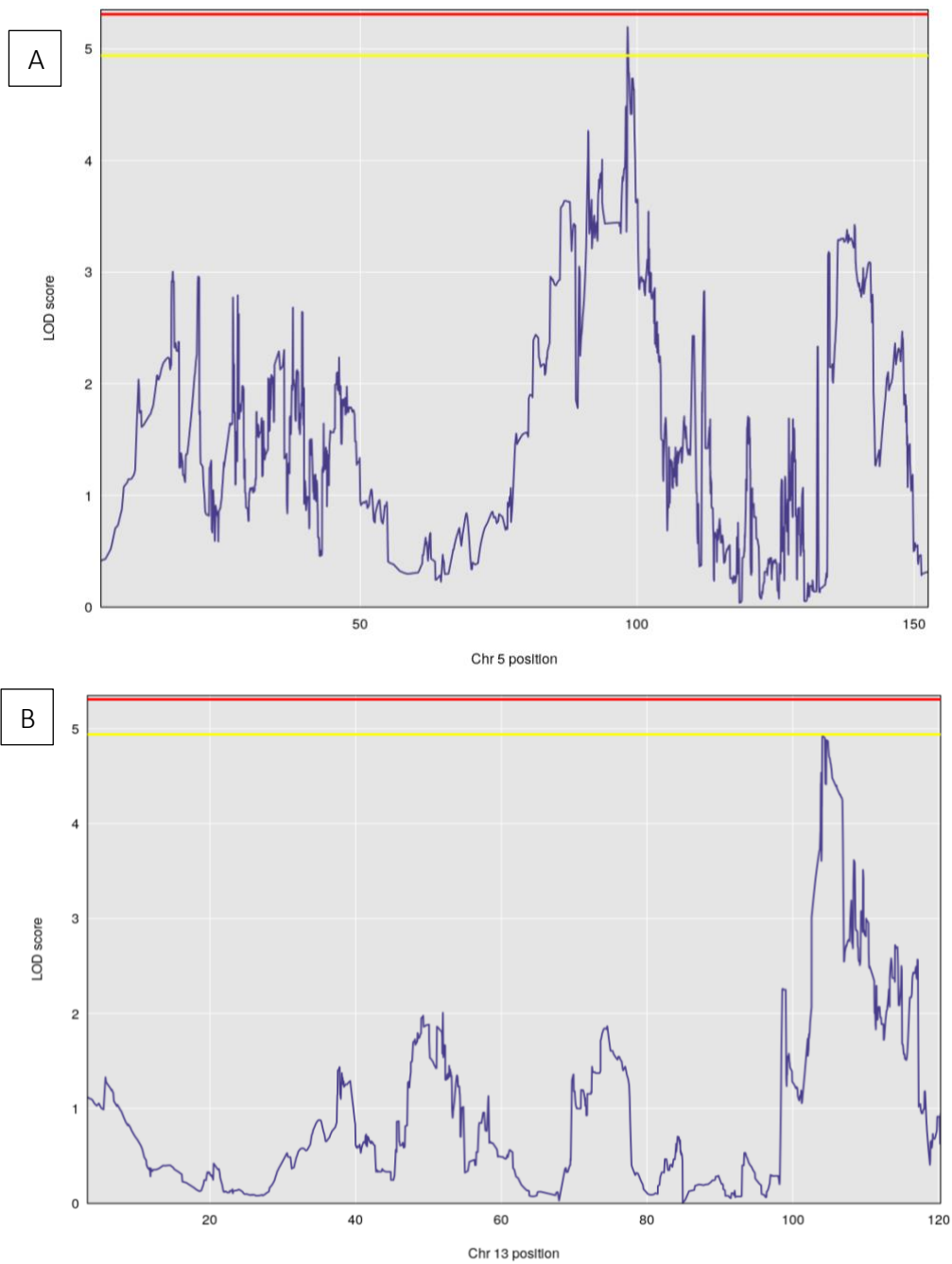


Figure 3.19. Visualization of the peak in chromosome 5 (A) and chromosome 13 (B), with the significance level lines: **red**: 5% and **yellow**: 10%

Candidate genes in each significant peak, and within the CI

The peaks and confidence intervals in ulna, femur and tibia, which were found significant are particularly interesting to describe in detail, as they are with close linkage to genes which are likely to affect the variance of the analysed phenotypes (Tab.3.12). The information on the candidate genes come from the MGI database.

Table 3.12. Candidate genes in peak position in each significant result per bone, and skeleton phenotype candidate genes in the confidence interval region

Bone	chromosome	Peak candidate gene	Skeleton phenotype candidate genes	Other phenotype candidate genes
Ulna	chr 6	<i>2010013B24Rik</i>	<i>Sox5, Kras,</i>	<i>Sspn</i>
	chr 13	<i>Trim23</i>	<i>Adamts6, Mast4, Cwc27</i>	<i>Trim23</i>
	chr 15	<i>Cdh10</i>	-	<i>Cdh10</i>
Femur	chr 8	<i>Gm32477</i>	<i>Cdh11</i>	<i>Cdh8, Got2</i>
Tibia	chr 5	<i>Gm34097</i>	<i>Prdm8, Bmp3, Prkg2,</i>	<i>Fgf5, Antxr2</i>
	chr 13	<i>Mast4</i>	<i>Adamts6, Cwc27</i>	<i>Trim23</i>

Chromosome 5

The candidate genes in chromosome 5 show very clear connection with skeletal morphology. The total number of genes in the CI is greater and include also those related to other phenotypes, such as for example *Fgf5* (fibroblast growth factor 5) which affects hair growth.

Prdm8 is a PR domain containing gene 8. It belongs to the Prdm gene family, which are known to be involved in processes of cell differentiation, and therefore are important in embryonic development, but also have been associated with cancer. They are characterised by PR domain. *Prdm8* is particularly important in the mouse nervous cell, and is active in cell's nucleus (Ross et al., 2012). The mutations of *Prdm8* are found to be related to abnormal tooth morphology and decreased caudal vertebrae number, but there is no evidence whether it affects long bone

properties. It is known to be expressed in muscle tissue of heart and tongue, but not in skeletal muscle. Postnatally it is expressed in the limb, however the results of its expression profile in tibia bone are ambiguous. As this gene is the closest one to the tibia length peak in chromosome 5 (0.3Mbp) it still might be a possible candidate affecting the tibia length. One of the interesting functions of the *Prdm8* is that it regulates mouse testis steroidogenesis (Eom et al., 2009). Since hormones are important environmental element contributing to skeleton, it might be a relevant trail to follow.

Bmp3 encodes bone morphogenetic protein 3 and is found within 1Mbp to the peak. The BMP3 is among the earliest discovered protein of the BMP family. It belongs to the transforming growth factor β (TGF- β) superfamily of signal molecules. Just as other genes of the family, the *Bmp3* is involved in numerous biological processes related to bone, including cartilage development, ossification and osteoblast differentiation. It is found in extracellular region and is active in cellular component. The BMP3 is a negative regulator of bone density, and targeted disruption induces the development of trabecular bone, which is porous form of a bone tissue (Bahamonde and Lyons, 2001). In homozygous knockout mice increased bone density was found, in contrast to bone defects such as tibia fracture when the *Bmp3* is overexpressed. In a way it is therefore restricting bone growth. The experiments on zebrafish showed that it is expressed in the embryo 48 hours after fertilization in pectoral fins and forming jaw. *Bmp-3* is also essential to skull development, and fine mapping of dog skull shape showed its association with variability of craniofacial shape fluctuations between different breeds. The *Bmp3* is expressed in perichondral cells which form connective tissue surrounding cartilage of developing bone. It is found to be expressed in mesenchyme of forming axial skeleton and limbs as early as TS13 (embryonic days 8-9.25). The BMP3 protein is essential also for repair process in the bone and is found in osteoblasts and osteocytes in fully-grown bone (Kokabu and Rosen, 2017).

Prkg2 encodes a protein cGMP-dependent kinase 2 (cGKII). *Prkg2* is located a little bit over 1Mbp from the tibia peak in chromosome 5. The function of this gene is regulation of intestinal secretion, as well as bone growth. Mutations in this gene in mice affect the skeleton in many ways, including shorten long bones, effecting from abnormal bone ossification. The evident

effect of *Prkg2* mutation is dwarfism, which was described not only in mice, but also humans, rats and even angus cattle (Tsuchida et al., 2008; Koltes et al., 2009). The study on mutant rats shows, that the protein cGKII is a molecular switch which slows down proliferation and begin hypertrophic differentiation of chondrocytes. Therefore, it proves to be a highly possible candidate because of developmental nature of the long bones, which is achieved by endochondral ossification. Importantly, the region of over 10 Mbp is conserved among human, rat and mouse. The cGKII deficient mice also exhibited faulty growth of the long bones.

Chromosome 6

The peak on chromosome 6 points to *2010013B24Rik*. It is a cDNA sequence established by the RIKEN project, and is found to be expressed in the adult mouse (Theiler stage 28) in femur and tibia. Two excellent candidate genes are found in the confidence interval: *Sox5* and *Kras*.

Sox5

The *Sox5* gene is found within 0.5Mbp from the ulna length peak on the chromosome 6. SOX5 belongs to the Sox family of 20 genes, which are key development genes of chordates. They encode proteins, which are characterised through the SRY (sex-determining of Y chromosome) which codes for high mobility group (HMG) protein. *Sox5* and *Sox6* belong to the D block of the Sox gene family (SoxD), both of them are highly similar and are expressed in cartilage. *Sox5*, *Sox6* and the *Sox9* are essential genes in chondrogenesis, but *Sox9* was shown to be necessary in earlier stages of embryonic development. Naturally, *Sox5* is found to be expressed in bones in animals postnatally, as well as in the fetus in mesenchyme, from which the limb forms. In humans SOX5 was also associated with atrial fibrillation, which is a heart condition, which causes irregular heart rate. Haploinsufficiency of *Sox5* has also been linked to a rare condition called Lamb-Shaffer syndrome, which causes mild craniofacial dysmorphism, intellectual disability and development delay. It shows the wide range of SOX5 function. It is though essential, that the bone has also multiple function, aside from locomotion.

Kras

Kras (Kirsten rat sarcoma virus) is found as close as 0.05 Mbp to the peak on 6th chromosome. It encodes a protein KRAS which is essential in the pathway MAPK/ERK, which is key in communication between cell and extracellular environment. Its mutations are known to be a cause of Noonan syndrome in humans, causing unusual skeletal morphology, but is also related to wide range of other conditions, such as acute myeloid leukaemia. It is a blood cancer, which has its beginning in the bone marrow. *Kras* has been associated with non-ossifying fibroma, common lesions of skeleton (Baumhoer et al., 2019).

Chromosome 8

In the peak on chromosome 8, *Gm32477* is present; It also is situated within the small QTL marker (*Desp1*). The QTL marker found within the peak on chromosome 8 was previously described as a region related to depression in mice, evaluated by the forced swimming test (FST)(Yoshikawa et al., 2002). More recent studies suggest that the method does not reflect depression, but rather mechanisms of coping with stress, and as such many factors could be represented by it (Armario, 2021). It would be therefore a very interesting region worth of further investigation.

Cdh11

Within the confidence interval of femur on chromosome 8, cadherin-11 gene can be found, at the minimum distance of 0.88Mbp from the peak. It is another cadherin gene found in this study and is often reported to be co-expressed with *Cdh10*, which is candidate gene of ulna length. Upstream of the peak, *Cdh8* is also situated within the CI, but it is further away from the peak (over 1Mbp). The human ortholog, *CDH11* is involved in Elshahy-Waters syndrome, a rare branchioskeletogenital condition affecting craniofacial shape and mental abilities among other issues. It is therefore a good candidate gene, as it shows that it affects the skeleton.

Chromosome 15

Cdh10 is a cadherin 10 gene, found within the ulna length peak on chromosome 15. According to the MGI database, mutant mice exhibit decreased circulating insulin level in males, and abnormal cholesterol homeostasis. Microphthalmia is also documented in female mutants. Although the role of this particular cadherin gene in skeleton or limb formation is not known, it might be a very interesting candidate, because bone has also endocrine regulation function. It is worth further studying in experimental manner, similar to *Cdh11* found in the femur peak. Cadherins are proteins responsible for cell-to-cell adhesion, essential in formation of tissues, and a key invention in metazoans relevant in cell migration during embryonic development. Consequently, the *Cdh10* is found to be expressed in embryo mesenchyme and forming limb buds at 22TS. Other cadherin-family genes, such as *Cdh11* and *Cdh2* have documented role in skeleton (Marie et al. 2013; Marie et al., 2014). Craniofacial-deafness-hand syndrome (CDHS) was associated with *CDH10* mutations in human, where one of the symptoms was ulna deformation (Sommer and Bartholomew, 2003). Just like *Cdh11*, *Cdh10* belongs to N-Cadherins. Overexpression can inhibit cell proliferation. In humans, somatic mutation of *CDH10* were found in the lung cells in people with lung cancer, together with mutations of *KRAS* gene as well as *PTEN*, among few other features. Interestingly, *Kras* is one of the candidate gene in ulna on chromosome 6, found very close to the peak, and *Pten* is found in the suggestive peak on chromosome 19 in humerus. The *Cdh10* was also found associated with autism spectrum disorder in rat model.

Chromosome 13

Peaks in chromosome 13 were observed in the genome scan results of the radius, ulna, scapula and tibia. Although it was only significant in the ulna, it can be speculated that this region was relevant in all of these bones, either as a result of pleiotropy or existing linkage of more than one gene. The lengths of forearm bones and shank bone (tibia) are strongly correlated, and especially in the females, scapula is also correlated with them.

As shown in Fig.3.20., the results point to roughly similar region, but the peaks do not point to exact same markers. To further confirm or exclude pleiotropy, different analyses might be necessary. The entire region, if combined from the earliest point of the confidence interval to the last one among phenotypes, is linked to several QTLs (according to MGI data), often mapped in skeleton-related traits: *Tbqt5* (tibia bone quality traits 5), *Skmw18*, 77, 78 79, 80 (Skeletal muscle weight), *Tailaq3/Taliq3* (tail length quality trait), *Fbtq6* (Femoral bone trait quality), *Egaq4* (early growth adjusted quality trait).

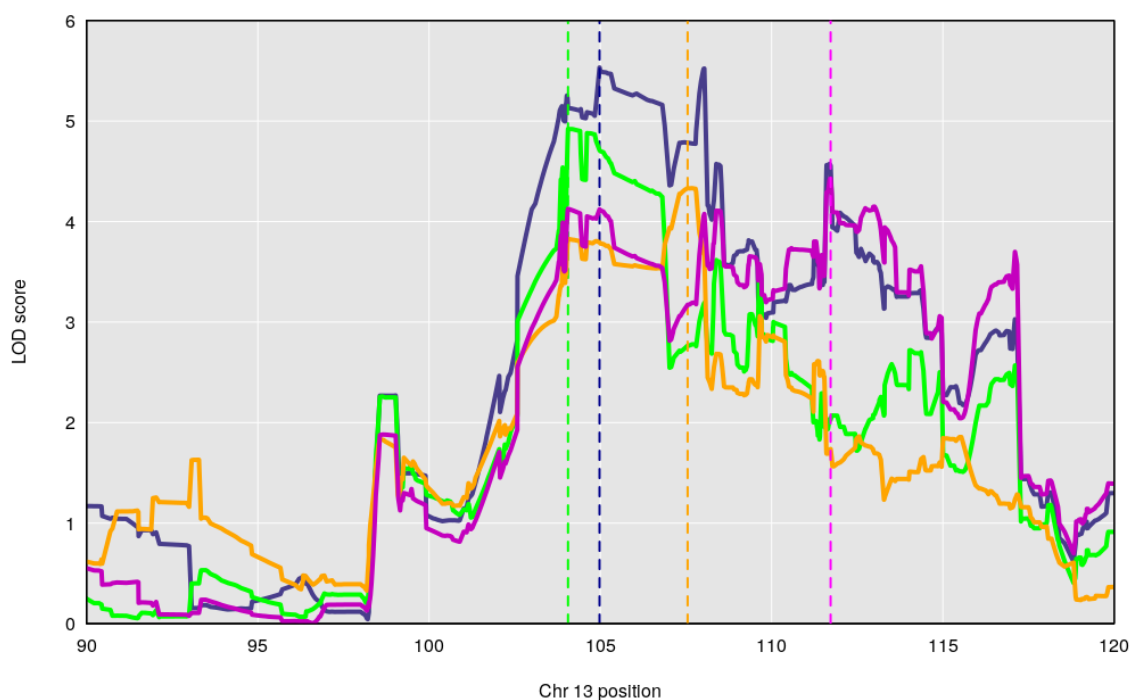


Figure 3.20. All suggestive peaks on chromosome 13: **dark blue** – ulna, **green** – tibia, **magenta** – radius, **orange** – scapula; vertical dashed lines show the position of highest LOD score of each phenotype

Genes in the CI region of the chromosome 13

Mast4 - stands for microtubule associated serine/threonine kinase family member 4.

This protein coding gene is experimentally proven to have effects on skeleton morphology. It is also related to the immune system phenotype responsible for lymphocyte numerousness. The mutant mice exhibit malocclusion, which is characterized with crooked bite. The *Mast4* is also expressed in long bones, such as femur and tibia, as well as muscles of the hindlimb. *Mast4* is

found within the peak of chromosome 13 in the tibia length, as well as within the confidence interval in ulna, in the distance of 0.8Mbp from the peak. In humans, *MAST4* is expressed in multiple myeloma bone marrow cells, which is a bone tissue cancer, and speculated is its role in osteoclast activation. Moreover, functional interaction with *PTEN* was reported (Zhang et al., 2018). As mentioned earlier, *Pten* was found in the suggestive peak of the humerus, and due to susceptibility of autoimmune disease and bone lesions reported in the G15 mice, such pathway could be highly likely to contribute to eventual length of long bones. On the other hand, *Pten* appears to be controlling *Kras* gene.

Adamts6 - disintegrin-like and metallopeptidase (reprolysin type) with thrombospondin type 1 motif, 6. *Adamts6* is a candidate gene found on chromosome 13 in ulna and tibia. In case of ulna, it is only 0.1 Mbp from the peak, and roughly 1.1 Mbp from the peak in tibia. Mutations of this gene were reported to affect skeleton, including abnormal hindlimb and vertebrae morphology, cleft palate and sternebra fusion. These reports make *Adamts6* a possible contributor to lengths of limb bones in G15 mice, however the evidence on how this gene is contributing to formation of skeleton is absent. The molecular function of the *Adamts6* is metal ion binding and the gene is also active in extracellular matrix. It is a known gene important in processes such as aorta, heart and kidney development as well as proteolysis. The gene has low expression in skeleton in most of the species and is not known to interact with other genes found in this study.

Trim23 is a tripartite motif-containing 23. It is a gene found in the peak region in ulna on the chromosome 13. It does not have recognized function in the limb skeleton; however, it is expressed postnatally in the femur and tibia. In the case of the femur, it was detected in femur diaphysis as well as metaphysis. The human ortholog of this gene, *TRIM23* is known to contribute to carcinogenesis when overexpressed (Han et al. 2020).

Cwc27 is a spliceosome-associated protein, found near the peak of ulna and tibia of the chromosome 13. The *Cwc27* is expressed in embryo mesenchyme, and in the limbs from the TS17. The spliceosome component *CWC27* in humans causes a rare condition of metaphyseal chondrodysplasia with retinal degeneration. Mutations of this gene have severe consequences in mouse, and are in most cases postnatally lethal. Embryos exhibit abnormalities, such as

growth retardation and lack of limb buds (Xu et al., 2017). It is therefore an excellent candidate gene to the zeugopod bones.

Other candidate genes from this study

Pten - Phosphate and tensin homolog, Mirzamohammadi et. al (2018) described pathoetiology of Feingold syndrome on mouse model, which causes skeletal development issues. Importantly the ***Pten*** mutation was related with macrocephaly, among other issues. ***Sspn*** - (Sarcospan) is a gene found roughly 0.6 Mbp from the peak in chromosome 6, but has no known function in long bone morphology. However, it is associated more with limb muscles than skeleton. ***Antxr2*** - anthrax toxin receptor 2.

Most candidate genes were within 1 Mbp distance from the LOD score peak (Tab.3.13). Aside from genes found within the respective peaks, candidate genes such as *Kras* and *Adamts6* were in the maximum distance of less than 0.5 Mbp.

Table 3.13. Position of the most relevant candidate genes (derived from the RGD resources for each gene in the in GRCh38/mm10 annotation) and their minimum and maximum distance to the peak (Mbp) LOD score in each phenotype

Bone	Chr	Gene	Gene pos_lo	Gene pos_hi	Peak position	min. distance	max. distance
ulna	chr6	<i>Sox5</i>	143.828425	144.782287	145.304160	0.52	1.48
		<i>Kras</i>	145.216699	145.250420	145.304160	0.05	0.09
	chr13	<i>Adamts6</i>	104.286518	104.496695	104.186732	0.10	0.31
		<i>Mast4</i>	102.732486	103.335099	104.186732	0.85	1.45
		<i>Cwc27</i>	104.631140	104.817110	104.186732	0.44	0.63
tibia	chr5	<i>Prdm8</i>	98.167203	98.187454	97.843261	0.32	0.34
		<i>Bmp3</i>	98.854415	98.884053	97.843261	1.01	1.04
		<i>Prkg2</i>	98.929773	99.037375	97.843261	1.09	1.19
	chr13	<i>Adamts6</i>	104.286518	104.496695	103.266184	1.02	1.23
		<i>Mast4</i>	102.732486	103.335099	103.266184	0.07	0.53
		<i>Cwc27</i>	104.631140	104.817110	103.266184	1.36	1.66
femur	chr8	<i>Cdh11</i>	102.632095	102.785493	101.749607	0.88	1.04
		<i>Cdh8</i>	99.024471	99.417666	101.749607	2.33	2.73

3.3.3. Bone covariates – mapping of residual bone values

As the first thing, permutations for the autosomes and the chromosome X were run for each of the model, and the thresholds at 0.05 and 0.1 significance level was acquired (Tab.3.14).

Table 3.14. Significance levels based on permutations of each covariate model

Bone	sign. Level	humerus	radius	ulna	scapula	femur	tibia
humerus as a covariate							
autosomes	0.05		5.30	5.31	5.67	5.33	5.31
	0.01		4.95	4.96	5.21	4.99	4.95
chr X	0.05		3.72	3.65	3.81	3.63	3.63
	0.01		3.33	3.26	3.38	3.25	3.25
ulna as a covariate							
autosomes	0.05	5.34	5.28		5.53	5.30	5.35
	0.01	4.96	4.94		5.11	4.93	4.98
chr X	0.05	3.48	3.52		3.81	3.63	3.63
	0.01	3.10	3.16		3.38	3.25	3.25
scapula as a covariate							
autosomes	0.05	5.33	5.35	5.33		5.36	5.32
	0.01	4.97	4.97	4.96		4.99	4.99
chr X	0.05	3.52	3.77	3.71		3.80	3.94
	0.01	3.14	3.36	3.32		3.39	3.53
femur as a covariate							
autosomes	0.05	5.38	5.35	5.32	5.46		5.35
	0.01	5.00	4.95	4.98	5.06		4.97
chr X	0.05	3.52	3.74	3.69	3.90		3.72
	0.01	3.15	3.34	3.31	3.48		3.33
tibia as a covariate							
autosomes	0.05	5.36	5.31	5.27	5.42	5.38	
	0.01	4.99	4.96	4.93	5.03	5.01	
chr X	0.05	3.50	3.59	3.61	4.02	3.72	
	0.01	3.13	3.21	3.25	3.58	3.32	

The genome scan was then run for each of the models, and the significant or close to significant peaks were listed (Tab.3.15). The numerous candidate regions identified in the above mapping models, clearly show that the covariation between different skeletal elements have genetic bases. In some cases, for example when the femur is a covariate to the ulna, we see the same candidate regions as for the ulna as an individual trait. It also was possible to find significant intervals in the elements such as the radius and scapula, for which none were found when they were analysed as individual traits. The humerus however, was still underrepresented, and only one peak was found on the chromosome X, close to suggestive level in tibia covariate model.

Table 3.15. List of significant and suggestive regions in each of the four models (GRCm38/mm10); rows in **bold** are significant at 0.05 level, lines in **blue** are significant at 0.1 level, lines in **dark red** are close to 0.1 significance level; * - marks intervals overlapping with the individual traits

Humerus as a covariate	chromosome	CI_lo (Mbp)	CI_hi (Mbp)	peak	size (Mbp)	Peak LOD	Peak marker
Radius	chr13	110.809512	114.172813	110.912761	3.36	5.90	UNC23366708*
Ulna	chr13	110.809512	114.172813	110.853764	3.36	5.05	UNC23365666
Femur	chr8	94.937544	103.530655	101.909615	8.59	5.05	UNC080531125*
Femur	chr18	82.238408	83.484377	82.947584	1.25	4.94	UNC29730171
Ulna as a covariate	chromosome	CI_lo	CI_hi	peak	size (Mbp)	Peak LOD	Peak marker
Radius	chr12	43.196752	44.57891	44.024835	1.38	5.10	UNC21005137
Scapula	chrX	138.968699	139.755063	139.425706	0.79	3.85	backupUNC200714769
Scapula	chrX	52.175460	92.534802	70.701585	40.36	3.75	UNC30941922
Scapula	chr19	40.660922	41.155811	41.018751	0.49	5.06	UNC30323050
Scapula	chr19	41.623728	42.239070	41.883114	0.62	5.06	UNC30334487
Tibia	chr7	50.593770	55.123751	50.996161	4.53	5.47	UNC12816185
Scapula as a covariate	chromosome	CI_lo	CI_hi	peak	size (Mbp)	Peak LOD	Peak marker
Femur	chr8	95.708605	103.078212	101.749610	7.37	5.23	UNC15386001*
Tibia	chr5	96.740873	97.577842	97.498701	0.84	5.45	JAX00133267*
Tibia	chr5	97.772694	99.642152	98.788981	1.87	6.25	JAX00589522
Femur as a covariate	chromosome	CI_lo	CI_hi	peak	size (Mbp)	Peak LOD	Peak marker
Ulna	chr15	8.929676	14.271753	12.815665	5.34	5.37	UNC150010223
Ulna	chr15	14.589430	15.307834	15.011232	0.72	5.02	UNC25088194
Ulna	chr15	18.535992	20.094186	18.688819	1.56	5.18	UNC25138352*
Ulna	chr13	101.723711	107.768813	102.998350	6.05	5.01	UNC23249870*
Ulna	chr6	147.396366	149.516148	149.298318	2.12	4.97	UNC12365003*
Scapula	chrX	86.045529	95.512422	87.001461	9.47	3.86	UNC31057902
Tibia	chr7	115.193996	116.898797	115.560466	1.70	4.94	UNC13672779
Tibia as a covariate	chromosome	CI_lo	CI_hi	peak	size (Mbp)	Peak LOD	Peak marker
Humerus	chrX	155.633055	157.187734	157.187734	1.55	3.11	UNC31498203
Radius	chr9	47.858302	48.007626	47.858302	0.15	5.36	UNC16312568
Ulna	chr1	88.781967	91.756731	91.103492	2.97	5.25	UNC1138455
Ulna	chr15	9.815496	13.144770	10.681208	3.33	5.64	backupUNC150003978
Femur	chr14	21.354907	21.518738	21.417047	0.16	5.11	UNC23675570
Femur	chr14	20.152337	21.035888	20.429890	0.88	5.07	UNC23664511
Femur	chrX	157.713777	159.875717	159.875717	2.16	3.97	UNC31517925

What is striking is that there was a large number of CI situated on chromosome X, including two peaks in the scapula and the ulna covariate, and one peak in the femur covariate model. Below I characterise significant results in each model.

I. Model: humerus is a covariate

Humerus is the bone with possibly more bias coming from the phenotyping method. Nevertheless, by using the best selected measurements of this bone as a covariate to the other phenotypes, a strong peak was identified in the radius bone. It is once again, a peak on chromosome 13, which overlaps to the same region as when radius was mapped as an individual bone (Fig.3.21 and 3.22).

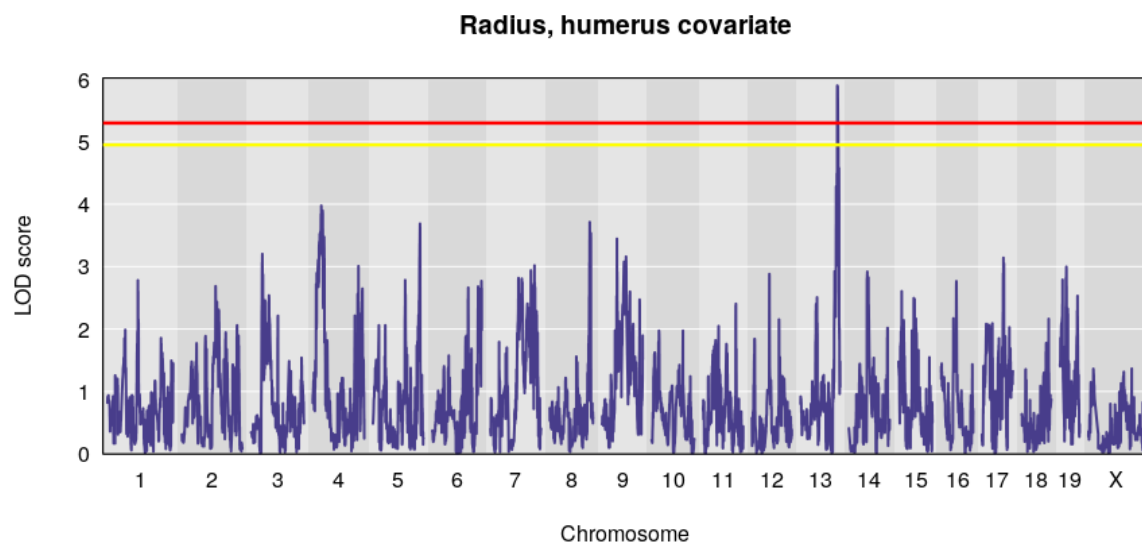


Figure 3.21. Radius LOD score graphs in the humerus covariate mapping model, with the significance level lines: **red**: 5% and **yellow**: 10%

Albeit with lower significance, the exact same region is present in the ulna in the model with the humerus covariate. Interestingly, it is not overlapping the CI region which was significant in the individual ulna bone length mapping (Fig.3.22).

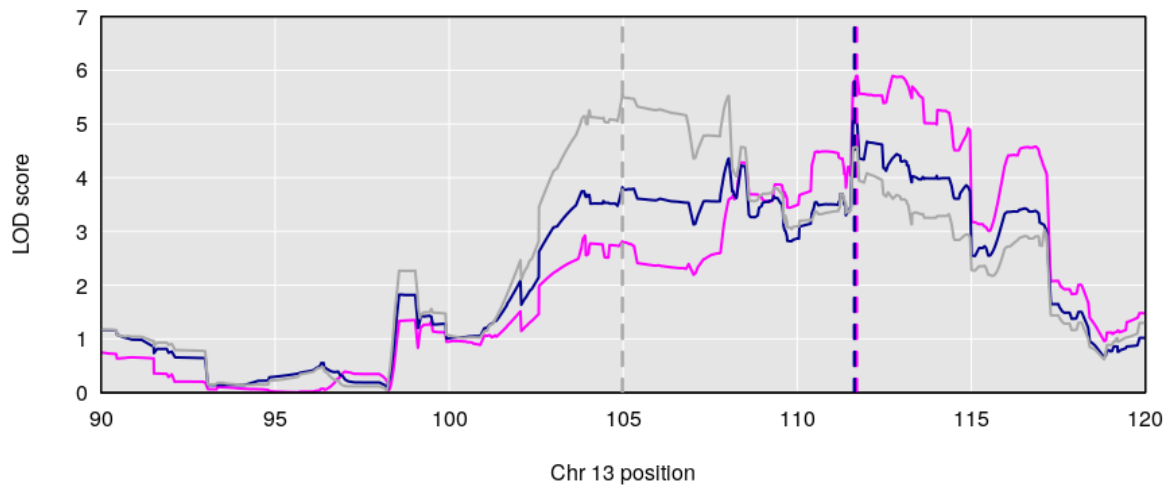


Fig.3.22. Significant peaks on chromosome 13, in the model with humerus covariate: **magenta** – radius, **dark blue** – ulna; the **dark grey** line and dashed vertical line represents the ulna peak in original raw mapping model

In case of the femur, on the chromosome 8 there was one peak which overlapped with the raw femur bone length confidence interval. However, the peak position was shifted, and was not found within the *Desp1* QTL marker (Fig.3.23, Tab.3.16). One peak was also very close to significance on the chromosome 18.

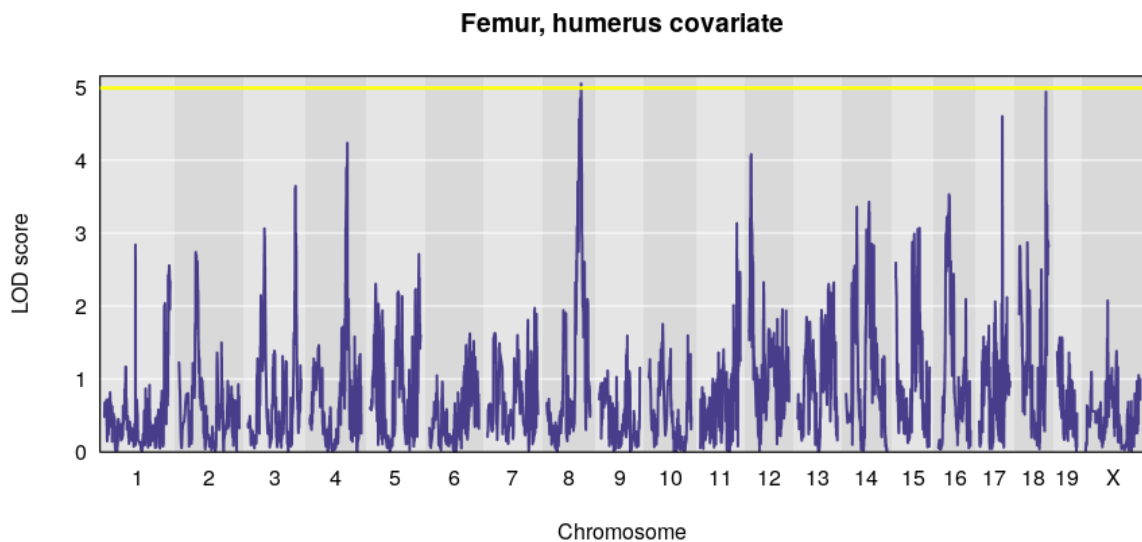


Figure 3.23. Femur LOD score graphs in the humerus covariate mapping model, with the significance level lines: **yellow**: 10%

Table 3.16. Peak candidate gene, and relevant phenotype candidate genes in the humerus covariate model

Humerus is a covariate	chromosome	Peak position (Mbp)	Peak candidate gene	candidate genes in CI
Radius	chr13	110.912761	-	<i>Map3k1, Il6st, Il31ra, Dhx29</i>
Ulna	chr13	110.853764	-	<i>Map3k1, Il6st, Il31ra, Dhx29</i>
Femur	chr8	101.909615	-	<i>Cdh8, Katnb1, Prss54,</i>
Femur	chr18	82.947584	<i>Zfp516</i>	<i>Zfp236, Mbp</i>

Excellent candidate genes were found in the CI in the radius and ulna with humerus covariate. Among them, *Il31ra* (interleukin 31 receptor A) and *Il6st* (interleukin 6 signal transducer) are especially recognised to affect long bones.

II. Model: ulna as a covariate

Ulna is characterised by strong correlation with bones such as radius, scapula and tibia. As previously mentioned, these bones displayed a peak in chromosome 13, which could affect their lengths through pleiotropy or because of existence of multiple genes within the region with a strong LD. When the ulna is modelled as a covariate to these bones, the peak in the chromosome 13 is no longer displayed. The radius bone displays strong suggestive peaks in the chromosome 12, as well as in chromosome 14 (below 0.1 significance level) (Fig.3.24).

As mentioned before, scapula shows two significant peaks in chromosome X, as well two peaks in chromosome 19, which are found just little below the level of statistical significance level, with the LOD scores of 5.06. In the tibia, a highly significant peak is present on the chromosome 7, with a LOD score of 5.47.

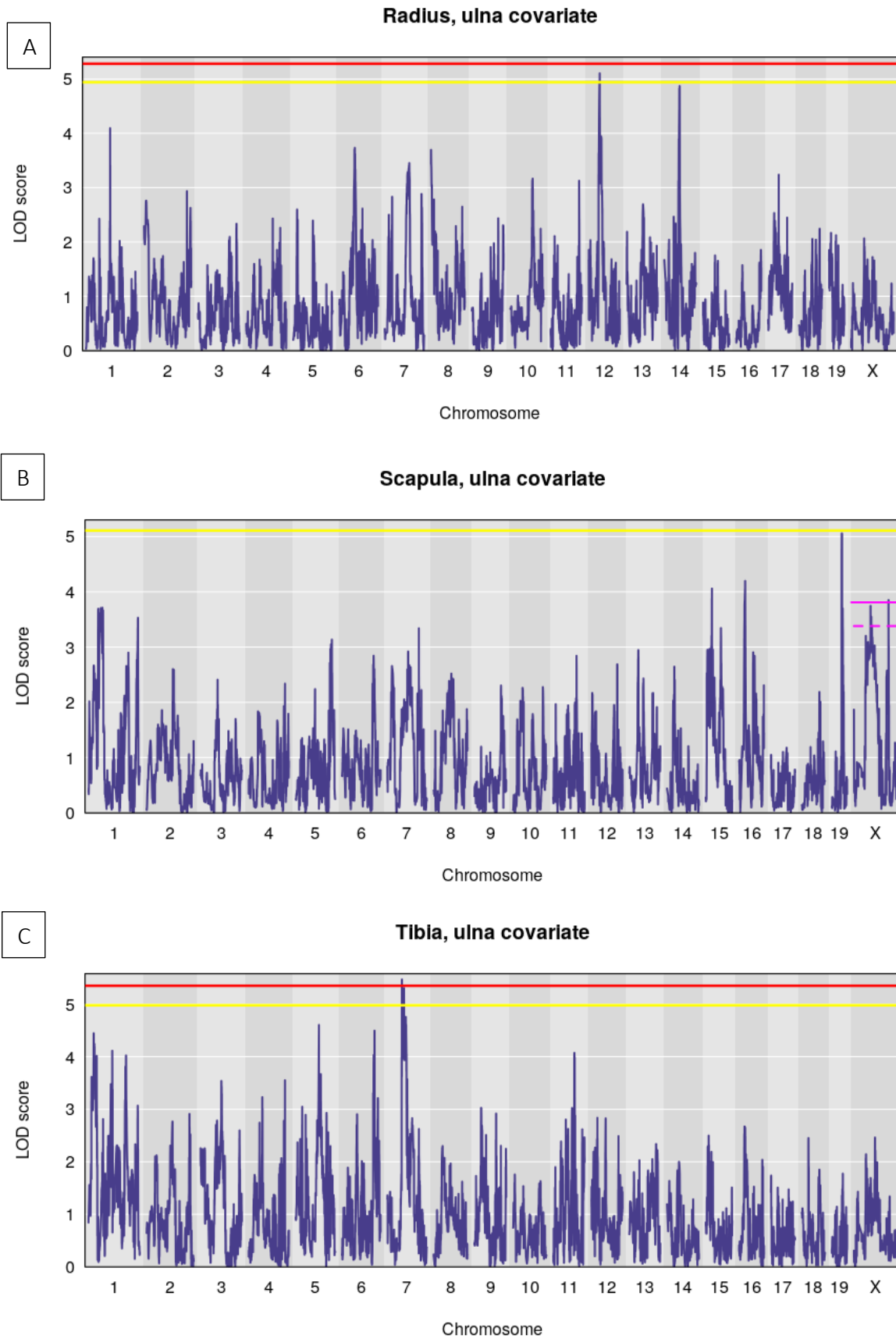


Figure 3.24. Relevant LOD score graphs of radius (A), scapula (B) and tibia (C) in ulna covariate model with the significance level lines: **red**: 5% and **yellow**: 10%, the vertical **magenta** lines indicate the significance levels in chromosome X (solid: 5%, dashed: 10%)

These results show, that although all these bones are correlated with each other, different genes are responsible for each of these connections.

Table 3.17. Peak candidate gene, and relevant phenotype candidate genes in ulna covariate model

Ulna is a covariate	chromosome	Peak position (Mbp)	Peak candidate gene	candidate genes in CI
Radius	chr12	44.024835	-	<i>Dnajb9, Pnpla8, Nrcam</i>
Scapula	chrX	139.425706	-	<i>Rnf128, Ripply1</i>
Scapula	chrX	70.701585	-	<i>Ids</i> , within proximity: <i>Mamld8, Mtm1</i>
Scapula	chr19	41.018751	-	<i>Dntt, Opalin, Tctn3</i>
Scapula	chr19	41.883114	<i>Rrp12</i>	<i>Sfrp5</i>
Tibia	chr7	50.996161	-	<i>Ano5, Nell1</i>

III. Model: scapula as a covariate

In the model where scapula is a covariate, only two bones showed significant or suggestive regions – femur and tibia (Fig.3.25). In the case of the femur, a peak in chromosome 8 overlaps with the peak found by scanning this bone as an individual trait. Reasonably close to the 0.1 significance level is a peak on chromosome 18.

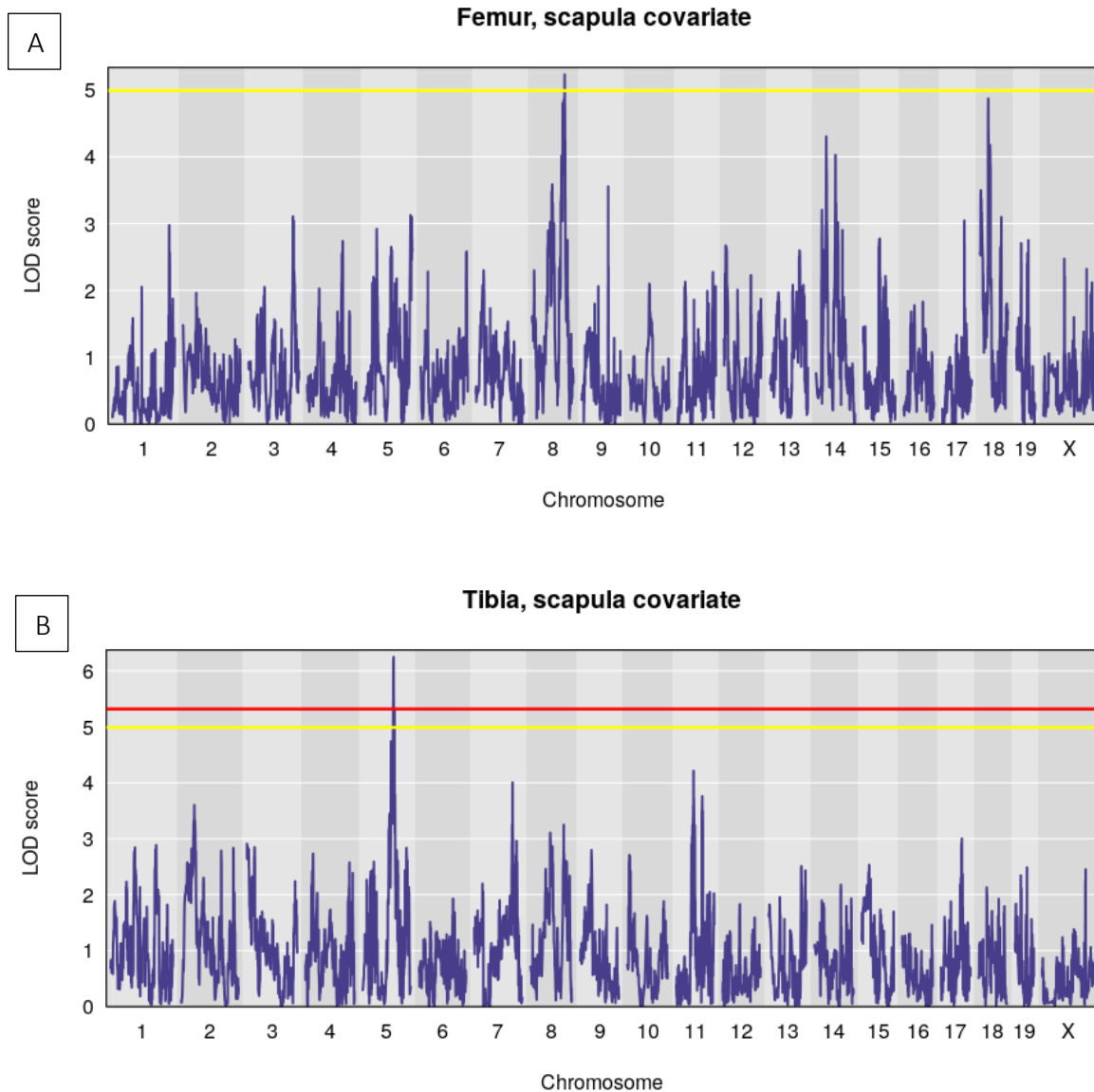


Figure 3.25. Relevant LOD score graphs of femur (A) and tibia (B) in scapula covariate model, with the significance level lines: red: 5% and yellow: 10%

Interestingly, in the tibia with the scapula as an additive covariate, chromosome 5 shows two significant peaks. There is one at 98 Mbp, with a confidence interval that overlaps with the peak in the tibia bone scan, and another one at 97 Mbp which is separated by large LOD drop (Fig.3.26).

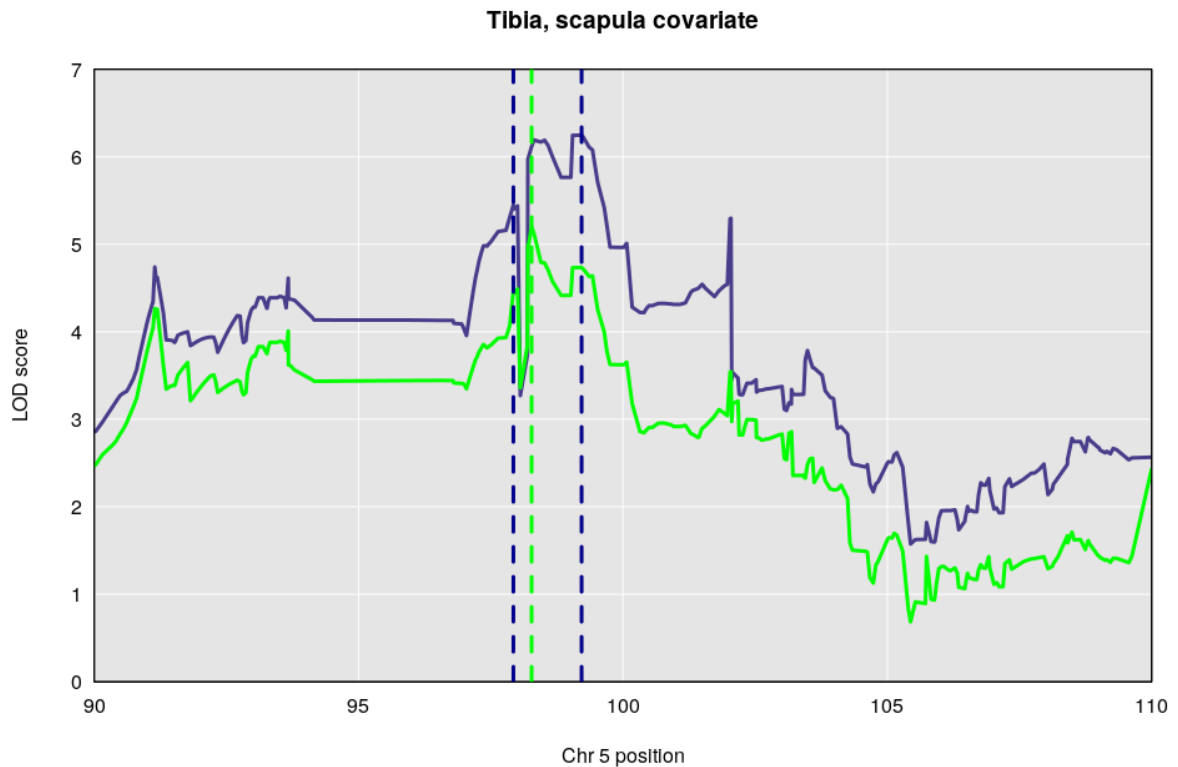


Figure 3.26. Position of the two LOD score peak on chromosome 5 in tibia with scapula as a covariate (blue dashed lines), and of the tibia as an individual bone (green colour lines)

Table 3.18. Peak candidate gene, and relevant phenotype candidate genes in the scapula covariate model

Scapula is a covariate	chromosome	Peak position (Mbp)	Peak candidate gene	candidate genes in CI
Femur	chr8	101.749610	-	<i>Cdh8, Cdh11</i>
Tibia	chr5	97.498701	<i>4930467D21Rik</i>	<i>Bmp2k, Fras1</i>
Tibia	chr5	98.788981	<i>Cfap299</i>	<i>Prdm8, Prkg2, Bmp3</i>

IV. Model: femur as a covariate

By using the femur as a covariate, new candidate intervals were identified in the ulna in the chromosome 15, aside from the one previously found for this bone. Here, the identified peaks in chromosome 13 and 6 could be caused either by lack of genetic covariation between these bones, or by the pleiotropic effect of candidate genes, similar as with femur and scapula covariate.

However, in this flipped model, we can also identify a peak in scapula on the chromosome X. Additionally, a peak in the tibia on chromosome 7 with LOD score of 4.94 was very close to the suggestive level of 4.97 LOD (Fig.3.27).

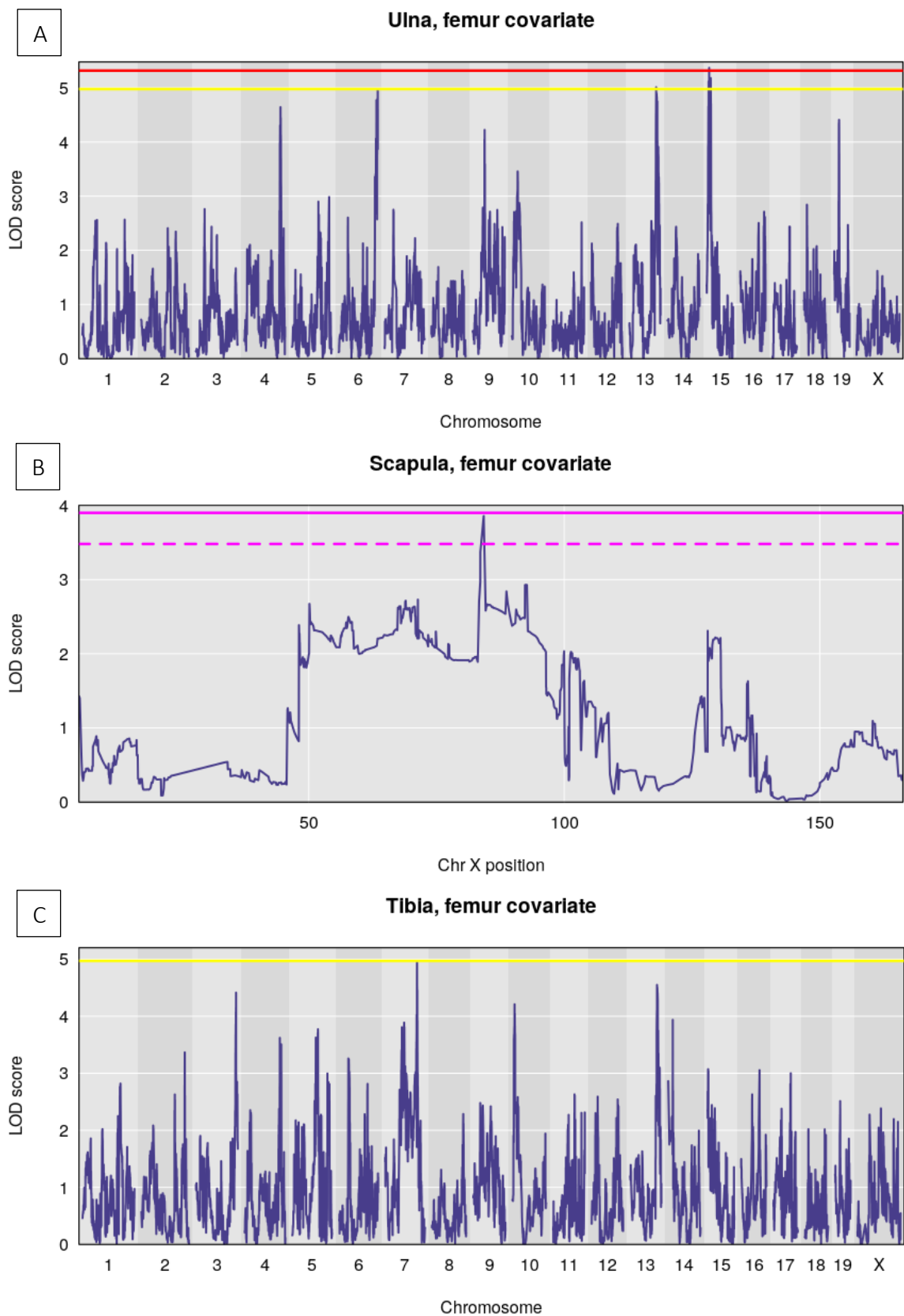


Figure 3.27. Relevant LOD score graphs of ulna (A), femur in the X chromosome (B) and tibia (C) in femur covariate model, with the significance level lines in autosomes: **red**: 5% and **yellow**: 10%, **red**: 5% and **yellow**: 10%, the vertical **magenta** lines indicate the significance levels in chromosome X (solid: 5%, dashed: 10%)

Table 3.19. Peak candidate gene, and relevant phenotype candidate genes in femur covariate model

Femur is a covariate	chromosome	Peak position (Mbp)	Peak candidate gene	candidate genes in CI
Ulna	chr15	12.815665	<i>6030458C11Rik</i>	<i>Prlr, Npr3, Spef2, Dnajc21, Rad1, Rai14, C1qtnf3, Golph3</i>
Ulna	chr15	15.011232	-	-
Ulna	chr15	18.688819	<i>C030047K22Rik</i>	<i>Cdh10</i>
Ulna	chr13	102.998350	<i>Mast4</i>	<i>Adamts6, Mast4, Cwc27, Nln</i>
Ulna	chr6	149.298318	-	
Scapula	chrX	87.001461	<i>Il1rapl1</i>	<i>Nr0b1, Gspt2, Amer1</i>
Tibia	chr7	115.560466	<i>Sox6</i>	<i>Sox6</i>

V. Model: tibia is a covariate

Tibia, radius and ulna belong to zeugopod part of the mouse limb. Therefore, genetic basis of phenotypically expressed correlation might be expected. One of the most interesting results is that the relationship of radius-tibia and ulna-tibia is controlled by the different set of QTL regions (Fig.3.28). Radius shows a significant peak at the chromosome 9 (5.36 LOD score), while the ulna bone shows two peaks at the chromosome 1 and chromosome 15 (5.25 and 5.64 LOD scores). The confidence interval of chromosome 15 is overlapping slightly with the peak on the same chromosome in femur covariate model and individual ulna mapping model.

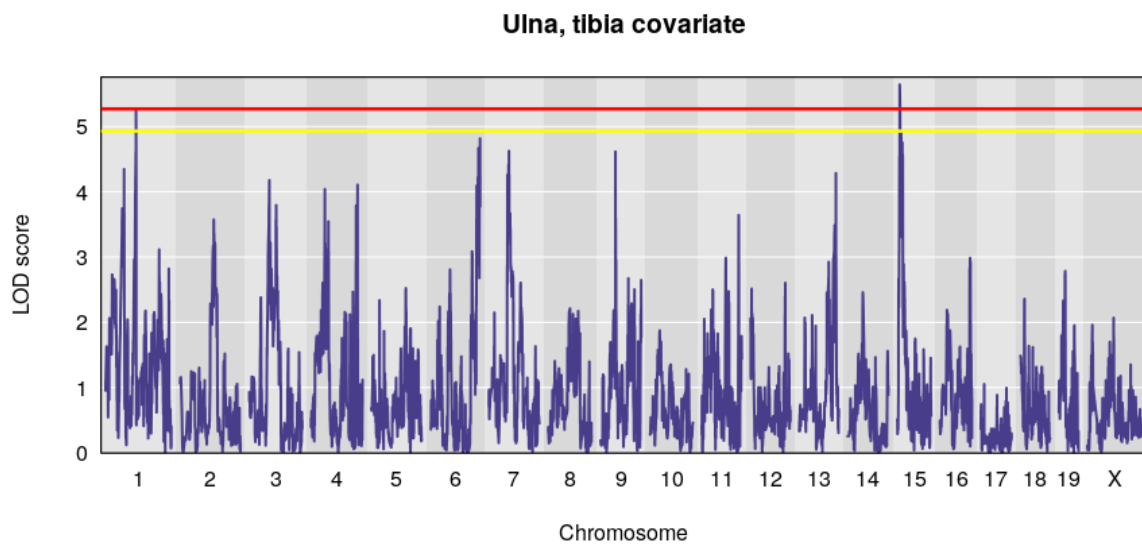
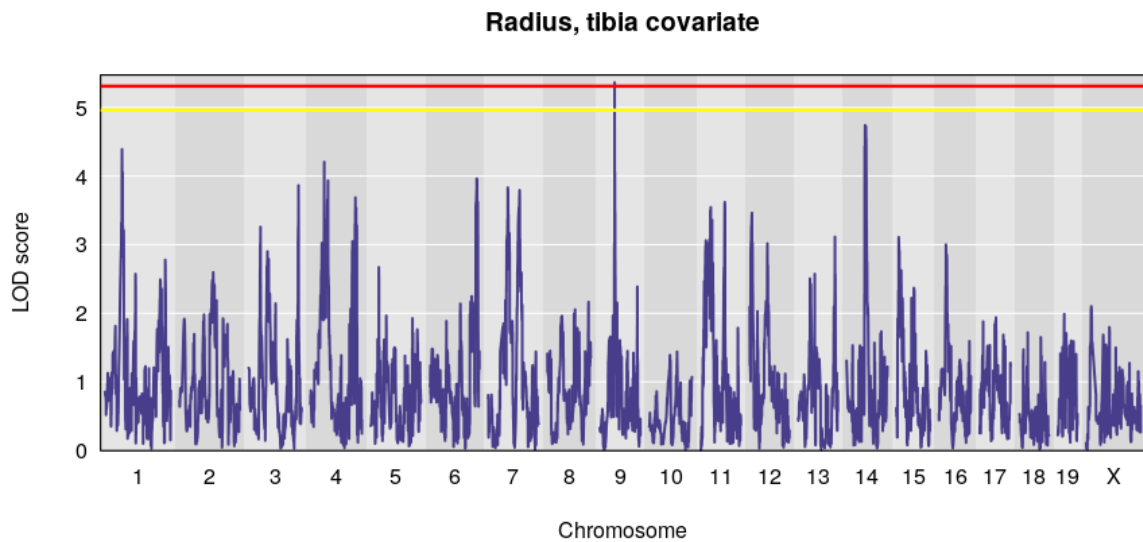


Figure 3.28. Relevant LOD score graphs of radius and ulna in the tibia covariate model, with the significance level lines: **red**: 5% and **yellow**: 10%

Femur and tibia which are bones of the hind limb show medium strength correlation in the population of G15 mice. Two peaks are nevertheless visible on the chromosome 14 within a suggestive significance level (with 5.11 and 5.07 LOD scores), and one on the chromosome X (3.97 LOD scores).

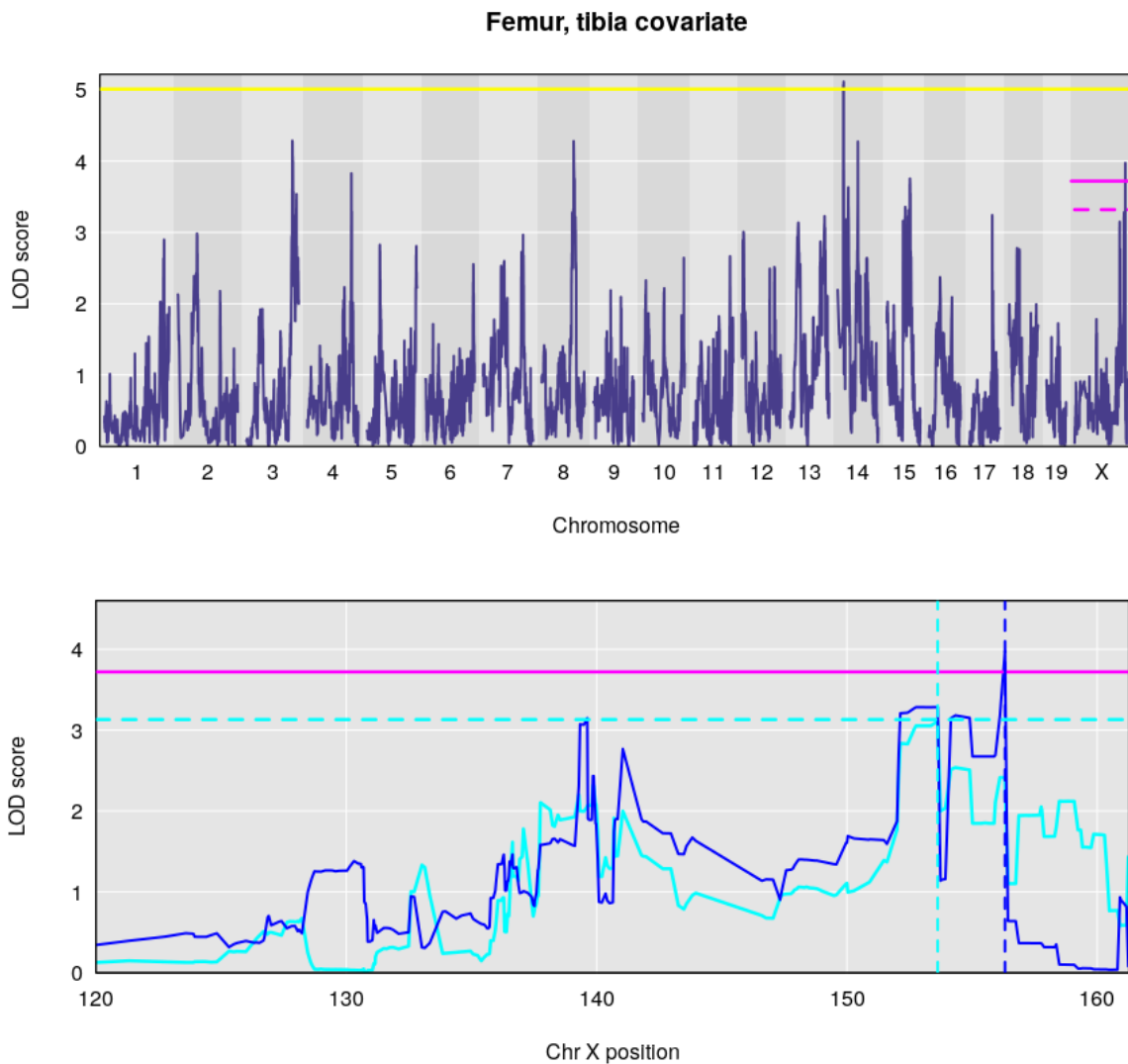


Figure 3.29. Relevant LOD score graphs of femur in the tibia covariate model (A), with the autosome significance level lines: red - 5% and yellow - 10% and closeup of the femur peak and suggestive humerus peak in chromosome X; the magenta horizontal line indicates significance level (5%) in femur, while cyan dashed line indicates suggestive level (10%) significance of humerus in the tibia covariate model

The candidate genes found in this model are known to have a strong impact on skeletal development (Tab.3.20.). Particularly, mutations in the X-linked *Rps6ka3* – a ribosomal protein S6 kinase polypeptide 3, is a known cause of Coffin-Lowry syndrome (Trivier et al., 1996). In the suggestive peak in the Humerus, which is in almost 3 Mbp distance from the Femur-Tibia peak, *Phex* is another excellent X-linked candidate acts upstream or within bone mineralization. It is implicated in hypophosphatemic rickets.

Table 3.20. Peak candidate gene, and relevant phenotype candidate genes in tibia covariate model

Tibia is a covariate	chromosome	Peak position (Mbp)	Peak candidate gene	candidate genes in CI
Humerus	chr X	157.187734	<i>Phex</i>	<i>Phex</i>
Radius	chr9	47.858302	<i>Cadm1</i>	<i>Cadm1</i>
Ulna	chr1	91.103492	<i>Lrrfip1</i>	<i>Agap1, Gbx2, Col6a3, Per2, Ube2f</i>
Ulna	chr15	10.681208	<i>Rai14</i>	<i>Prlr, Npr3, Spef2, Dnajc21, Rad1, Rai14, C1qtnf3, Golph3</i>
Femur	chr14	21.417047	<i>Adk</i>	<i>Kat6b</i>
Femur	chr14	20.429890	<i>Cfap70</i>	<i>Anxa7, Myoz1, Ndst2, Plau, Vcl,</i>
Femur	chrX	159.875717	<i>Sh3kbp1</i>	<i>Rps6ka3</i>

3. 3. DISCUSSION

The G15 mice mostly show expected morphological integration patterns, as expressed by the correlation between lengths of the limb bones. Very strong correlations are observed within the front limb zeugopod (radius and ulna), and between hind limb zeugopod (tibia), as compared to lower covariation between bones of different developmental modules. This agrees with the observation in mice from other populations, as well as general tetrapod pattern.

One of the integral parts of diversification between the front and hind limbs is a decreasing phenotypic covariance, resulting from the reduction of common developmental factors and evolutionary pressure favouring distinct function of each pair of limbs (Young, 2013). As previously mentioned, the front and hind limbs of the murine rodents present a certain degree of morphological and functional disconnection. The front limb bears similarity to that of the primates, including the human where dexterity of autopod is further specialised. In both examples, the elements of zeugopod allows the rotation of the palm through the radius, which articulates with the wrist bones and the ulna. This pattern of two independent zeugopod bones is not kept in the hind limb bones of the mouse, where the tibia is fused with the fibula.

Hox genes are one of the most important in patterning of the formation of the limb morphology, for example through expression in diversifying distal radius among hominids (Davis et al., 1995; Reno et al., 2008; Kamiyama et al., 2012;). Although no *Hox* gene was found in the genome mapping presented in my study, multiple other large effect genes were detected within the confidence intervals. That includes such as *Sox5* in the ulna and *Bmp3* in the tibia. Furtherly, the region on chromosome 13, which was significant in the ulna and tibia lengths of G15 mice, has been previously reported in several studies. It was associated with skeletal properties in mice, such as lengths of the ulna, tibia and femur as well as traits within the skull and other relevant phenotypes (Jiao et al., 2007; Kenney-Hunt et al., 2008). Furtherly, the region was also associated with mineral bone density (Sabsovich et al., 2008). In the mentioned studies, and in the G15 mapping, the interval wraps major QTL markers, such as the *Tbqt5* (tibia bone quality traits 5) and *Fbtq6* (femoral bone trait QTL 6) which are clearly important to skeletal phenotypes, including those of different embryonic origin, as evidenced by frequent identification and provide insight into possible pleiotropic interactions. Jiao et al.

(2007) has reported the chromosome 13 QTL region (from 59 to 73 cM of genetic location in the F2 population of C57BL/6J and C3H/HeJ mice, relevant to the bone hardness and stiffness. However, due to the limited number of markers in older QTL mapping attempts, it was often impossible to narrow down the list of candidate genes in this region. In my study, the confidence interval on this chromosome is almost the same in the mapping effort of the ulna and tibia lengths, where the peaks are within 1 Mbp distance of each other. Although in the setup of the G15 mapping experiment it could be expected to find large effect candidate genes, the role of either *Mast4* or *Adamts6* found within both confidence intervals is not clear in the long bone formation. The *Cwc27*, which is also in proximity, might provide more interesting background, as well as other less known protein coding genes.

The radius was characterised by relatively large ME, and as in the humerus and scapula there were no significant regions mapped in this study for these phenotypes alone, which could be a consequence of small sample size. Of interest was a distinctive peak on chromosome 13, which encompasses a slightly different region in the ulna and tibia. It became highly significant, when the humerus was used as a covariate, proving that at least part of the radius variance was controlled by this peak. In this model, the peak in chromosome 13 defined by the ulna has shifted to the same position as the radius. The presence of interesting candidate genes in both candidate intervals suggests that the QTL marker *Tibqt5*, is a chromosome region that encompasses independent genes affecting the individual lengths of ulna and tibia as well as skeletal proportions of the front limb zeugopod. Additionally, it calls for attention, that developing different methods of approximating the significance of the genome scan in a small population might be necessary.

Using another bone as a covariate allowed me to find more candidate intervals associated with the radius. Among the relationship QTLs, the region in the chromosome 12 in the model of ulna covariate and radius as a trait roughly matches the region found previously in the femur-humerus model (Pavlicev et al., 2013). In the NCBImm37 assembly, the mapped region in this study, with 1.5 LOD score dropped from the peak covered the region from 41.881972-45.679897 Mbp, while in the mentioned Pavlicev study (2013), with 1 LOD score drop: 41.765398-48.199933 Mbp. The location of the peak was shifted by almost 3 Mbp. In both studies, *Dnajb9* was a candidate gene found within the confidence interval. *Dnajb9* is a DnaJ heat shock protein family (Hsp40) member B9. The other protein coding gene which is present

in both confidence intervals is *Nrcam* which might be a contributor to the morphology of forelimbs. It should be mentioned that neither has a known role in skeleton formation, although both genes are expressed in the long bones. *Nrcam* is an important neuronal cell-cell adhesion protein. Mice with mutations in the gene experience paralysis and loss of function of the forelimbs. It was also linked to postnatal growth retardation (Douglas et al., 2009). On the other hand, *Dnajb9* is a possible contributor in early osteoarthritis (de Kroon et al., 2018) which would indicate a role in chondrocytes. The described region on chromosome 12 is positioned within the QTL markers previously described as contributing to limb bone length (*Lmblgq5*) and femur midshaft diameter (*Femd7*). Furthermore, the previously mentioned mapping study on a C57BL/6J and C3H/HeJ cross also identified a region covering from 17-38 cM as determining hardness and stiffness of the tibia, while the peak in the G15 covariate model corresponds to genetic position of around 20 cM. These mapping results might indicate a wider role of this region in skeleton or other limb-related tissues, such as cartilage or interosseous membrane present between the radius and ulna.

One of the important findings in this study is that the rQTL intervals of radius and ulna with the tibia bone as a covariate do not match. Together with the fibula, these elements are serially homologous, due to their development, but since in mice fibula forms a complex with the tibia bone, it is difficult to measure its individual length and was not included in this experimental setup.

When tibia was used as a covariate to radius, a peak in chromosome 9 reached the significance threshold of 0.05. In a short 0.15 Mbp interval, and within the peak is a gene involved in cell-cell adhesion gene, *Cadm1*. *Cadm1* is a type of a calcium dependent cell adhesion protein and was reported as related to low bone mineral content (Bassett et al., 2012). In ulna with the tibia covariate model two peaks are present in the chromosome 1, and 15. Chromosome 15 appears to have a very important role in the ulna bone, with a suggestive peak in this trait alone (within the *Cdh10* gene), three independent peaks in the model with femur, and finally with tibia covariate (Fig.3.30.). The confidence interval, as mentioned before, matches mostly between the femur and tibia model, so it can be concluded that it encompasses genes relevant to individuation of the fore- and hind limb.

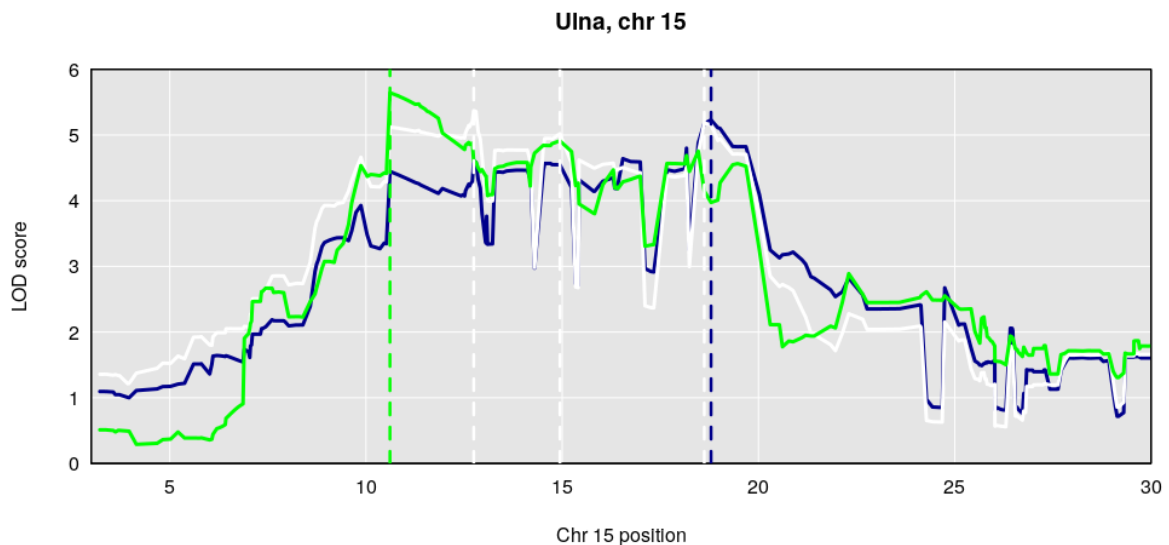


Figure 3.30. Genome scan outcome on chromosome 15, **dark blue** solid and vertical dashed lines mark the ulna as a separate trait, **green** is specific to the results with the tibia as a covariate, and **white** is specific to the femur covariate

The peak on chromosome 1 does not appear in other phenotypes or models, and it was suggestive in the tibia model. A close-by peak was also identified by Škrabar (2018) (Škrabar et al., 2018), as affecting the femur when the ulna was a covariate, which might indicate that this region has a relation to general skeleton proportions. The tibia bone also shows a significant peak in the model with the ulna as covariate (thus the opposite model), which is found within the chromosome 7. *Nell1* and *Ano5* are skeleton relevant genes, among which *Nell1* (NEL-like 1) is situated within proximity to the peak. This protein coding gene is inhibiting osteoblast proliferation, while positively regulating bone mineralisation. It has been found to affect early cranial suture closing when overexpressed (Zhang et al., 2002). *Ano5* is associated with gnathodiaphyseal dysplasia, which affects anatomy of long bones and mandible (Riminucci et al., 2001; Otaify et al., 2018). It was reported, that inactivation of this gene increases osteoblastogenesis (Wang et al., 2019).

One of the very interesting findings of this chapter, is a strong correlation between scapula and zeugopod bones expressed in females, which is evident in the G15 and also in the AH mice (but only with the tibia, which is probably associated with the measurement method). The shoulder blade bone seems also to be more correlated with body weight than the other bones. Although so different in development than the long bones, the mammalian scapula shape defines the type of movement (gait), and predominantly contributes to propulsive movement of the limb,

in a similar way to femur in the leg (Fischer et al., 2002; Muñoz et al., 2019). No suggestive QTL is found in scapula as a separate trait (although it also exhibits relatively large peaks on chromosome X and chromosome 13) or when the tibia was used as a covariate. However, in the flipped model of the tibia with scapula as covariate, I found two close-by peaks on chromosome 5. In addition to the CI with extremely relevant genes such as *Bmp3* and *Prkg2*, the second one points to an excellent candidate, a *Bmp2k*, with function on osteoblasts differentiation (Kearns et al., 2001) and regulation of bone mineralisation. This finding might be very important in order to better understand mineral bone density differences in males and females, which could be what *Bmp2k* contributes to. The BMPs belong to TGF-beta signalling (transforming growth factor beta) and are essential in condensation of cartilage. Although this is not an X-chromosome gene, its effect might be mediated by other genes or hormones, which is then exhibited as a different correlation between scapula and tibia in males and females. For example, muscle forces have also a great impact on mineralisation of this bone (Karunaratne et al., 2012).

In many species of mammals, the proportions and shape of specific bones are known to vary strongly between males and females, with classic examples such as pelvic bone, skull or digit length ratio. Since proportion of limb bones are related to body mass of animals we could expect, that due to male mice being heavier than females, all of the bones would also be longer in males. This is the case in the Iranian mice, however in the G15 mice, both bones of the leg are longer in females – even after correcting the data for weight residual. It might be speculated, whether the reasonably large body mass of G15 females is somewhat related to differences in the correlation of hind limb bones and scapula, or their length compared to males. Yet, it was reported, that human bone properties such as BMD and BMC differ despite similar body sized males and females (same age)(Nieves et al., 2005). Among laboratory mouse strains, the C57BL/6J also was reported to exhibit longer hind limb bones in females (Škrabar, 2018). This most popular mouse strain is reported with low bone density, and occurring ankylosing enthesopathy of tarsal joints, as reported by the Jaxon Laboratory. In addition, other researchers have reported that female CD-1 mice at 8 and 18 months of age had longer femurs than males (He et al., 2006). The sex differences in bone length are also related to timing of their development, where rapid growth of the femur lasts 8 weeks in females, while males last for 12 weeks (Bab et al., 2007). It was reported, that androgen activity affects the larger size of bones in males (Sims et al., 2002).

The G15 mice were characterised by overall heavier body weight than the Iranian mice, and this difference is especially noticeable between females (Fig.3.31). While the mean male weight of AH mice is 33.25 grams, the weight of G15 males is on average 36.80 grams. Females, on the other hand weight 24.19 and 32.50 gram respectively.

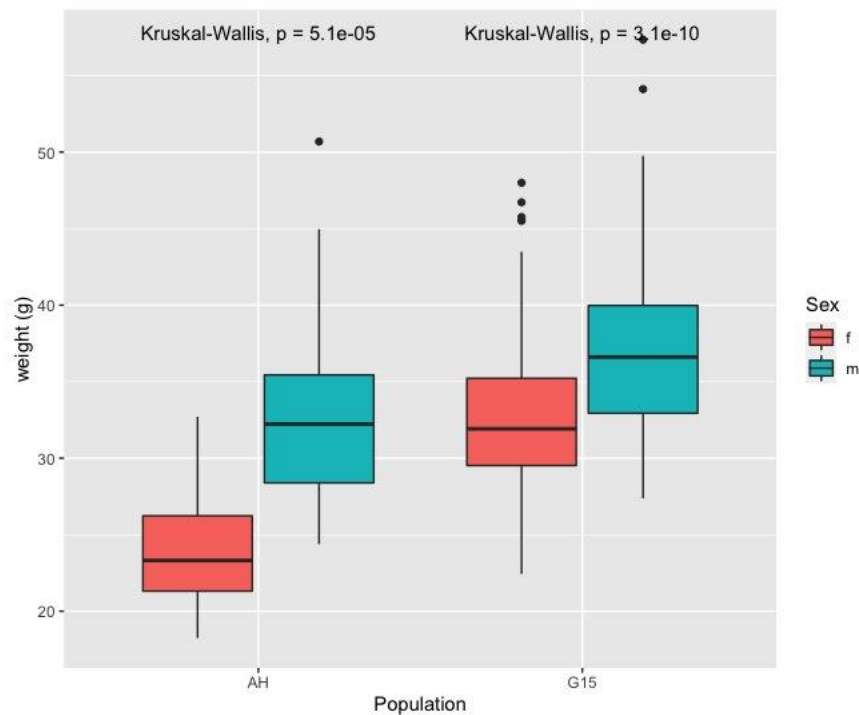


Figure 3.31. Weight differences of males and females in AH and G15 mice; Kruskal-Wallis statistics: AH mice chi-squared = 16.4, df =1; G15 mice = chi-squared = 39.6, df = 1

Weight of mice is a highly varied feature, depending on the strain and also age. It is important, that there were a few female G15 younger than 100 days. Also, the weight of normal *M. m. castaneus* is in overall lower than for example B6 mice which, similar to the AH mice is mostly of *domesticus* origin.

The X chromosome regions are found in the bone covariate models. Three peaks are found in the scapula – two with the ulna covariate and one with the femur. In the model with the tibia as covariate, I found candidate genes on the X chromosome related to the femur, which to some extent might explain proportions observed in this experimental population. In the

confidence interval, the *Rps6ka3* provides exceptionally interesting ground to study changing bone length proportions. It has been associated with skeletal abnormalities and mental retardation associated with Coffin-Lowry syndrome (CLS), and it had been shown that it is indispensable for osteoblasts in developing mouse embryo. It also upregulates the *Sox8* (Wu et al., 2021). The lower limb discrepancy was reported in humans with CLS.

While the *Rps6ka3* is a candidate gene for the femur with tibia covariate, in the opposite model only one gene, the *Sox6* is close to achieving statistical support. It is the second *Sox* family candidate gene in this study, first being the *Sox5* in chromosome 6 linked to ulna length. Although here, the peak is below suggestive level, it is an exceptionally good candidate gene, and it could be speculated that this low LOD score could be related to small sample size or measurement error.

In hybrids, mapped intervals in the X-chromosome are often disproportionately large, which is also found here. This is consistent with Turner and Harr (Turner and Harr, 2014), and what is even more interesting, one of the regions with the peak at 70 Mbp matches a region found by these authors, where it was contributing to weight of mice testis. In this study, it was a suggestive region to the scapula when the ulna was a covariate, where it encompasses over 40 Mbp of the chromosome, as well as with femur covariate, but the peaks are not close. This result might be related to the distinct *castaneus* allele present in the population, causing the large X effect. The region, also present in the scapula as a separate trait (with no significance), contains many skeleton relevant genes, such as *Il1rap1* (within the peak), *Ids*, *Maml8* or *Mtm1*. Second, chromosome X CI in the scapula with ulna covariate is significant at 0.05 level, close to interesting gene *Ripply1* (rippy transcriptional repressor 1). It is essential to somite rostral/caudal axis specification by regulating *Mesp2* expression. (Takahashi et al., 2010)

There was only a single research on the *Desp1* QTL region (Yoshikawa et al., 2002), which here was mapped as relevant to length of femur. It was also present in the model with the ulna as a covariate. Due to the phenotyping method, it is possible that for example length of thigh muscles is reflected in the mapping, so more fitting method, such as μ CT measurement could be tested. Only predicted genes are identified in the peak, and *Cdh11* as well as the *Cdh8* are found in a large distance from the peak.

4. General Conclusions

In this thesis, I have shown that x-ray-based bone measurement, as well as micro-tomography-based measurements (in the Chapter I) can be valuable in understanding proportions and genetic architecture of the limb bones. Polygenic nature of bone lengths and correlation between them was further confirmed in this study. Different bone correlations between male and female Iranian as well as G15 mice were noticed and possible genetic contribution have been suggested. Many of the relationship QTL (covariate models) track to loci which were not identified for separate traits, especially in the models where the tibia was a covariate. These candidates might be contributing to individuation of specific trait.

More precise analyses will be necessary in identifying specific genes contributing to those phenotypes, and how do they contribute to the evolution of homologous, repeated bone elements of the limb. As the debate on exact homology of the bones within zeugopodium (radius, ulna, tibia and fibula) is not resolved, unique candidate genes found in each of the covariate models might provide new insight on this topic. Possibly one or more of them could contribute to functional specialization of the front limb in murine rodents.



Supplementary material

Chapter: Limb bone morphometrics in Iranian mice

Supplementary Table 2.1. List of specimens used in the chapter II; the name is specific with the breeding patterns of the MPI; AH_1 and AH_2 mice were bred in separate building, but come from the same mouse outbred stock;

Mouse ID	Room	sex	born
70767	AH_2	f	15.07.2018
70768	AH_2	f	15.07.2018
70747	AH_2	f	12.07.2018
70748	AH_2	f	12.07.2018
70749	AH_2	f	12.07.2018
70750	AH_2	f	12.07.2018
70908	AH_2	f	16.07.2018
70909	AH_2	f	16.07.2018
70910	AH_2	f	16.07.2018
70646	AH_2	f	10.07.2018
70647	AH_2	f	10.07.2018
71202	AH_1	f	16.07.2018
71201	AH_1	f	16.07.2018
71200	AH_1	f	16.07.2018
71199	AH_1	f	16.07.2018
71205	AH_1	f	16.07.2018
71204	AH_1	f	16.07.2018
71203	AH_1	f	16.07.2018
70522	AH_2	m	08.07.2018
70523	AH_2	m	08.07.2018
70524	AH_2	m	08.07.2018
70741	AH_2	m	09.07.2018
70744	AH_2	m	12.07.2018
70745	AH_2	m	12.07.2018
70765	AH_2	m	15.07.2018
70766	AH_2	m	15.07.2018
70903	AH_2	m	16.07.2018
70904	AH_2	m	16.07.2018
70905	AH_2	m	16.07.2018
70906	AH_2	m	16.07.2018
71044	AH_2	m	27.07.2018
71046	AH_2	m	27.07.2018
71198	AH_1	m	16.07.2018
71197	AH_1	m	16.07.2018
71196	AH_1	m	16.07.2018
71191	AH_1	m	16.07.2018

Supplementary Table 2.2. Summary of Shapiro-Wilk test of normality with W and p values in each trait as well as weight of the animals.

Bone	Statistic	all AH mice	females	males
Humerus	W	0.98	0.97	0.91
	p	0.63	0.80	0.08
Radius	W	0.99	0.96	0.97
	p	0.96	0.66	0.72
Ulna	W	0.98	0.94	0.97
	p	0.72	0.29	0.81
Scapula	W	0.97	0.97	0.95
	p	0.36	0.79	0.40
Femur	W	0.98	0.96	0.93
	p	0.70	0.62	0.19
Tibia	W	0.95	0.92	0.95
	p	0.14	0.14	0.46
Weight	W	0.94	0.94	0.91
	p	0.04	0.24	0.10

Supplementary Table 2.3. PCA scores of each bone in females, males and weight residual dataset.

Group	Males		Females		All*	
	PC1 (58%)	PC2 (16%)	PC1 (65%)	PC2 (18%)	PC1 (72%)	PC2 (13%)
Humerus	0.41701	-0.00941	0.30559	0.27037	-0.39284	-0.10548
Radius	0.45660	0.33333	0.35017	-0.66413	-0.41301	0.50357
Ulna	0.44502	0.42252	0.41310	-0.48870	-0.41091	0.54652
Scapula	0.25594	-0.80432	0.43301	0.42534	-0.36572	-0.59418
Femur	0.42097	-0.24251	0.45885	0.18725	-0.43222	-0.16661
Tibia	0.42054	-0.06743	0.46401	0.17614	-0.43091	-0.23623

Supplementary Table 3.1. t-test results of male-female differences in G15 mice;

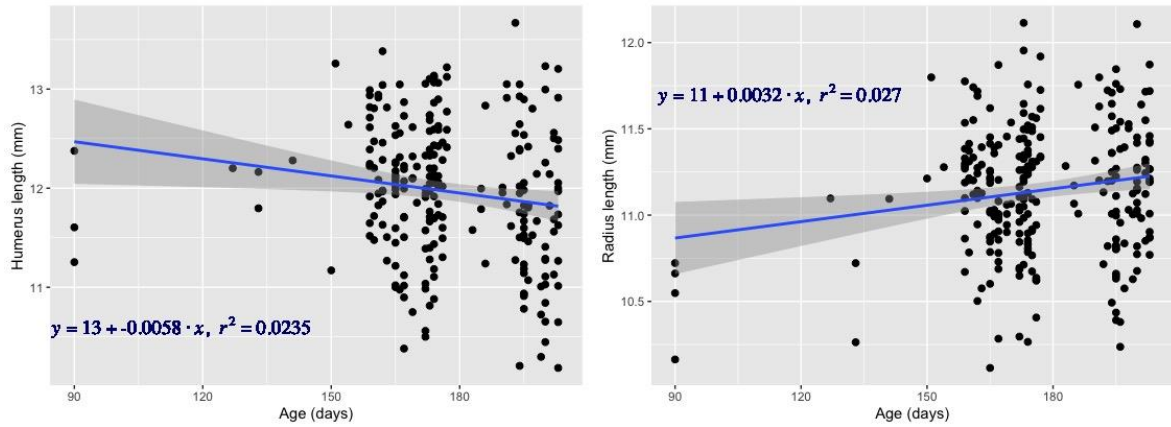
Bone	t-test		
	df	t	p
Humerus	217.18	-5.53	<0.0001
Radius	202.98	-3.18	0.002
Ulna	205.12	-4.3991	<0.0001
Scapula	192.44	-2.52	0.01
Femur	210.44	3.9649	0.0001
Tibia	200.44	3.1	0.002
Mean weight (grams)	Wilcoxon Test		
	W	p	
	4280.5	<0.0001	
Mean Age (days)			
	10888	<0.0001	

Supplementary Table 3.2. ANOVA results of the covariate models in G15 mice

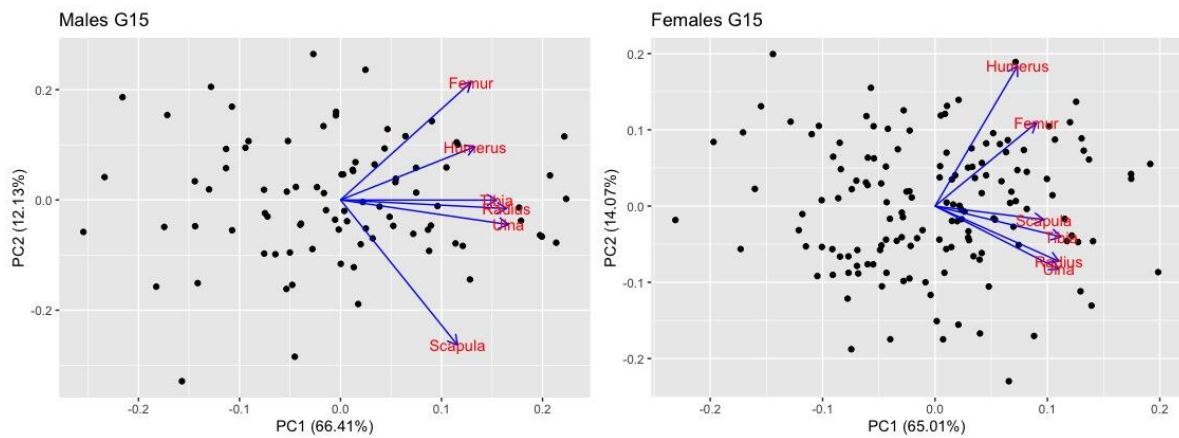
HUMERUS	Df	Sum sq	Mean sq	F value	Pr(>F)
Weight	1	19.92	19.9199	52.3431	6.96E-12
Age	1	4.874	4.8743	12.8082	0.0004212
Sex	1	1.91	1.9097	5.018	0.0260448
Weight:Age	1	0.021	0.0209	0.0549	0.8149162
Weight:Sex	1	0.394	0.3938	1.0349	0.3100847
Age:Sex	1	0.488	0.488	1.2822	0.2586718
Weight:Age:Sex	1	0.082	0.0817	0.2146	0.6436426
Residuals	229	87.149	0.3806		
RADIUS	Df	Sum sq	Mean sq	F value	Pr(>F)
Weight	1	7.6931	7.6931	72.7257	1.42E-15
Age	1	0.412	0.412	3.895	0.04953
Sex	1	0.0422	0.0422	0.3985	0.52843
Weight:Age	1	0.0659	0.0659	0.6228	0.43074
Weight:Sex	1	0.1411	0.1411	1.3339	0.24922
Age:Sex	1	0.6676	0.6676	6.3114	0.01262
Weight:Age:Sex	1	0.0034	0.0034	0.0326	0.85691
Residuals	251	26.5512	0.1058		
ULNA	Df	Sum sq	Mean sq	F value	Pr(>F)
Weight	1	12.919	12.9189	94.0658	2.00E-16
Age	1	0.267	0.2672	1.9457	0.16429
Sex	1	0.324	0.3242	2.3605	0.1257
Weight:Age	1	0.19	0.19	1.3833	0.24066
Weight:Sex	1	0.148	0.1485	1.0809	0.29949
Age:Sex	1	0.577	0.5773	4.2036	0.04138
Weight:Age:Sex	1	0.026	0.0264	0.1921	0.66157
Residuals	251	34.472	0.1373		

Supplementary Table 3.2. ANOVA results of the covariate models in G15 mice (continued)

SCAPULA	Df	Sum sq	Mean sq	F value	Pr(>F)
Weight	1	13.491	13.4905	49.9353	1.59E-11
Age	1	0.666	0.6659	2.4648	0.1177
Sex	1	0.023	0.0228	0.0844	0.7716
Weight:Age	1	0.069	0.0693	0.2566	0.6129
Weight:Sex	1	0.022	0.0221	0.0819	0.7749
Age:Sex	1	0.318	0.3181	1.1776	0.2789
Weight:Age:Sex	1	0.266	0.2657	0.9836	0.3223
Residuals	249	67.27	0.2702		
FEMUR	Df	Sum sq	Mean sq	F value	Pr(>F)
Weight	1	2.283	2.283	4.4384	0.03613
Age	1	0.24	0.24	0.4667	0.49516
Sex	1	13.759	13.7595	26.7497	4.74E-07
Weight:Age	1	0.434	0.4342	0.844	0.35913
Weight:Sex	1	0.155	0.155	0.3013	0.58353
Age:Sex	1	0.05	0.0503	0.0978	0.75472
Weight:Age:Sex	1	0.04	0.0396	0.077	0.78157
Residuals	251	129.109	0.5144		
TIBIA	Df	Sum sq	Mean sq	F value	Pr(>F)
Weight	1	7.04	7.0404	23.1193	2.63E-06
Age	1	2.24	2.2403	7.3566	0.007145
Sex	1	8.354	8.354	27.4328	3.45E-07
Weight:Age	1	0.09	0.0897	0.2944	0.587903
Weight:Sex	1	0.159	0.1586	0.5207	0.471231
Age:Sex	1	1.355	1.3549	4.4491	0.035914
Weight:Age:Sex	1	0.011	0.0111	0.0365	0.848707
Residuals	250	76.132	0.3045		



Supplementary Figure 3.1. Relation of bone length and age of the G15 mice; Humerus: F-statistics = 5.65, DF = 235, p-value = 0.02; Radius: F-statistics = 7.12, DF = 257, p-value = 0.008;



Supplementary Figure 3.2. PCA graphs of the G15 mice bone lengths in males (A) and females (B); the data are not corrected for covariates.

Supplementary Table 3.3. PCA scores of each bone in females, males and weight residual dataset in the G15 mice

Bone	Males G15		Females G15		All G15	
	PC1	PC2	PC1	PC2	PC1	PC2
Humerus	0.3586662	0.18947016	0.2927857	0.54456578	0.3264329	0.57695432
Radius	0.4414649	0.13050404	0.4360753	-0.2150576	0.4665363	-0.293158
Ulna	0.4491283	0.04217168	0.4371212	-0.2635272	0.4645064	-0.3482093
Scapula	0.320293	-0.5373883	0.3810814	0.01385739	0.3838985	-0.1869315
Femur	0.3462806	0.4305626	0.3432515	0.58005408	0.3455954	0.6451925
Tibia	0.4140707	0.16412894	0.4390102	-0.0362853	0.439551	-0.0933576

BIBLIOGRAPHY

- Akiyama, H., Kim, J.-E., Nakashima, K., Balmes, G., Iwai, N., Deng, J.M., Zhang, Z., Martin, J.F., Behringer, R.R., Nakamura, T., de Crombrugge, B. (2005) Osteo-chondroprogenitor cells are derived from Sox9 expressing precursors. *Proceedings of the National Academy of Sciences of the United States of America*, 102, 14665–14670.
- Annys, E., Billington, R., Clayton, R., Bremm, K.-D., Graziano, M., McKelvie, J., Ragan, I., Schwarz, M., van der Laan, J.W., Wood, C., Öberg, M., Wester, P., Woodward, K.N. (2014) Advancing the 3Rs in regulatory toxicology – carcinogenicity testing: scope for harmonisation and advancing the 3Rs in regulated sectors of the European Union. *Regulatory Toxicology and Pharmacology*. 69, 234–242.
- Armario, A. (2021) The forced swim test: Historical, conceptual and methodological considerations and its relationship with individual behavioral traits. *Neurosci. Biobehav. Rev.* 128, 74–86.
- Arostegui, M., Underhill, T.M. (2021) Murine Limb Bud Organ Cultures for Studying Musculoskeletal Development, in: Hilton, M.J. (Ed.), *Skeletal Development and Repair: Methods and Protocols*, *Methods in Molecular Biology*. Springer US, New York, NY, pp. 115–137.
- Atchley, W.R., Hall, B.K. (1991) A model for development and evolution of complex morphological structures. *Biological Reviews of the Cambridge Philosophical Society*, 66, 101–157.
- Azevedo, L., Suriano, G., van Asch, B., Harding, R.M., Amorim, A. (2006) Epistatic interactions: how strong in disease and evolution? *Trends in Genetics*, 22, 581–585.
- Bab, I.A., Hajbi-Yonissi, C., Gabet, Y., Müller, R. (2007) *Micro-tomographic atlas of the mouse skeleton*. Springer Science & Business Media, Boston, MA, pp. 117-201.
- Bahamonde, M.E., Lyons, K.M. (2001) BMP3: to be or not to be a BMP. *The Journal of Bone and Joint Surgery, American Volume*, 83-A Suppl 1, S56-62.
- Bailey, A.A., Wahlsten, D., Hurd, P.L. (2005) Digit ratio (2D:4D) and behavioral differences between inbred mouse strains. *Genes, Brain and Behavior*, 4, 318–323.
- Bard, J.L., Kaufman, M.H., Dubreuil, C., Brune, R.M., Burger, A., Baldock, R.A., Davidson, D.R. (1998) An internet-accessible database of mouse developmental anatomy based on a systematic nomenclature. *Mechanisms of Development*, 74, 111–120.
- Barrett, J.M., Tapias, M.G.R., Shepherd, G.M.G. (2020) Manual dexterity of mice during food-handling involves the thumb and a set of fast basic movements. *PLoS One* 15, e0226774.
- Bassett, J.H.D., Gogakos, A., White, J.K., Evans, H., Jacques, R.M., van der Spek, A.H., Sanger Mouse Genetics Project, Ramirez-Solis, R., Ryder, E., Sunter, D., Boyde, A., Campbell, M.J., Croucher, P.I., Williams, G.R. (2012) Rapid-throughput skeletal phenotyping of 100 knockout mice identifies 9 new genes that determine bone strength. *PLoS Genetics* 8, e1002858.
- Bassett, J.H.D., Williams, G.R. (2016) Role of Thyroid Hormones in Skeletal Development and Bone Maintenance. *Endocrine Review*, 37, 135–187.

- Baumhoer, D., Kovac, M., Sperveslage, J., Ameline, B., Strobl, A.-C., Krause, A., Trautmann, M., Wardelmann, E., Nathrath, M., Höller, S., Harges, J., Gosheger, G., Krieg, A.H., Vieth, V., Tirabosco, R., Amary, F., Flanagan, A.M., Hartmann, W. (2019) Activating mutations in the MAP-kinase pathway define non-ossifying fibroma of bone. *The Journal of Pathology*, 248, 116–122.
- Beck, J.A., Lloyd, S., Hafezparast, M., Lennon-Pierce, M., Eppig, J.T., Festing, M.F.W., Fisher, E.M.C. (2000) Genealogies of mouse inbred strains. *Nature Genetics* 24, 23–25.
- Belheouane, M., Gupta, Y., Künzel, S., Ibrahim, S., Baines, J.F. (2017) Improved detection of gene-microbe interactions in the mouse skin microbiota using high-resolution QTL mapping of 16S rRNA transcripts. *Microbiome* 5, 59.
- Berman, S.L. (1985) Convergent evolution in the hindlimb of bipedal rodents. *Journal of Zoological Systematics and Evolutionary Research*, 23, 59–77.
- Bhattacharyya, M.K., Smith, A.M., Ellis, T.H.N., Hedley, C., Martin, C. (1990) The wrinkled-seed character of pea described by Mendel is caused by a transposon-like insertion in a gene encoding starch-branching enzyme. *Cell* 60, 115–122.
- Bierne, N., Lenormand, T., Bonhomme, F., David, P. (2002) Deleterious mutations in a hybrid zone: can mutational load decrease the barrier to gene flow? *Genetics Research*, 80, 197–204.
- Bolton, M., Stanbury, A., Baylis, A.M.M., Cuthbert, R. (2014) Impact of introduced house mice (*Mus musculus*) on burrowing seabirds on Steeple Jason and Grand Jason Islands, Falklands, South Atlantic. *Polar Biology*, 37, 1659–1668.
- Botstein, D., White, R.L., Skolnick, M., Davis, R.W. (1980) Construction of a genetic linkage map in man using restriction fragment length polymorphisms. *American Journal of Human Genetics*. 32, 314–331.
- Broman, K.W. (2001) Review of statistical methods for QTL mapping in experimental crosses. *Lab Animal*, 30, 44–52.
- Broman, K.W., Sen, Ś., Owens, S.E., Manichaikul, A., Southard-Smith, E.M., Churchill, G.A. (2006) The X chromosome in quantitative trait locus mapping. *Genetics* 174, 2151–2158.
- Broman, W. K., Saunak, Ś. (2009) A guide to QTL mapping with R/QTL. Springer US, New York, NY, pp 1-20.
- Bućan, M., Abel, T. (2002) The mouse: genetics meets behaviour. *Nature Review Genetics* 3, 114–123.
- Buerstmayr, H., Ban, T., Anderson, J.A. (2009) QTL mapping and marker-assisted selection for Fusarium head blight resistance in wheat: a review. *Plant Breeding*, 128, 1–26.
- Bundschu, K., Knobloch, K.-P., Ullrich, M., Schinke, T., Amling, M., Engelhardt, C.M., Renné, T., Walter, U., Schuh, K. (2005) Gene disruption of Spred-2 causes dwarfism. *The Journal of Biological Chemistry*. 280, 28572–28580.
- Cantley, M.D., Bartold, P.M., Marino, V., Reid, R.C., Fairlie, D.P., Wyszynski, R.N., Zilm, P.S., Haynes, D.R. (2009) The use of live-animal micro-computed tomography to determine the effect of a novel phospholipase A2 inhibitor on alveolar bone loss in an in vivo mouse model of periodontitis. *Journal Periodontal Research*, 44, 317–322.

- Capellini, T.D., Handschuh, K., Quintana, L., Ferretti, E., Di Giacomo, G., Fantini, S., Vaccari, G., Clarke, S.L., Wenger, A.M., Bejerano, G., Sharpe, J., Zappavigna, V., Selleri, L. (2011) Control of pelvic girdle development by genes of the Pbx family and Emx2. *Developmental Dynamics*, 240, 1173–1189.
- Carter, D.R., Mikić, B., Padian, K. (1998) Epigenetic mechanical factors in the evolution of long bone epiphyses. *Zoological Journal of the Linnean Society*, 123, 163–178.
- Carver, E.A., Stubbs, L. (1997) Zooming in on the human-mouse comparative map: genome conservation re-examined on a high-resolution scale. *Genome Research*, 7, 1123–1137.
- Castro, J.P., Yancoskie, M.N., Marchini, M., Belohlavy, S., Hiramatsu, L., Kučka, M., Beluch, W.H., Naumann, R., Skuplik, I., Cobb, J., Barton, N.H., Rolian, C., Chan, Y.F. (2019) An integrative genomic analysis of the Longshanks selection experiment for longer limbs in mice. *eLife* 8, e42014.
- Chaim, A.B., Borovsky, Y., Rao, G., Gur, A., Zamir, D., Paran, I. (2006) Comparative QTL mapping of fruit size and shape in tomato and pepper. *Israel Journal of Plant Sciences*, 54, 191–203.
- Chesler, E.J., Gatti, D.M., Morgan, A.P., Strobel, M., Trepanier, L., Oberbeck, D., McWeeney, S., Hitzemann, R., Ferris, M., McMullan, R., Clayshuttle, A., Bell, T.A., de Villena, F.P.-M., Churchill, G.A. (2016) Diversity Outbred Mice at 21: Maintaining Allelic Variation in the Face of Selection. *G3 Genes Genomes Genetics* 6, 3893–3902.
- Christiansen, P. (2002) Mass allometry of the appendicular skeleton in terrestrial mammals. *Journal of Morphology*, 251, 195–209.
- Christiansen, P., 1999. Scaling of the limb long bones to body mass in terrestrial mammals. *Journal of Morphology*, 239, 167–190.
- Christiansen, P., Fariña, R.A. (2004) Mass prediction in theropod dinosaurs. *Hist. Biol.* 16, 85–92.
- Churakov, G., Sadasivuni, M.K., Rosenbloom, K.R., Huchon, D., Brosius, J., Schmitz, J. (2010) Rodent Evolution: Back to the Root. *Molecular Biology Evolution* 27, 1315–1326.
- Churchill, G.A., Gatti, D.M., Munger, S.C., Svenson, K.L. (2012) The diversity outbred mouse population. *Mammalian Genome*, 23, 713–718.
- Claude J (2008) *Morphometrics With R*. Springer, Berlin, pp. 25-65.
- Cooper, K.L. (2011) The Lesser Egyptian Jerboa, *Jaculus jaculus*: A Unique Rodent Model for Evolution and Development. *Cold Spring Harbour Protocol*, 12, 1451-1456.
- Cooper, K.L., Sears, K.E., Uygur, A., Maier, J., Baczkowski, K.-S., Brosnahan, M., Antczak, D., Skidmore, J.A., Tabin, C.J. (2014) Patterning and post-patterning modes of evolutionary digit loss in mammals. *Nature*, 511, 41–45.
- Cooper, W.J., Steppan, S.J., Cooper, W.J., Steppan, S.J. (2010) Developmental constraint on the evolution of marsupial forelimb morphology. *Australian Journal of Zoology*, 58, 1–15.
- Cretekos, C.J., Wang, Y., Green, E.D., Martin, J.F., Rasweiler, J.J., Behringer, R.R. (2008) Regulatory divergence modifies limb length between mammals. *Genes Development*, 22, 141–151.
- Darvasi, A., Soller, M. (1995) Advanced intercross lines, an experimental population for fine genetic mapping. *Genetics*, 141, 1199–1207.

- Davis, A.P., Witte, D.P., Hsieh-Li, H.M., Potter, S.S., Capecchi, M.R. (1995) Absence of radius and ulna in mice lacking *hoxa-11* and *hoxd-11*. *Nature*, 375, 791–795.
- de Kroon, L.M.G., van den Akker, G.G.H., Brachvogel, B., Narcisi, R., Belluoccio, D., Jenner, F., Bateman, J.F., Little, C.B., Brama, P.A.J., Blaney Davidson, E.N., van der Kraan, P.M., van Osch, G.J.V.M. (2018) Identification of TGF β -related genes regulated in murine osteoarthritis and chondrocyte hypertrophy by comparison of multiple microarray datasets. *Bone* 116, 67–77.
- Dirckx, N., Moorer, M.C., Clemens, T.L., Riddle, R.C. (2019) The role of osteoblasts in energy homeostasis. *Nature Review Endocrinology*, 15, 651–665.
- Douglas, D.S., Moran, J.L., Bermingham, J.R., Chen, X.-J., Brindley, D.N., Soliven, B., Beier, D.R., Popko, B. (2009) Concurrent *Lpin1* and *Nrcam* mouse mutations result in severe peripheral neuropathy with transitory hindlimb paralysis. *Journal Neuroscience*, 29, 12089–12100.
- Duggan, B.M., Hocking, P.M., Schwarz, T., Clements, D.N. (2015) Differences in hindlimb morphology of ducks and chickens: effects of domestication and selection. *Genetics Selection Evolution*, 47, 88
- Eom, G.H., Kim, K., Kim, S.-M., Kee, H.J., Kim, J.-Y., Jin, H.M., Kim, J.-R., Kim, J.H., Choe, N., Kim, K.-B., Lee, J., Kook, H., Kim, N., Seo, S.-B. (2009) Histone methyltransferase PRDM8 regulates mouse testis steroidogenesis. *Biochemical and Biophysical Research Communications*, 388, 131–136.
- Ernst, C.W., Steibel, J.P. (2013) Molecular advances in QTL discovery and application in pig breeding. *Trends in Genetic*, 29, 215–224.
- Eyal, S., Rubin, S., Krief, S., Levin, L., Zelzer, E. (2019) Common cellular origin and diverging developmental programs for different sesamoid bones. *Development*, 146 (4), 167452.
- Fischer, M.S., Schilling, N., Schmidt, M., Haarhaus, D., Witte, H. (2002) Basic limb kinematics of small therian mammals. *Journal of Experimental Biology*, 205, 1315–1338.
- Franz-Odenaal, T.A. (2011) Induction and patterning of intramembranous bone. *Frontiers in Bioscience, Landmark Edition*, 16, 2734–2746.
- Galis, F., van Alphen, J.J.M., Metz, J.A.J. (2001) Why five fingers? Evolutionary constraints on digit numbers. *Trends in Ecology and Evolution*, 16, 637–646.
- Galli, A., Robay, D., Osterwalder, M., Bao, X., Bénazet, J.-D., Tariq, M., Paro, R., Mackem, S., Zeller, R. (2010) Distinct roles of *Hand2* in initiating polarity and posterior *Shh* expression during the onset of mouse limb bud development. *PLoS Genetics*, 6, e1000901.
- García-Esponda, C.M., Calanoce, A.R., Candela, A.M. (2021) Brachiocephalic muscular arrangements in cavioid rodents (Caviomorpha): a functional, anatomical, and evolutionary study. *Journal of Mammalian Evolution*, 28, 529–541.
- Gargiulo, S., Greco, A., Gramanzini, M., Esposito, S., Affuso, A., Brunetti, A., Vesce, G. (2012) Mice anesthesia, analgesia, and care, Part I: anesthetic considerations in preclinical research. *ILAR Journal*, 53, 55-69.
- Gonzales, N.M., Palmer, A.A. (2014) Fine mapping QTLs in advanced interbred lines and other outbred populations. *Mammalian Genome*, 25, 271–292.

- Gough-Palmer, A.L., Maclachlan, J., Routh, A. (2008) Paws for thought: comparative radiologic anatomy of the mammalian forelimb. *RadioGraphics* 28, 501–510.
- Grenier, J.K., Carroll, S.B. (2000) Functional evolution of the Ultrabithorax protein. *Proceedings of the National Academy of Sciences of the United States of America*, 97, 704–709.
- Grisart, B., Coppieters, W., Farnir, F., Karim, L., Ford, C., Berzi, P., Cambisano, N., Mni, M., Reid, S., Simon, P., Spelman, R., Georges, M., Snell, R. (2002) Positional Candidate Cloning of a QTL in Dairy Cattle: Identification of a Missense Mutation in the Bovine DGAT1 Gene with Major Effect on Milk Yield and Composition. *Genome Research*, 12, 222–231.
- Gros, J., Tabin, C.J. (2014) Vertebrate limb bud formation is initiated by localized epithelial-to-mesenchymal transition. *Science* 343, 1253–1256.
- Hager, E.R., Harringmeyer, O.S., Wooldridge, T.B., Theingi, S., Gable, J.T., McFadden, S., Neugeboren, B., Turner, K.M., Hoekstra, H.E. (2021) A chromosomal inversion drives evolution of multiple adaptive traits in deer mice. *bioRxiv* 2021.01.21.427490
- Hallgrímsson, B., Jamniczky, H., Young, N.M., Rolian, C., Parsons, T.E., Boughner, J.C., Marcucio, R.S. (2009) Deciphering the palimpsest: studying the relationship between morphological integration and phenotypic covariation. *Evolutionary Biology*, 36, 355–376.
- Hardouin, E.A., Orth, A., Teschke, M., Darvish, J., Tautz, D., Bonhomme, F. (2015) Eurasian house mouse (*Mus musculus* L.) differentiation at microsatellite loci identifies the Iranian plateau as a phylogeographic hotspot. *BMC Evolutionary Biology*, 15, 26.
- Harr, B., et al., n.d. Genomic resources for wild populations of the house mouse, *Mus musculus* and its close relative *Mus spretus* | Scientific Data [WWW Document]. URL <https://www.nature.com/articles/sdata201675> (accessed 12.10.21).
- He, J., Rosen, C.J., Adams, D.J., Kream, B.E. (2006) Postnatal growth and bone mass in mice with IGF-I haploinsufficiency. *Bone* 38, 826–835.
- Hirasawa, T., Kuratani, S. (2015) Evolution of the vertebrate skeleton: morphology, embryology, and development. *Zoology Letters* 1, 2.
- Huchon, D., Madsen, O., Sibbald, M.J.J.B., Ament, K., Stanhope, M.J., Catzeflis, F., de Jong, W.W., Douzery, E.J.P. (2002) Rodent phylogeny and a timescale for the evolution of Glires: evidence from an extensive taxon sampling using three nuclear genes. *Molecular Biology and Evolution* 19, 1053–1065.
- Hung, I.H., Yu, K., Lavine, K.J., Ornitz, D.M. (2007) FGF9 regulates early hypertrophic chondrocyte differentiation and skeletal vascularization in the developing stylopod. *Developmental Biology*, 307, 300–313.
- Ingham, P.W., McMahon, A.P. (2001) Hedgehog signaling in animal development: paradigms and principles. *Genes and Development*, 15, 3059–3087.
- Ishikawa, A., Namikawa, T. (2004) Mapping major quantitative trait loci for postnatal growth in an intersubspecific backcross between C57BL/6J and Philippine wild mice by using principal component analysis. *Genes and Genetic Systems*, 79, 27–39.
- Jiao, Y., Chiu, H., Fan, Z., Jiao, F., Eckstein, E.C., Beamer, W.G., Gu, W. (2007) Quantitative trait loci that determine mouse tibial nanoindentation properties in an F2 population derived from C57BL/6J X C3H/HeJ. *Calcified Tissue International*, 80, 383–390.

- Jiménez, J.A., Hughes, K.A., Alaks, G., Graham, L., Lacy, R.C. (1994) An experimental study of inbreeding depression in a natural habitat. *Science*, 266, 271–273.
- Kalichman, L., Batsevich, V., Kobylansky, E. (2019) Heritability estimation of 2D:4D finger ratio in a Chuvashian population-based sample. *American Journal of Human Biology*. 31, e23212.
- Kamiyama, N., Seki, R., Yokoyama, H., Tamura, K. (2012) Heterochronically early decline of Hox expression prior to cartilage formation in the avian hindlimb zeugopod. *Development, Growth & Differentiation*, 54, 619–632.
- Kang, H.M., Zaitlen, N.A., Wade, C.M., Kirby, A., Heckerman, D., Daly, M.J., Eskin, E. (2008) Efficient control of population structure in model organism association mapping. *Genetics*, 178, 1709–1723.
- Karunaratne, A., Davis, G.R., Hiller, J., Esapa, C.T., Terrill, N.J., Brown, S.D.M., Cox, R.D., Thakker, R.V., Gupta, H.S. (2012) Hypophosphatemic rickets is associated with disruption of mineral orientation at the nanoscale in the flat scapula bones of rachitic mice with development. *Bone*, 51, 553–562.
- Keane, T.M., Goodstadt, L., Danecek, P., White, M.A., Wong, K., Yalcin, et al. (2011) Mouse genomic variation and its effect on phenotypes and gene regulation. *Nature*, 477, 289–294.
- Kearns, A.E., Donohue, M.M., Sanyal, B., Demay, M.B. (2001) Cloning and characterization of a novel protein kinase that impairs osteoblast differentiation in vitro. *The Journal of Biological Chemistry*. 276, 42213–42218.
- Kemble, H., Nghe, P., Tenailon, O. (2019) Recent insights into the genotype–phenotype relationship from massively parallel genetic assays. *Evolutionary Applications*, 12, 1721–1742.
- Kenney-Hunt, J.P., Wang, B., Norgard, E.A., Fawcett, G., Falk, D., Pletscher, L.S., Jarvis, J.P., Roseman, C., Wolf, J., Cheverud, J.M. (2008) Pleiotropic patterns of quantitative trait loci for 70 murine skeletal traits. *Genetics*, 178, 2275–2288.
- Kim, M.S., Patel, K.P., Teng, A.K., Berens, A.J., Lachance, J. (2018) Genetic disease risks can be misestimated across global populations. *Genome Biology*, 19, 179.
- Kimura, Y., Matsunami, H., Inoue, T., Shimamura, K., Uchida, N., Ueno, T., Miyazaki, T., Takeichi, M. (1995) Cadherin-11 expressed in association with mesenchymal morphogenesis in the head, somite, and limb bud of early mouse embryos. *Developmental Biology*, 169, 347–358.
- Klingenberg, C.P. (2014) Studying morphological integration and modularity at multiple levels: concepts and analysis. *Philosophical Transactions of the Royal Society B: Biological Sciences*, 369, 20130249.
- Knott, S.A., Elsen, J.M., Haley, C.S. (1996) Methods for multiple marker mapping of quantitative trait loci in half-sib populations 10. *Theoretische und angewandte Genetik*, 93, 71–80.
- Kokabu, S., Rosen, V. (2017) BMP3 expression by osteoblast lineage cells is regulated by canonical Wnt signaling. *FEBS Open Bio*, 8, 168–176.
- Koller, D.L., Rodriguez, L.A., Christian, J.C., Slemenda, C.W., Econs, M.J., Hui, S.L., Morin, P., Conneally, P.M., Joslyn, G., Curran, M.E., Peacock, M., Johnston, C.C., Foroud, T. (1998)

- Linkage of a QTL Contributing to Normal Variation in Bone Mineral Density to Chromosome 11q12–13. *Journal of Bone Mineral Research*, 13, 1903–1908.
- Koltes, J.E., Mishra, B.P., Kumar, D., Kataria, R.S., Totir, L.R., Fernando, R.L., Cobbold, R., Steffen, D., Coppieters, W., Georges, M., Reecy, J.M. (2009) A nonsense mutation in cGMP-dependent type II protein kinase (PRKG2) causes dwarfism in American Angus cattle. *Proceedings of the National Academy of Sciences*, 106, 19250–19255.
- Lázaro, J., Nováková, L., Hertel, M., Taylor, J.R.E., Muturi, M., Zub, K., Dechmann, D.K.N. (2021) Geographic patterns in seasonal changes of body mass, skull, and brain size of common shrews. *Ecology and Evolution*, 11, 2431–2448.
- Leamy, L.J., Pomp, D., Eisen, E.J., Cheverud, J.M. (2002) Pleiotropy of quantitative trait loci for organ weights and limb bone lengths in mice. *Physiology Genomics*, 10, 21–29.
- Lee, B.T., Barber, G.P., Benet-Pagès, A., Casper, J., Clawson, H., Diekhans, M., Fischer, C., Gonzalez, J.N., Hinrichs, A.S., Lee, C.M., Muthuraman, P., Nassar, L.R., Nguy, B., Pereira, T., Perez, G., Raney, B.J., Rosenbloom, K.R., Schmelter, D., Speir, M.L., Wick, B.D., Zweig, A.S., Haussler, D., Kuhn, R.M., Haeussler, M., Kent, W.J. (2022) The UCSC Genome Browser database: 2022 update. *Nucleic Acids Research*, 50, D1115–D1122.
- Li, W.-H., Ellsworth, D.L., Krushkal, J., Chang, B.H.-J., Hewett-Emmett, D. (1996) Rates of nucleotide substitution in primates and rodents and the generation–time effect hypothesis. *Molecular Phylogenetic Evolution*, 5, 182–187.
- Lieberman, D.E., Polk, J.D., Demes, B. (2004) Predicting long bone loading from cross-sectional geometry. *American Journal of Physical Anthropology*, 123, 156–171.
- Lilje, K.E., Tardieu, C., Fischer, M.S. (2003) Scaling of long bones in ruminants with respect to the scapula. *Journal of Zoological Systematics and Evolutionary Research*, 41, 118–126.
- Liu, J., Luo, W., Qin, N., Ding, P., Zhang, H., Yang, C., Mu, Y., Tang, H., Liu, Y., Li, W., Jiang, Q., Chen, G., Wei, Y., Zheng, Y., Liu, C., Lan, X., Ma, J. (2018) A 55 K SNP array-based genetic map and its utilization in QTL mapping for productive tiller number in common wheat. *Theoretical and Applied Genetics*, 131, 2439–2450.
- Loebel, D.A.F., Hor, A.C.C., Bildsoe, H.K., Tam, P.P.L. (2014) Timed deletion of *twist1* in the limb bud reveals age-specific impacts on autopod and zeugopod patterning. *PLoS One*, 9, e98945.
- Lynch, N.E., Lynch, S.A., McMenemy, J., Webb, D. (2009) Bannayan-Riley-Ruvalcaba syndrome: a cause of extreme macrocephaly and neurodevelopmental delay. *Archives of Disease in Childhood*, 94, 553–554.
- Mallet, C., Billet, G., Houssaye, A., Cornette, R. (2020) A first glimpse at the influence of body mass in the morphological integration of the limb long bones: an investigation in modern rhinoceroses. *Journal of Anatomy*, 237, 704–726.
- Manning, J.T., Bundred, P.E., Newton, D.J., Flanagan, B.F. (2003) The second to fourth digit ratio and variation in the androgen receptor gene. *Evolution and Human Behavior*, 24, 399–405.
- Marchini, M., Rolian, C. (2018) Artificial selection sheds light on developmental mechanisms of limb elongation. *Evolution*, 72, 825–837.

- Marchini, M., Sparrow, L.M., Cosman, M.N., Dowhanik, A., Krueger, C.B., Hallgrímsson, B., Rolian, C. (2014) Impacts of genetic correlation on the independent evolution of body mass and skeletal size in mammals. *BMC Evolutionary Biology*, 14, 258.
- Marie, P.J., Haÿ, E., Modrowski, D., Revollo, L., Mbalaviele, G., Civitelli, R. (2014) Cadherin-mediated cell-cell adhesion and signaling in the skeleton. *Calcified Tissue International*, 94, 46–54.
- Martínez-Abadías, N., Heuzé, Y., Wang, Y., Jabs, E.W., Aldridge, K., Richtsmeier, J.T. (2011) FGF/FGFR Signaling coordinates skull development by modulating magnitude of morphological integration: evidence from apert syndrome mouse models. *PLoS One* 6, e26425.
- Martín-Serra, A., Figueirido, B., Pérez-Claros, J.A., Palmqvist, P. (2015) Patterns of morphological integration in the appendicular skeleton of mammalian carnivores. *Evolution* 69, 321–340.
- McGinley, J.C., Kozin, S.H. (2001) Interosseous membrane anatomy and functional mechanics. *Clinical Orthopaedics and Related Research*, 108–122.
- McGonnell, I.M. (2001) The evolution of the pectoral girdle. *Journal of Anatomy*, 199, 189–194.
- Monteiro, A. (2021) Distinguishing serial homologs from novel traits: Experimental limitations and ideas for improvements. *BioEssays* 43, 2000162.
- Morikawa, Y., D’Autrèaux, F., Gershon, M.D., Cserjesi, P. (2007) Hand2 determines the noradrenergic phenotype in the mouse sympathetic nervous system. *Developmental Biology*, 307, 114–126.
- Mouse Genome Sequencing Consortium (2002) Initial sequencing and comparative analysis of the mouse genome. *Nature*, 420, 520–562.
- Mullin, S.K., Taylor, P.J. (2002) The effects of parallax on geometric morphometric data. *Computers in Biology and Medicine*, 32, 455–464.
- Muñoz, N.A., Toledo, N., Candela, A.M., Vizcaíno, S.F. (2019) Functional morphology of the forelimb of Early Miocene caviomorph rodents from Patagonia. *Lethaia* 52, 91–106.
- Navarro, N., Murat Maga, A. (2018) Genetic mapping of molar size relations identifies inhibitory locus for third molars in mice. *Heredity* 121, 1–11.
- Negrão, S., Cecília Almadanim, M., Pires, I.S., Abreu, I.A., Maroco, J., Courtois, B., Gregorio, G.B., McNally, K.L., Margarida Oliveira, M. (2013) New allelic variants found in key rice salt-tolerance genes: an association study. *Plant Biotechnology Journal*, 11, 87–100.
- Nieves, J.W., Formica, C., Ruffing, J., Zion, M., Garrett, P., Lindsay, R., Cosman, F. (2005) Males have larger skeletal size and bone mass than females, despite comparable body size. *Journal of Bone and Mineral Research*, 20, 529–535.
- Noden, D.M., Schneider, R.A. (2006) Neural crest cells and the community of plan for craniofacial development, in: Saint-Jeannet, J.-P. (Ed.), *Neural crest induction and differentiation, advances in experimental medicine and biology*. Springer US, Boston, MA, pp. 1–23.
- Noirrit-Esclassan, E., Valera, M.-C., Tremollières, F., Arnal, J.-F., Lenfant, F., Fontaine, C., Vinel, A. (2021) Critical role of estrogens on bone homeostasis in both male and female: from

- physiology to medical implications. *International Journal of Molecular Sciences*. 22, 1568.
- Oberlender, S.A., Tuan, R.S. (1994) Spatiotemporal profile of N-cadherin expression in the developing limb mesenchyme. *Cell Adhesion and Communication*, 2, 521–537.
- Olsson, I.A.S., Silva, S.P. da, Townend, D., Sandøe, P. (2016) Protecting animals and enabling research in the european union: an overview of development and implementation of directive 2010/63/EU. *ILAR J.* 57, 347–357.
- Ongom, P.O., Ejeta, G. (2018) Mating design and genetic structure of a multi-parent advanced generation intercross (MAGIC) population of sorghum (*Sorghum bicolor* (L.) Moench). *G3 Genes Genomes Genetics* 8, 331–341.
- Orr, H.A. (1998) The population genetics of adaptation: the distribution of factors fixed during adaptive evolution. *Evolution* 52, 935–949.
- Otaify, G.A., Whyte, M.P., Gottesman, G.S., McAlister, W.H., Eric Gordon, J., Hollander, A., Andrews, M.V., El-Mofty, S.K., Chen, W.-S., Veis, D.V., Stolina, M., Woo, A.S., Katsonis, P., Lichtarge, O., Zhang, F., Shinawi, M. (2018) Gnathodiaphyseal dysplasia: severe atypical presentation with novel heterozygous mutation of the anoctamin gene (ANO5). *Bone* 107, 161–171.
- Ovchinnikov, D. (2009) Alcian blue/alizarin red staining of cartilage and bone in mouse. *Cold Spring Harbour Protocols*, pdb.prot517
- Pallares, L.F., Carbonetto, P., Gopalakrishnan, S., Parker, C.C., Ackert-Bicknell, C.L., Palmer, A.A., Tautz, D. (2015) Mapping of Craniofacial Traits in Outbred Mice Identifies Major Developmental Genes Involved in Shape Determination. *PLoS Genetics*, 11, e1005607.
- Pallares, L.F., Harr, B., Turner, L.M., Tautz, D. (2014) Use of a natural hybrid zone for genomewide association mapping of craniofacial traits in the house mouse. *Molecular Ecology*, 23, 5756–5770.
- Pan, J., Wang, B., Li, W., Zhou, X., Scherr, T., Yang, Y., Price, C., Wang, L. (2012) Elevated cross-talk between subchondral bone and cartilage in osteoarthritic joints. *Bone, Osteoarthritis* 51, 212–217.
- Parker, C.C., Chen, H., Flagel, S.B., Geurts, A.M., Richards, J.B., Robinson, T.E., Solberg Woods, L.C., Palmer, A.A. (2014) Rats are the smart choice: rationale for a renewed focus on rats in behavioral genetics. *Neuropharmacology, NIDA 40th Anniversary Issue* 76, 250–258.
- Parker, C.C., Cheng, R., Sokoloff, G., Lim, J.E., Skol, A.D., Abney, M., Palmer, A.A. (2011) Fine-mapping alleles for body weight in LG/J × SM/J F2 and F34 advanced intercross lines. *Mammalian Genome*, 22, 563–571.
- Parmenter, M.D., Gray, M.M., Hogan, C.A., Ford, I.N., Broman, K.W., Vinyard, C.J., Payseur, B.A. (2016) Genetics of skeletal evolution in unusually large mice from Gough Island. *Genetics*, 204, 1559–1572.
- Paschalis, E., Recker, R., Dicarlo, E., Doty, S., Atti, E., Boskey, A. (2003) Distribution of collagen cross-links in normal human trabecular bone. *Journal of Bone and Mineral Research*, 18, 1942–1946.

- Pavlicev, M., Wagner, G.P., Noonan, J.P., Hallgrímsson, B., Cheverud, J.M. (2013) Genomic correlates of relationship QTL involved in fore- versus hind limb divergence in mice. *Genome Biology and Evolution*, 5, 1926–1936.
- Perez, M.J., Barquez, R.M., Diaz, M.M. (2017) Morphology of the limbs in the semi-fossorial desert rodent species of *Tympanoctomys* (Octodontidae, Rodentia). *ZooKeys*, 710, 77–96.
- Perilli, E., Cantley, M., Marino, V., Crotti, T.N., Smith, M.D., Haynes, D.R., Dharmapatni, A. a. S.S.K. (2015) Quantifying not only bone loss, but also soft tissue swelling, in a murine inflammatory arthritis model using micro-computed tomography. *Scandinavian Journal of Immunology*, 81, 142–150.
- Petit, F., Sears, K.E., Ahituv, N. (2017) Limb development: a paradigm of gene regulation. *Nature Review Genetics*, 18, 245–258.
- Pham, H.T., Kram, V., Dar, Q.-A., Komori, T., Ji, Y., Mohassel, P., Rooney, J., Li, L., Kilts, T.M., Bonnemann, C., Lamande, S., Young, M.F. (2020) Collagen VI α 2 chain deficiency causes trabecular bone loss by potentially promoting osteoclast differentiation through enhanced TNF α signaling. *Scientific Reports*, 10, 13749.
- Pruszkowska-Przybylska, P., Kobus, M., Iljin, A., Wiktorska, J.A., Żądzińska, E., Sitek, A. (2021) Thyroid diseases and second to fourth digit ratio in Polish adults. *Scientific Report*, 11, 18979.
- Quintana-Murci, L., Barreiro, L.B. (2010) The role played by natural selection on Mendelian traits in humans. *Annals of the New York Academy of Sciences*, 1214, 1–17.
- Reno, P.L., McCollum, M.A., Cohn, M.J., Meindl, R.S., Hamrick, M., Lovejoy, C.O. (2008) Patterns of correlation and covariation of anthropoid distal forelimb segments correspond to *Hoxd* expression territories. *Journal of Experimental Zoology Part B: Molecular and Developmental Evolution*. 310B, 240–258.
- Riminucci, M., Collins, M.T., Corsi, A., Boyde, A., Murphey, M.D., Wientroub, S., Kuznetsov, S.A., Cherman, N., Robey, P.G., Bianco, P. (2001) Gnathodiaphyseal dysplasia: a syndrome of fibro-osseous lesions of jawbones, bone fragility, and long bone bowing. *Journal of Bone and Mineral Research*, 16, 1710–1718.
- Rosemann, M., Gonzalez-Vasconcellos, I., Domke, T., Kuosaite, V., Schneider, R., Kremer, M., Favor, J., Nathrath, M., Atkinson, M.J. (2014) A *Rb1* promoter variant with reduced activity contributes to osteosarcoma susceptibility in irradiated mice. *Molecular Cancer*, 13, 182.
- Ross, S.E., McCord, A.E., Jung, C., Atan, D., Mok, S.I., Hemberg, M., Kim, T.-K., Salogiannis, J., Hu, L., Cohen, S., Lin, Y., Harrar, D., McInnes, R.R., Greenberg, M.E. (2012) *Bhlhb5* and *Prdm8* form a repressor complex involved in neuronal circuit assembly. *Neuron*, 73, 292–303.
- Ruff, C. (1987) Structural allometry of the femur and tibia in Hominoidea and Macaca. *Folia Primatologica*, 48, 9–49.
- Sabsovich, I., Clark, J.D., Liao, G., Peltz, G., Lindsey, D.P., Jacobs, C.R., Yao, W., Guo, T.-Z., Kingery, W.S. (2008) Bone microstructure and its associated genetic variability in 12 inbred mouse strains: μ CT study and in silico genome scan. *Bone*, 42, 439–451.

- Samocha, K.E., Lim, J.E., Cheng, R., Sokoloff, G., Palmer, A.A. (2010) Fine mapping of QTL for prepulse inhibition in LG/J and SM/J mice using F2 and advanced intercross lines. *Genes, Brain and Behavior*, 9, 759–767.
- Sanger, T.J., Norgard, E.A., Pletscher, L.S., Bevilacqua, M., Brooks, V.R., Sandell, L.J., Cheverud, J.M. (2011) Developmental and genetic origins of murine long bone length variation. *Journal of Experimental Zoology Part B: Molecular and Developmental Evolution*, 316B, 146–161.
- Saxena, A., Sharma, V., Muthuirulan, P., Neufeld, S.J., Tran, M.P., Gutierrez, H.L., Chen, K.D., Erberich, J.M., Birmingham, A., Capellini, T.D., Cobb, J., Hiller, M., Cooper, K.L. (2021) Interspecies transcriptomics identify genes that underlie disproportionate foot growth in jerboas. *Current Biology*, 32, 289–303.
- Schacherer, J. (2016) Beyond the simplicity of Mendelian inheritance. *Comptes Rendus Biologies*, 339, 284–288.
- Schindelin, J., Arganda-Carreras, I., Frise, E., Kaynig, V., Longair, M., Pietzsch, T., Preibisch, S., Rueden, C., Saalfeld, S., Schmid, B., Tinevez, J.-Y., White, D.J., Hartenstein, V., Eliceiri, K., Tomancak, P., Cardona, A. (2012) Fiji: an open-source platform for biological-image analysis. *Nature Methods*, 9, 676–682.
- Schmidt, M., Fischer, M.S. (2009) Morphological integration in mammalian limb proportions: dissociation between function and development. *Evolution* 63, 749–766.
- Schunke, A.C., Bromiley, P.A., Tautz, D., Thacker, N.A. (2012) TINA manual landmarking tool: software for the precise digitization of 3D landmarks. *Frontiers in Zoology*, 9, 6.
- Sears, K.E. (2008) Molecular determinants of bat wing development. *Cells Tissues Organs* 187, 6–12.
- Sears, K.E., Behringer, R.R., Rasweiler IV, J.J., Niswander, L.A. (2007) The evolutionary and developmental basis of parallel reduction in mammalian zeugopod elements. *The American Naturalist*, 169, 105–117.
- Seeman, E., Hopper, J.L., Young, N.R., Formica, C., Goss, P., Tsalamandris, C. (1996) Do genetic factors explain associations between muscle strength, lean mass, and bone density? A twin study. *American Journal of Physiology-Endocrinology and Metabolism*, 270, E320–E327.
- Shikhaliev, P., Tartoni, N. (2019) Improving spatial resolution in X-ray microscopy by using tilted angle detector: A simulation study. *ArXiv191001383 Phys*.
- Shubin, N.H., Daeschler, E.B., Jenkins, F.A. (2006) The pectoral fin of *Tiktaalik roseae* and the origin of the tetrapod limb. *Nature*, 440, 764–771.
- Sims, N.A., Dupont, S., Krust, A., Clement-Lacroix, P., Minet, D., Resche-Rigon, M., Gaillard-Kelly, M., Baron, R. (2002) Deletion of estrogen receptors reveals a regulatory role for estrogen receptors-beta in bone remodeling in females but not in males. *Bone*, 30, 18–25.
- Škrabar, N., Turner, L.M., Pallares, L.F., Harr, B., Tautz, D. (2018) Using the *Mus musculus* hybrid zone to assess covariation and genetic architecture of limb bone lengths. *Molecular Ecology Resources*, 18, 908–921.

- Škrabar, Neva, 2018. Phenotypic variability and genetic architecture of limbs in populations and strains of the house mouse (*Mus musculus*). Max-Planck-Institut für Evolutionsbiologie, Ploen.
- Smith, J.R., Hayman, G.T., Wang, S.-J., Laulederkind, S.J.F., Hoffman, M.J., Kaldunski, M.L., Tutaj, M., Thota, J., Nalabolu, H.S., Ellanki, S.L.R., Tutaj, M.A., De Pons, J.L., Kwitek, A.E., Dwinell, M.R., Shimoyama, M.E. (2020) The Year of the Rat: The Rat Genome Database at 20: a multi-species knowledgebase and analysis platform. *Nucleic Acids Research*, 48, D731–D742.
- Solberg Woods, L.C. (2014) QTL mapping in outbred populations: successes and challenges. *Physiological Genomics*, 46, 81–90.
- Sommer, A., Bartholomew, D.W. (2003) Craniofacial-deafness-hand syndrome revisited. *American Journal of Medical Genetics. Part A*, 123A, 91–94.
- Srinivas, G., Möller, S., Wang, J., Künzel, S., Zillikens, D., Baines, J.F., Ibrahim, S.M. (2013) Genome-wide mapping of gene-microbiota interactions in susceptibility to autoimmune skin blistering. *Nature Communications*, 4, 2462.
- Stallings, W.M., Gillmore, G.M. (1971) A note on “accuracy” and “precision.” *Journal of Educational Measurement*, 8, 127–129.
- Sugiyama, F., Churchill, G.A., Higgins, D.C., Johns, C., Makaritsis, K.P., Gavras, H., Paigen, B. (2001) Concordance of murine quantitative trait loci for salt-induced hypertension with rat and human loci. *Genomics*, 71, 70–77.
- Sun, D., Zhou, X., Yu, Z., Xu, S., Seim, I., Yang, G. (2019) Accelerated evolution and diversifying selection drove the adaptation of cetacean bone microstructure. *BMC Evolutionary Biology*, 19, 194.
- Sunyaev, S., Ramensky, V., Koch, I., Lathe III, W., Kondrashov, A.S., Bork, P. (2001) Prediction of deleterious human alleles. *Human Molecular Genetics*, 10, 591–597.
- Svenson, K.L., Gatti, D.M., Valdar, W., Welsh, C.E., Cheng, R., Chesler, E.J., Palmer, A.A., McMillan, L., Churchill, G.A. (2012) High-resolution genetic mapping using the Mouse Diversity Outbred Population. *Genetics*, 190, 437–447.
- Swank, S., Sanger, T.J., Stuart, Y.E. (2021) (Non)Parallel developmental mechanisms in vertebrate appendage reduction and loss. *Ecology and Evolution*, 11, 15484–15497.
- Takahashi, J., Ohbayashi, A., Oginuma, M., Saito, D., Mochizuki, A., Saga, Y., Takada, S. (2010) Analysis of Ripply1/2-deficient mouse embryos reveals a mechanism underlying the rostro-caudal patterning within a somite. *Developmental Biology* 342, 134–145.
- Tam, V., Patel, N., Turcotte, M., Bossé, Y., Paré, G., Meyre, D. (2019) Benefits and limitations of genome-wide association studies. *Nature Reviews Genetics* 20, 467–484.
- The 3Rs | NC3Rs [WWW Document], n.d. URL <https://nc3rs.org.uk/the-3rs> (accessed 11.1.21).
- The, B., Mol, L., Diercks, R.L., Ooijen, P.M.A. van, Verdonchot, N. (2006) Correction of error in two-dimensional wear measurements of cemented hip arthroplasties. *Clinical Orthopaedics and Related Research*, 442, 180–186.
- Thompson, Z., Miclau, T., Hu, D., Helms, J.A. (2002) A model for intramembranous ossification during fracture healing. *Journal of Orthopaedic Research: Official Publication of the Orthopaedic Research Society*, 20, 1091–1098.

- Tommasini, S.M., Hu, B., Nadeau, J.H., Jepsen, K.J. (2009) Phenotypic integration among trabecular and cortical bone traits establishes mechanical functionality of inbred mouse vertebrae. *Journal of Bone and Mineral Research*, 24, 606–620.
- Trivier, E., De Cesare, D., Jacquot, S., Pannetier, S., Zackai, E., Young, I., Mandel, J.L., Sassone-Corsi, P., Hanauer, A. (1996) Mutations in the kinase Rsk-2 associated with Coffin-Lowry syndrome. *Nature*, 384, 567–570.
- Tsuchida, A., Yokoi, N., Namae, M., Fuse, M., Masuyama, T., Sasaki, M., Kawazu, S., Komeda, K. (2008) Phenotypic characterization of the Komeda miniature rat Ishikawa, an animal model of dwarfism caused by a mutation in Prkg2. *Comparative Medicine*, 58, 560–567.
- Turner, L.M., Harr, B. (2014) Genome-wide mapping in a house mouse hybrid zone reveals hybrid sterility loci and Dobzhansky-Muller interactions. *eLife* 3, e02504.
- Vu, Vincent Q. (2011) ggbiplot: A ggplot2 based biplot. R package version 0.55.
- Wagner, G.P. (2005) The developmental evolution of avian digit homology: An update. *Theory in Bioscience*, 124, 165–183.
- Wang, M., Xu, S. (2019) Statistical power in genome-wide association studies and quantitative trait locus mapping. *Heredity*, 123, 287–306.
- Wang, X., Liu, X., Dong, R., Liang, C., Reichenberger, E.J., Hu, Y. (2019) Genetic disruption of anoctamin 5 in mice replicates human gnathodiaphyseal dysplasia (GDD). *Calcified Tissue International*, 104, 679–689.
- Waxman, D., Welch, J.J. (2005) Fisher’s microscope and Haldane’s ellipse. *The American Naturalist*, 166, 447–457.
- Weatherholt, A.M., Fuchs, R.K., Warden, S.J. (2012) Specialized connective tissue: bone, the structural framework of the upper extremity. *Journal of Hand Therapy*, 25, 123–132.
- Wei T., S.V. (2021) R package “corrplot”: Visualization of a Correlation Matrix. (Version 0.90).
- Wu, S., Shao, M., Zhang, Y., Shi, D. (2021) Activation of RSK2 upregulates SOX8 to promote methotrexate resistance in gestational trophoblastic neoplasia. *Laboratory Investigation*, 101, 1494–1504.
- Wuschke, S., Dahm, S., Schmidt, C., Joost, H.-G., Al-Hasani, H. (2007) A meta-analysis of quantitative trait loci associated with body weight and adiposity in mice. *International Journal of Obesity*, 31, 829–841.
- Xu, M., Xie, Y., Abouzeid, H., Gordon, C.T., Fiorentino, A., Sun, Z., et. al (2017) Mutations in the spliceosome component CWC27 cause retinal degeneration with or without additional developmental anomalies. *American Journal of Human Genetics*, 100, 592–604.
- Yan, Y.L., Miller, C.T., Nissen, R.M., Singer, A., Liu, D., Kirn, A., Draper, B., Willoughby, J., Morcos, P.A., Amsterdam, A., Chung, B.-C., Westerfield, M., Haffter, P., Hopkins, N., Kimmel, C., Postlethwait, J.H., Nissen, R. (2002) A zebrafish sox9 gene required for cartilage morphogenesis. *Development (Cambridge, England)*, 129, 5065–5079.
- Yang, H., Wang, J.R., Didion, J.P., Buus, R.J., Bell, T.A., Welsh, C.E., Bonhomme, F., Yu, A.H.-T., Nachman, M.W., Pialek, J., Tucker, P., Boursot, P., McMillan, L., Churchill, G.A., de Villena, F.P.-M. (2011) Subspecific origin and haplotype diversity in the laboratory mouse. *Nature Genetics* 43, 648–655.

- Yoshikawa, T., Watanabe, A., Ishitsuka, Y., Nakaya, A., Nakatani, N. (2002) Identification of multiple genetic loci linked to the propensity for “behavioral despair” in mice. *Genome Research*, 12, 357–366.
- Youlten, S.E., Baldock, P.A. (2019) Using mouse genetics to understand human skeletal disease. *Bone, Skeletal Genomics: State-of-the-Art and Future Directions* 126, 27–36.
- Young, M., Selleri, L., Capellini, T.D. (2019) Genetics of scapula and pelvis development: An evolutionary perspective. *Current Topics in Developmental Biology*, 132, 311–349.
- Young, N.M. (2013) Macroevolutionary diversity of amniote limb proportions predicted by developmental interactions. *Journal of Experimental Zoology Part B: Molecular and Developmental Evolution*, 320, 420–427.
- Young, N.M., Hallgrímsson, B. (2005) Serial homology and the evolution of mammalian limb covariation structure. *Evolution*, 59, 2691–2704.
- Young, N.M., Hallgrímsson, B., Garland, T. (2009) Epigenetic effects on integration of limb lengths in a mouse model: selective breeding for high voluntary locomotor activity. *Evolutionary Biology*, 36, 88.
- Yu, J., Pressoir, G., Briggs, W.H., Vroh Bi, I., Yamasaki, M., Doebley, J.F., McMullen, M.D., Gaut, B.S., Nielsen, D.M., Holland, J.B., Kresovich, S., Buckler, E.S. (2006) A unified mixed-model method for association mapping that accounts for multiple levels of relatedness. *Nature Genetics* 38, 203–208.
- Zeller, R., López-Ríos, J., Zuniga, A. (2009) Vertebrate limb bud development: moving towards integrative analysis of organogenesis. *Nature Review Genetics*, 10, 845–858.
- Zhang, Danfeng, Huang, J., Zhang, W., Pan, L., Zhang, Dan, Zhao, P., Wang, F., Luo, H., He, J., Qin, Y., Qu, Y., Guo, T., Niu, T., Zheng, Y. (2018) Young female patients with multiple myeloma have low occurrence of osteolytic lesion. *Bone* 110, 21–28.
- Zhang, G., Cohn, M.J. (2008) Genome duplication and the origin of the vertebrate skeleton. *Current Opinion in Genetics & Development*, 18, 387–393.
- Zhang, X., Kuroda, S., Carpenter, D., Nishimura, I., Soo, C., Moats, R., Iida, K., Wisner, E., Hu, F.-Y., Miao, S., Beanes, S., Dang, C., Vastardis, H., Longaker, M., Tanizawa, K., Kanayama, N., Saito, N., Ting, K. (2002) Craniosynostosis in transgenic mice overexpressing *Nell-1*. *The Journal of Clinical Investigation*, 110, 861–870.
- Zimmerman, H., Yin, Z., Zou, F., Everett, E.T. (2019) Interfrontal bone among inbred strains of mice and QTL mapping. *Frontiers in Genetics*, 10, 291.
- Zwick, M.E., Cutler, D.J., Chakravarti, A. (2000) Patterns of genetic variation in mendelian and complex traits. *Annual Review of Genomics and Human Genetics*, 1, 387–407.

List of Figures

Figure 1.1.	11
Examples of simple cross designs used in QTL mapping – backcross, and intercross which after multiple generations is referred as an advanced intercross (A); Cross design of the diversity outbred (DO) mice (B);	
Figure 1.2.	15
Concept of integrated bone elements as in the example of the house mouse;	
Figure 2.1.	28
The Faxitron x-ray machine used in the experiment (A), and the settings of the machine used in this study (B)	
Figure 2.2.....	29
Examples roentgen pictures of front (A) and hind (B) part of the AH mouse	
Figure 2.3.	30
Inserting a mouse body into the ScanCo micro-tomograph (A); parameters of the scanner in AH mice (B).	
Figure 2.4.	34
Heatmaps of Pearson’s correlation of bones measurements in x-ray-based (a) and μ CT-based (b) measurements	
Figure 2.5.	35
Violin plots representing male (M) and female (F) distribution of each bone length in the AH mice;	
Figure 2.8.....	37
Relation of weight and bone length in female AH mice;	
Figure 2.9.....	38
Male scapula correlation with the weight of animals;	
Figure 2.10.....	39
Correlation between bones in μ CT-based measurement for raw female (f-r) and male (m-r) data, and for weight residual dataset (female: f-w, males: m-w).	
Figure 2.11.....	40
Residual weight measurements of AH mice show division between male and female. The ulna and radius show a similar direction of variance.	
Figure 2.12.....	41
PCA showing loadings of each trait in males (a) and females (b) AH mice	
Figure 2.13.	43
Front limb bone length proportions in males and females.	

Figure 3.1.	50
Schematic figure of the G15 mice breeding; the three parental lines are laboratory inbred mice of <i>M. m. domesticus</i> origin, which were crossed for 15 generations together with the wild-type mice <i>M. m. castaneus</i>	
Figure 3.2.....	52
Spreadsheet example for calculating the length of each bone in first and second attempt.	
Figure 3.3.	55
Example of the new Excel spreadsheet layout used to calculate the bone lengths.	
Figure 3.4.	56
Bone length change due to quality in humerus and femur	
Figure 3.5.....	60
Frequency histograms of each measured bone, raw dataset, both sexes; left-side tail is observed in humerus;	
Figure 3.6.....	62
Frequency histograms of the final measurement of G15 mice (phenotyped and genotyped specimens)	
Figure 3.7.....	64
Violin plots representing male (M) and female (F) distribution each bone length in G15 mice;	
Figure 3.8.....	66
Relation of weight and bone length G15 mice;	
Figure 3.9.....	67
Correlation between bone length in G15 mice (both sexes, no covariates added, all results are significant with $p < 0.05$), with r values in the upper squares; method: Pearson product moment correlation, complete pairwise observation	
Figure 3.10.....	68
Correlation patterns between bone length in females (a) and males (b); method: Pearson product moment correlation (Pearson's R), complete pairwise observation, all results are significant with $p < 0.05$	
Figure 3.11.....	69
PCA graph on weight residual dataset (complete observation) of the G15 mice with eigenvectors for each bone	
Figure 3.12.....	72
LOD scores in each chromosome in the humerus phenotype	
Figure 3.13.....	73
LOD scores in each chromosome in the scapula phenotype	

Figure 3.14.....	74
LOD scores in each chromosome in the radius phenotype	
Figure 3.15.....	76
LOD scores in each chromosome in the ulna phenotype	
Figure 3.16.....	77
Peaks in Ulna on chromosome 6 (A), 13 (B) and 15 (C)	
Figure 3.17.....	78
LOD scores in each chromosome in the femur phenotype (A) and visualization of the peak in chromosome 8 (B)	
Figure 3.18.....	79
LOD scores in each chromosome in the tibia phenotype	
Figure 3.19.....	80
Visualization of the peak in chromosome 5 (A) and chromosome 13 (B)	
Figure 3.20.....	86
All suggestive peaks on chromosome 13: dark blue – ulna, green – tibia, magenta – radius, orange – scapula;	
Figure 3.21.....	93
Radius LOD score graphs in the humerus covariate mapping model, with the significance level lines	
Fig.3.22.....	94
Significant peaks on chromosome 13, in the model with humerus covariate: magenta – radius, dark blue – ulna; the dark grey line and dashed vertical line represents the ulna peak in original raw mapping model.	
Figure 3.23.....	94
Femur LOD score graphs in the humerus covariate mapping model	
Figure 3.24.....	96
Relevant LOD score graphs of radius, scapula and tibia in ulna covariate model.	
Figure 3.25.....	98
Relevant LOD score graphs of femur and tibia in scapula covariate model.	
Figure 3.26.	99
Position of the two LOD score peak on chromosome 5 in tibia with scapula as a covariate (blue dashed lines), and of the tibia as an individual bone (green colour line)	

Figure 3.27.....	101
Relevant LOD score graphs of ulna (A), femur in the X chromosome (B) and tibia (C) in femur covariate model	
Figure 3.28.....	103
Relevant LOD score graphs of radius and ulna in the tibia covariate model.	
Figure 3.29.	104
Relevant LOD score graphs of femur in the tibia covariate model (A), with the autosome significance level lines and closeup of the femur peak and suggestive humerus peak in chromosome X (B)	
Figure 3.30.....	109
Genome scan outcome on chromosome 15, dark blue solid and vertical dashed lines mark the ulna as a separate trait, green is specific to the results with the tibia as a covariate, and white is specific to the femur covariate.	
Figure 3.31.....	111
Weight differences of males and females in AH and G15 mice;	

List of Tables

Table 2.1.....	31
List of landmark anatomical positions in each measured bone	
Table 2.2.....	33
Basic statistic of ex-vivo morphometric measurements	
Table 2.3.....	36
Length properties (the values are given in milimeters) of each measured bone in females and males and the statistical test (Wilcoxon test) of the bone length and weight difference in males and females;	
Table 2.4.....	37
Kendall's tau correlation between weight and bone length in cumulated samples, females and males.	
Table 3.1.....	53
List of anatomical placements of landmarks	
Table 3.2.....	53
Summary of the two sets of measurements;	
Table 3.3.....	59
Cumulated measurements on 292 mice of each bone and measurement error percentage;	

Table 3.4.....	61
Number of measurements in each quality score per bone	
Table 3.5.....	61
Primary statistical results of the genotyped and phenotyped mice.	
Table 3.6.....	63
Female and male statistics in the G15 mice; lengths are given in millimetres	
Table 3.7.....	65
Level of significance of ANOVA test between bone length and covariate, including combination of two of more covariates.	
Table 3.8.....	70
Autosome significance threshold in each bone (number of permutations: 10,000)	
Table 3.9.....	70
Chromosome X significance threshold in each bone (number of permutations: 14,9367)	
Table 3.10.....	71
List of highest LOD peaks in humerus, radius and scapula which did not reach significance; confidence interval (CI) and peak position converted to GRCm38	
Table 3.11.....	75
Highest LOD peaks significant in the bones (blue colour represents significance at the level 10%), the position of the peak and confidence intervals was converted to the GRCm38.	
Table 3.12.....	81
Candidate genes in peak position in each significant result per bone, and skeleton phenotype candidate genes in the confidence interval region	
Table 3.13.....	89
Position of skeleton phenotype candidate genes (in GRCm38 as derived from the RGD resources for each gene) and their minimum and maximum distance to the peak (Mbp)	
Table 3.14.....	90
Significance levels based on permutations of each covariate model	
Table 3.15.....	92
List of significant and suggestive regions in each of the four models;	
Table 3.16.....	95
Peak candidate gene, and relevant phenotype candidate genes in the humerus covariate model	
Table 3.17.....	97
Peak candidate gene, and relevant phenotype candidate genes in ulna covariate model	

Table 3.18.....	99
Peak candidate gene, and relevant phenotype candidate genes in the scapula covariate model	
Table 3.19.....	102
Peak candidate gene, and relevant phenotype candidate genes in femur covariate model	
Table 3.20.....	105
Peak candidate gene, and relevant phenotype candidate genes in tibia covariate model	
Supplementary Table 2.1.....	114
List of specimens used in the chapter II; the name is specific with the breeding patterns of the MPI;	
Supplementary Table 2.2.....	115
Summary of Shapiro-Wilk test of normality with W and p values in each trait as well as weight of the animals.	
Supplementary Table 2.3.....	115
PCA scores of each bone in females, males and weight residual dataset.	
Supplementary Table 3.1.....	116
t-test results of male-female differences in G15 mice;	
Supplementary Table 3.2.....	117
ANOVA results of the covariate models in G15 mice	
Supplementary Table 3.3.....	119
PCA scores of each bone in females, males and weight residual dataset in the G15 mice	

Acknowledgements

I would like to express my gratitude to the examining committee, Prof. Dr. Paul Rainey, Prof. Dr. Eva Stukenbrock and Prof. Dr. John Baines as well as the Chair of the Disputation for their time and contribution in the final step of pursuing my doctoral degree. I would like to thank my supervisors: Paul and Diethard, for their involvement in the process and allowing me to complete my research. I am extremely thankful to dr. Dave Rogers, who patiently guided me in my work until its successful completion. After all the upside downs, I can now see myself as a scientist, and it just wouldn't be possible without his help. I would also want to thank dr. Carsten Fortmann-Grote, for the bioinformatics help, and enabling me to use the computing cluster. Furtherly, I am extremely grateful to dr. Meriem Belheouane, who helped me with the G15 genome data, and also explained the mapping models, which ultimately led me to really enjoy my work in the field of quantitative genetics. Neva, thank you enormously for all the patient help with geometric morphometrics and genetics at the start of my journey, as well as the lovely chats in our old office with Rebecca and also Yoland. Thanks to dr. Derek Caetano-Anolles for his supervision within the first six months of my work. I would also want to thank the Mouse House team, especially Christine and Heike and Elke. I am also very happy for the encouragement and patient explanations of German bureaucracy by Angela, Britta (and her sweetest dog, Merlin). I also want to acknowledge the IT team of the MPI, especially Derk, who is always around to help.

This thesis would not come to life, if it was not for the support which I received from co-workers, my family and friends. First, I would like to thank my beloved sister, Angelika. You were always there for me, since the time we were little children. You heard me out every time I felt discouraged, and aided me with kind words. I enjoyed the time we spent together in Tenerife during the winter break, eating ice cream and watching whales! And just laughing at funny things, such as "bobek" is when we can forget about life difficulties and enjoy our companion. I also want to mention my parents for their support, and the nice, welcome time whenever I was back home, with Kamila and her family – Emilia, Nina and Tomek (and our beloved dogs – Lisia and Zara).

The list of my friends within the institute is so long I might not include everyone! But if you are reading this, you are probably one of them! First, Lize - I just loved spending time together, and I can't even imagine where would this thesis be if not for you. Your kind words and all the advice were always valuable to me. And also, meta! Ela, I loved to spend time with you and having delicious vegan food! Ana, let's not forget about the cucumbers and non-vegan treats at the Christmas market. And of course, all the amazing travels and chats. Maria, I am super happy to know you, and to attend karate together! Life in Ploen would not be the same without the fun we had together in the Dōjō. Carolina, Karen, Ezgi (thank you for the milk rice), Zahra, Filipa, Bilal, Roman, Devika, Johana, Federica, Nico, Malavi, Elio – I just love you guys! The BBQs, Aquavit and defences parties in the old cafeteria are the nicest memories, which I will not forget. Maryam, thank you for all the lovely chats about genetics and teaching me Persian with Zahra and Nazanin. Elena, I remember traveling with you and Joanna to the sea side! Thank you for all the nice chats, and your encouragements. Thanks to Loukas, for always being kind neighbour! And cheers to the IMPRS batch 2017!

Finally, I would also like to acknowledge members - and my friends, of the Microbial Population Biology Department: Joanna, Norma, Elisa, Bram, Charly and others, for the encouragement and the cherished time I had - while working with you.

Authors' contributions

Chapter II: Wioleta J. Rasmus designed the study, performed the phenotyping of mice, as well as the QTL mapping of the G15 mice; dr. Meriem Belheouane prepared the micro array data files for analyses in the r/qt12 package.

Declaration

I declare that,

- i. apart from the supervisor's guidance the content and design of the thesis is my own work;
- ii. this thesis has not been submitted either partially or completely as part of a doctoral degree to another examining institution. No materials are published or submitted for publication other than indicated in this thesis;
- iii. this thesis was prepared with regard to the Rules of Good Scientific Practice of the German Research Foundation;
- iv. no academic degree has ever been withdrawn;

Wioleta Joanna Rasmus

Plön, April 2022

Outline of the Academic career

Wioleta Joanna Rasmus

Nationality: Polish

Date and place of birth: 03 April 1991; Elblag, Poland

Education

2007 – 2010

3rd John Paul II High School in Elblag, Poland

2011 – 2014

Bachelor of Science Degree;
Oceanography
Department of Oceanography and Geography
University of Gdansk, Poland

2014 – 2017

Master of Science Degree;
Marine Biology, Oceanography
Department of Oceanography and Geography
University of Gdansk, Poland

Thesis: Planktonic Ostracoda in the Frontal Zones of the Drake Passage

Since February 2018

Doctor of Philosophy degree;
Department of Microbial Population Biology
Max Planck Institute for Evolutionary Biology
Ploen Germany

Thesis: Morphometric properties and quantitative trait loci mapping of the mouse limb skeleton